

**EXPLORING THE METABOLIC INTERSECTION OF JUGLONE  
AND PHYLLOQUINONE BIOSYNTHESIS**

by

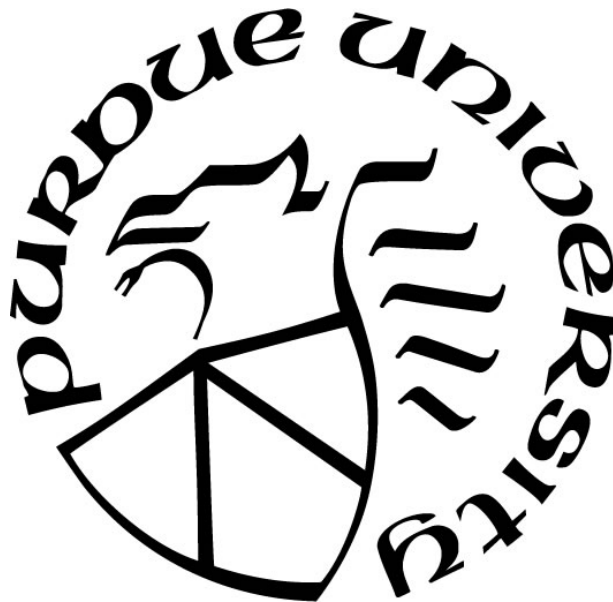
**Rachel M. McCoy**

**A Dissertation**

*Submitted to the Faculty of Purdue University*

*In Partial Fulfillment of the Requirements for the degree of*

**Doctor of Philosophy**



Department of Horticulture

West Lafayette, Indiana

May 2020

**THE PURDUE UNIVERSITY GRADUATE SCHOOL  
STATEMENT OF COMMITTEE APPROVAL**

**Dr. Joshua R. Widhalm**

Department of Horticulture and Landscape Architecture

**Dr. Clint Chapple**

Department of Biochemistry

**Dr. Brian Dilkes**

Department of Biochemistry

**Dr. Sharon Kessler**

Department of Botany and Plant Pathology

**Approved by:**

Dr. Aaron J. Patton

*In memoriam:*

Leslie N. McCoy

1956-2016

Pamela R. Kinnen

1961-2017

Wish you were here.

## ACKNOWLEDGMENTS

The end of a long journey is a time for reflection and gratitude. I did not accomplish this alone and am grateful for the training, support, and friendship I have received along the way. I've been impacted by so many people during this time, but some require special recognition.

First and foremost, the work herein would not have been possible without the support of my advisor, Dr. Josh Widhalm. I am eternally grateful for his mentorship, especially during tumultuous times in my life. Regardless of the situation, he has always been on my side and in my corner. Thanks for your patience, understanding, and faith in me.

I would also like to acknowledge the superb mentoring I received from my committee members. Thanks to my past committee members, past and present. Thanks to Drs. David Rhodes, Lori Hoagland, and Natalia Dudareva for your feedback and insight. Thanks to Dr. Sharon Kessler for helping me cross the finish line. Special thanks to Drs. Clint Chapple and Brian Dilkes, who have been with me since the beginning. I am so grateful for your support and perspective over the years.

Dr. Gordon McNickle was instrumental in the development of chapter 4 of my thesis. After one of the most interesting classes I've ever taken, he said something along the lines of "we could publish this" and now a class project is a chapter of my thesis. I've learned a lot and had a lot of fun doing it.

I couldn't have finished this degree without the amazing support I received from my friends. Especially, thanks to Dr. Ruthie S. Arieti, Dr. Laura K. Henry, Dr. Brittany F. Peterson, and soon-to-be-doctor Fabiola Muro-Villanueva. Without your support and encouragement, I would not be where I am today. Words cannot describe how much of an impact each of you have had on me, both professionally and personally. Thank you.

Thank you to my family. Thanks, Liam, for helping keep me sane during quarantine and being such a sweet kid. Thanks, Stephanie, for the adventures. Thanks to Dan for always being willing to go to a garden with me. Thanks to Jane for her wit and often unsolicited advice. Miss you.

None of this would have been possible without the unwavering support from my partner, Kyle A. Robison. Words cannot express the depth of my gratitude for his patience, strength, encouragement, and care throughout this degree. Thanks for being the loudest cheerleader in my life and believing in me even when I didn't.

Lastly, I would like to thank my parents, Les McCoy and Pam Kinnen, for raising me to be the person I am today. Though I wish they were still here with me, I know they would be proud.

## TABLE OF CONTENTS

LIST OF TABLES .....	8
LIST OF FIGURES .....	9
ABSTRACT .....	11
CHAPTER 1. LITERATURE REVIEW .....	12
1.1 Preface .....	12
1.2 1,4-naphthoquinones .....	13
1.2.1 Vitamin K .....	14
1.2.2 Juglone .....	19
Mechanism/mode of action .....	20
Biosynthesis of juglone .....	20
1.3 Allelopathy and biotechnology .....	21
1.4 References .....	22
CHAPTER 2. THE ORIGIN AND BIOSYNTHESIS OF THE NAPHTHALENOID MOIETY OF JUGLONE IN BLACK WALNUT .....	27
2.1 Abstract .....	27
2.2 Introduction .....	28
2.3 Materials and Methods .....	30
2.3.1 Plant materials and general experimental procedures .....	30
2.3.2 Metabolic profiling .....	31
2.3.3 RNA extraction, library construction, and sequencing .....	31
2.3.4 Bioinformatics analysis .....	32
2.3.5 qPCR analysis .....	33
2.3.6 Stable isotope labeling of juglone by feeding <sup>13</sup> C-glutamate .....	33
2.4 Results .....	34
2.4.1 Spatial accumulation of juglone and phylloquinone in black walnut tissues .....	34
2.4.2 Transcriptome sequencing, quality control, de novo assembly, and annotation .....	36
2.4.3 Summary and GO enrichment analyses of DEGs .....	36
2.4.4 Phylloquinone pathway gene expression analysis .....	38

2.4.5	Juglone is de novo synthesized from an intermediate of the phylloquinone pathway in black walnut roots.....	40
2.5	Discussion.....	42
2.6	References .....	45
CHAPTER 3. INVESTIGATING THE SUBCELLULAR ARCHITECTURE OF THE PHYLLOQUINONE PATHWAY.....		49
3.1	Abstract.....	49
3.2	Introduction .....	50
3.3	Results .....	53
3.3.1	<i>At1g60550</i> functions as a peroxisomal DHNS .....	53
3.3.2	<i>Arabidopsis</i> AAE14 is localized to both chloroplasts and peroxisomes.....	56
3.3.3	OSB-CoA ligase activity is necessary in both chloroplasts and peroxisomes .....	58
3.4	Discussion.....	60
3.5	Materials and methods.....	64
3.5.1	Chemical reagents and general experimental procedures .....	64
3.5.2	Plant materials and growth conditions .....	64
3.5.3	Plant genotyping and quantitative expression analysis .....	64
3.5.4	Generation of <i>At1g60550-RNAi</i> lines.....	65
3.5.5	Generation of transgenic <i>Arabidopsis</i> with a single organellar OSB-CoA ligase ..	65
3.5.6	Functional complementation of <i>E. coli</i> and menaquinone analysis .....	66
3.5.7	Subcellular localization .....	67
3.5.8	Phylloquinone analysis.....	67
3.6	References .....	68
CHAPTER 4. ALLELOPATHY AS AN EVOLUTIONARILY STABLE STRATEGY .....		72
4.1	Abstract.....	72
4.2	Introduction .....	72
4.3	Model.....	74
4.3.1	Evolutionarily stable strategy definition .....	75
4.4	Results .....	76
4.4.1	Pure evolutionarily stable strategies.....	76
4.4.2	Mixed evolutionarily stable strategies.....	76

4.5	Discussion.....	78
4.6	Conclusion.....	82
4.7	References .....	82
CHAPTER 5. CONCLUSIONS AND FUTURE DIRECTIONS .....		88
5.1	Conclusion.....	88
5.2	Remaining questions .....	88
5.3	Future applications .....	90
5.4	References .....	91
APPENDIX A. SUPPLEMENTAL INFORMATION FROM MCCOY ET AL. 2018 (CHAPTER 2).....		92
APPENDIX B. SUPPLEMENTAL INFORMATION FROM CHAPTER 3 .....		98
APPENDIX C. SUPPLEMENTAL INFORMATION FROM CHAPTER 4 .....		108
PUBLICATIONS.....		111

## LIST OF TABLES

Table 1.1 Phylloquinone biosynthetic genes in <i>Arabidopsis</i> and their <i>E. coli</i> menaquinone biosynthetic homologs. Localization is indicated for the <i>Arabidopsis</i> proteins. ....	16
Table 3.1 Phenotyping results observed in progeny of heterozygous plants expressing <i>35S-EcMenE-PTS1</i> . p-value reported for a $\chi^2$ test (df=1). The null hypothesis ( $H_0 = 3:1$ ratio of green to white plants) will be rejected at a p-value $< 0.05$ . Failure to reject the null hypothesis (p-value $> 0.05$ ) indicates the progeny followed a 3:1 ratio. ....	59
Table 3.2 Genotyping results from $>20$ green plants in progeny of heterozygous plants expressing <i>35S-EcMenE-PTS1</i> . p-value reported for a $\chi^2$ test (df=2). The null hypothesis ( $H_0 = 1:2:0$ ratio) will be rejected at a p-value $< 0.05$ . ....	59
Table 3.3 Genotyping results from Basta-selected, green primary transformants of <i>AAE14/aae14</i> plants transformed with <i>35S-AAE14-plastidial</i> .....	60

## LIST OF FIGURES

Figure 1.1 Structure of selected 1,4-NQs.....	12
Figure 1.2 Redox states of 1,4-NQs.....	15
Figure 1.3 The phyloquinone biosynthetic pathway. Question markers indicate areas of uncertainty. See text for abbreviations.....	17
Figure 2.1 The proposed connection between phyloquinone and juglone biosynthesis in <i>Juglans nigra</i> (black walnut). Presented is the phyloquinone pathway as elucidated via genetic and biochemical studies in <i>Arabidopsis thaliana</i> . The product of the phyloquinone pathway is its reduced form, phyloquinol, which spontaneously re-oxidizes to phyloquinone in the presence of molecular oxygen. We hypothesize that in black walnut, the naphthalenoid moiety of juglone originates from 1,4-dihydroxynaphthoic acid (DHNA) derived from the phyloquinone pathway. Subcellular architecture is not depicted. Boxed numbers next to arrows indicate identified enzymes: 1, isochorismate synthase; 2, PHYLLLO, trifunctional 2-succinyl-5-enolpyruvyl-6-hydroxy-2-cyclohexene-2-carboxylate (SEPHCHC) synthase, 2-succinyl-6-hydroxy-2,4-cyclohexadiene-2-carboxylate (SHCHC) synthase, and <i>o</i> -succinylbenzoate (OSB) synthase; 3, OSB-CoA ligase; 4, 1,4-dihydroxy-2-naphthoyl-CoA (DHNA-CoA) synthase; 5, DHNA-CoA thioesterase; 6, DHNA phytyl transferase; 7, NAD(P)H dehydrogenase C1 (NDC1); 8, demethylphyloquinone methyltransferase. Numbers in brackets next to arrows indicate official Enzyme Commission numbers. Open block arrow indicates steps of the shikimate pathway. $\alpha$ -KG, $\alpha$ -ketoglutarate; 1,4-NQ, 1,4-naphthoquinone; L-Glu, L-Glutamate. ....	29
Figure 2.2 Pool sizes of phyloquinone and free juglone in <i>Juglans nigra</i> (black walnut) organs. (a) Phyloquinone levels. (b) Free juglone levels. All data are means $\pm$ SEM ( $n = \geq 3$ biological replicates). Different letters indicate significant differences via Analysis of Variance (ANOVA) followed by Post-hoc Tukey test ( $\alpha = 0.05$ ). ....	35
Figure 2.3 GO term enrichment in DEGs between roots and leaves of <i>Juglans nigra</i> (black walnut). Black shading in bars indicates higher expression in roots, and white shading indicates higher expression in leaves. Numbers above bars are total DEGs for each GO term.....	37
Figure 2.4 Relative expression pattern of phyloquinone pathway genes in <i>Juglans nigra</i> (black walnut) roots and leaves. (a) The phyloquinone pathway. See Figure 2.1 legend for abbreviations. (b) Expression pattern of phyloquinone pathway genes based on normalized DESeq2 counts. Log <sub>2</sub> fold-differences (FD) in roots compared to leaves are presented with negative numbers, which indicate lower mRNA accumulation in roots. Numbers in brackets are percent expression relative to ICS expression, based on normalized DESeq2 counts in the cognate organ. + indicates significant differential expression in leaves versus roots as calculated by DESeq2 ( $p < 0.001$ ). (c) Relative gene expression in roots compared to leaves set at 100% as inferred by qPCR. Data are means $\pm$ SEM ( $n = 3$ biological replicates), * $p < 0.05$ and ** $p < 0.01$ by Students <i>t</i> -test relative to leaves.....	40
Figure 2.5 Isotopic labeling of juglone from <sup>13</sup> C <sub>5</sub> <sup>15</sup> N <sub>1</sub> -L-glutamate (Glu-[ <sup>13</sup> C <sub>5</sub> <sup>15</sup> N <sub>1</sub> ]). (a) Scheme depicting labeling pattern of Glu-[ <sup>13</sup> C <sub>5</sub> <sup>15</sup> N <sub>1</sub> ] incorporated into the structure of juglone via DHNA derived from the phyloquinone pathway. (b) Time course of percent labeling of the L-glutamate	

pool in axenically grown *Juglans nigra* (black walnut) roots fed with 25 mM Glu- $^{13}\text{C}_5^{15}\text{N}_1$ . The glutamate pool was labeled by over 90% within 30 min and remained constant over the 96 hr experiment. (c) Time course of percent labeling of the free juglone pool in axenically grown black walnut roots fed with 25 mM Glu- $^{13}\text{C}_5^{15}\text{N}_1$ . Each time point represents the average percent labeling in glutamate or juglone from two independent feeding experiments..... 41

Figure 2.6 Juglone accumulates in *Juglans nigra* (black walnut) root periderm. (a) Black walnut root cross section depicting dissected sections of periderm and vascular tissue. (b) Profiling of free juglone in periderm and vascular tissue. Data are means  $\pm$  SEM ( $n = 3$  biological replicates),  $**p < 0.001$  by Students *t*-test relative to periderm. .... 44

Figure 3.1 The phylloquinone pathway is in both the chloroplast and the peroxisome. See text for abbreviations. .... 51

Figure 3.2 Subcellular localization of At1g60550 in *Nicotiana benthamiana* leaves. a.-d. Transient co-expression of GFP-alone and peroxisomal marker: a. autofluorescence of chlorophyll, b. GFP-alone, c. peroxisomal marker with mCherry, d. merged image. e.-h. Transient co-expression of At1g60550-GFP and peroxisomal marker: e. autofluorescence of chlorophyll, f. At1g60550-GFP, g. peroxisomal marker with mCherry, h. merged image. .... 54

Figure 3.3 Phylloquinone extraction from primary transformants with the *At1g60550-RNAi* construct. Error bars are standard deviation.  $n=2-3$  leaves from an individual plant. Green bars indicate lines taken to the next generation for RNA and phylloquinone profiling..... 55

Figure 3.4 Synthetic construct used to examine subcellular localization of OSB-CoA ligase (AAE14). GFP was placed in-frame in the middle of the *AAE14* cDNA. *pAAE14* is the 2.5 kb native *aae14* promoter used to drive expression. .... 56

Figure 3.5 AAE14 is localized to the chloroplast and the peroxisome under its native promoter. a.-c. Transient co-expression of AAE14-GFP and a peroxisomal marker in *Nicotiana benthamiana*: a. GFP-tagged AAE14, b. peroxisomal marker tagged with mCherry, c. merged image. d.-f. Transient expression of AAE14 in *N. benthamiana*: d. GFP-tagged AAE14, e. autofluorescence of chlorophyll, f. merged image. g.-i. Stable expression of AAE14-GFP in *Arabidopsis thaliana*: g. GFP-tagged AAE14, h. autofluorescence of chlorophyll, i. merged image. .... 57

Figure 3.6 a. Established pathway architecture for synthesis of 4-hydroxybenzoic acid in relation to ubiquinone biosynthesis. b. Proposed new model for the subcellular architecture of the phylloquinone pathway. .... 61

Figure 4.1 Symmetric pay-off matrix for competition between plants that either produce allelochemicals (+A) or not (-A). See text for parameter definitions. .... 75

Figure 4.2 Isoclines that depict ESS states in *B* and *C* phase space depending on the value of *T* (columns) or *a* (rows). The dashed line represents the isocline  $B = 2C2a - 1$ . The solid line represents the isocline  $B = 2C - T2a - 1$ . White space is the area of parameter space where production of allelochemicals (+A) is the ESS. Dark grey is where not producing allelochemicals is the ESS (-A). The space in between (light grey) is where priority effect (PE) occurs..... 77

Figure 5.1 Bioinformatics strategy to identify and prioritize candidates for functional testing of involvement in juglone biosynthesis. Genes highlighted in gray will be screened first..... 89

## ABSTRACT

Juglone is a 1,4-naphthoquinone (1,4-NQ) and the allelochemical responsible for the well-known toxic effects of black walnut (*Juglans nigra*) and other members of the Juglandaceae. Juglone affects a variety of weed species via a mode of action unlike any commercially available herbicides, and thus has the potential to be used as a new natural product-based herbicide. However, lack of knowledge about its metabolism precludes introducing juglone biosynthesis traits into resistant crops through biotechnology. Herein, we established that juglone is derived from the phylloquinone pathway at the level of the intermediate 1,4-dihydroxy-2-naphthoic acid (DHNA). Phylloquinone is a primary 1,4-NQ made by all plants for photosynthetic electron transport. Despite the fundamental importance of phylloquinone, there are still unanswered questions about the subcellular architecture of the phylloquinone pathway. In chapter 3, we show that *o*-succinylbenzoate CoA-ligase is localized to both chloroplasts and peroxisomes and that its activity is vital in both organelles. The required dual localization of CoA ligase activity is a theme common to other plant pathways with CoA metabolic steps occurring in peroxisomes and thus leads us to propose a revised model of the phylloquinone pathway. Lastly, given the potential of introducing juglone biosynthesis as part of novel weed management strategies, we investigated the circumstances, costs, and benefits of producing allelochemicals in crops using an evolutionary game theory model. Together, this work (i) shows that the phylloquinone pathway provides crops with the biosynthetic framework to produce juglone, (ii) sheds new light on the phylloquinone pathway architecture, and (iii) reveals the circumstances in which producing an allelochemical will be an evolutionarily stable strategy. We envision these results will assist biotechnological efforts to utilize juglone as a novel, natural product-based herbicide.

## CHAPTER 1. LITERATURE REVIEW

### 1.1 Preface

The toxic effects of walnuts have been known for millennia. Pliny the Elder (23-79 C.E.) remarked "the shadow of the walnut tree is poison to all plants within its compass<sup>1</sup>." In the 1920s, it was discovered that the primary compound associated with this toxicity was juglone (5-hydroxy-1,4-naphthoquinone; Figure 1.1)<sup>2</sup>. Since, it has been established that juglone is an allelochemical responsible for the toxic effects of black walnut on surrounding plants. Allelochemicals are natural products that participate in allelopathy, the phenomena in which one plant releases a toxic compound into the environment to inhibit growth and development of neighboring plants. In addition, juglone has a mode of action unlike any commercial herbicide<sup>3</sup>. Therefore, juglone has the potential to be utilized as a natural product-based herbicide, but in order to harness that potential, the biosynthesis of juglone in black walnut needs to be elucidated.

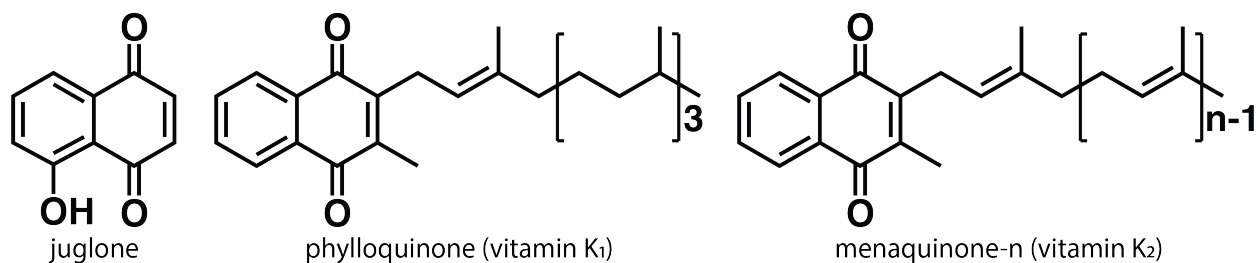


Figure 1.1 Structure of selected 1,4-NQs.

Juglone is part of a class of natural products called the 1,4-naphthoquinones (1,4-NQs). 1,4-NQs are redox-active molecules composed of a cyclic diketone fused to an aromatic ring (Figure 1.1). All plants make the 1,4-NQ phyloquinone (2-methyl-3-phytyl-1,4-naphthoquinone; vitamin K<sub>1</sub>) for use in photosynthetic electron transport<sup>4</sup>, but some plants additionally make specialized 1,4-NQs. To date, very little is known about the biosynthesis of specialized 1,4-NQs, like juglone, though it appears production of various specialized 1,4-NQs has independently evolved in diverse lineages multiple times using at least four different biosynthetic pathways<sup>4</sup>. Labeling data suggested that juglone can be derived from 1,4-dihydroxy-2-naphthoic acid (DHNA), which is also an intermediate in the phyloquinone pathway<sup>5,6</sup>, but it remains an open question whether juglone and phyloquinone metabolism share a pathway. In chapter 2, I present

evidence that established the juglone pathway branches off the phylloquinone pathway at the level of DHNA.

Further, despite the fundamental importance of phylloquinone, there are still questions about its biosynthesis. The pathway to make phylloquinone is thought to be split between the chloroplast and the peroxisome, but it is still unclear where exactly the split occurs, as an enzyme at the branchpoint is thought to be localized to both organelles. Chapter 3 explores the subcellular architecture of the phylloquinone pathway.

In chapter 2, I demonstrated that juglone and phylloquinone share a pathway, and this opens up the possibility that other 1,4-NQ-based allelochemicals are also derived from DHNA via the phylloquinone pathway. However, though the metabolic framework is there, it remains unknown what other circumstances factor into the evolution of allelochemicals. More broadly, it is unknown under what circumstances plants evolve to produce allelochemicals. The ability to make an allelochemical could convey competitive advantage but appears to have evolved relatively rarely in plants. In chapter 4, a game theoretic model was developed to probe the costs and benefits of evolving allelopathy and when allelopathy is an evolutionarily stable strategy.

## 1.2 1,4-naphthoquinones

1,4-naphthoquinones (1,4-NQs) are a diverse class of compounds synthesized by organisms in all kingdoms of life. The 1,4-NQ core structure is a cyclized diketone with carbonyl groups in the *para* position fused to an aromatic ring (Figure 1.2). This core structure can then be modified by the addition of moieties including but not limited to methyl, hydroxyl, carbonyl, and prenyl groups<sup>4</sup>. 1,4-NQs are redox active molecules in living systems, as the naphthoquinone moiety can exist as a fully oxidized quinone, a semiquinone or a reduced quinol (Figure 1.2).

Plants produce hundreds of specialized 1,4-NQs, many of which are promising targets for herbicides and therapeutics<sup>4</sup>. To make this variety of specialized 1,4-NQs, plants utilize at least four different pathways: a polyketide synthase pathway, a pathway that begins with conjugation of 4-hydroxybenzoic acid and geranyl diphosphate, one that begins with combination of homogentisate and dimethylallyl pyrophosphate, and the *o*-succinylbenzoate (OSB) pathway. In contrast to the other pathways for making specialized 1,4-NQs, the OSB pathway is present in all plants as its product, 1,4-dihydroxy-2-naphthoic acid (DHNA), is precursor to phylloquinone (vitamin K<sub>1</sub>), an essential metabolite in plants, green algae, and some cyanobacteria<sup>7</sup>.

### 1.2.1 Vitamin K

Vitamin K was first discovered in 1935 as an anti-hemorrhagic vitamin necessary in chicken diets to prevent them from developing a disorder of blood clotting<sup>8</sup>. Henrik Dam (1935) called it “vitamin K” for *koagulation*, the German and Scandinavian spelling of coagulation. He determined that, distinct from vitamins A and D, vitamin K was a fat-soluble vitamin present in some animal and plant parts<sup>8</sup>. Vitamin K<sub>1</sub> was isolated from alfalfa<sup>9</sup>, and the structure identified as phylloquinone (2-methyl-3-phytyl-1,4-naphthoquinone)<sup>10</sup> in 1939. Shortly afterwards, vitamin K<sub>2</sub> was isolated from decomposing fish meal<sup>11</sup> and identified as menaquinone<sup>12</sup>. Almquist and Stokstad (1935) deduced that while fresh fish meal was not able to prevent this dietary coagulation disorder, putrefied fish meal could and postulated that the preventative qualities of putrefied fish meal were due to microorganisms<sup>13</sup>. Indeed, menaquinone is made by many bacteria and differs from phylloquinone only in the length and degree of saturation of the prenyl side chain (Figure 1.1).

The vitamins K function as redox active molecules in living systems. The naphthoquinone moiety can exist as a fully oxidized quinone, a semiquinone, or a reduced quinol. The even more oxidized epoxide is formed by enzymatic action in animal cells<sup>14</sup>. In humans and other mammals, vitamin K is necessary for the  $\gamma$ -carboxylation of some glutamate residues in proteins that bind calcium<sup>15</sup>. Some animal proteins involved in blood coagulation have  $\gamma$ -carboxyglutamate (Gla) residues that participate in calcium ion binding and are formed in a coupled reaction to the epoxidation of vitamin K. Menaquinone is made by many bacteria and is used as an electron carrier in anaerobic respiration.

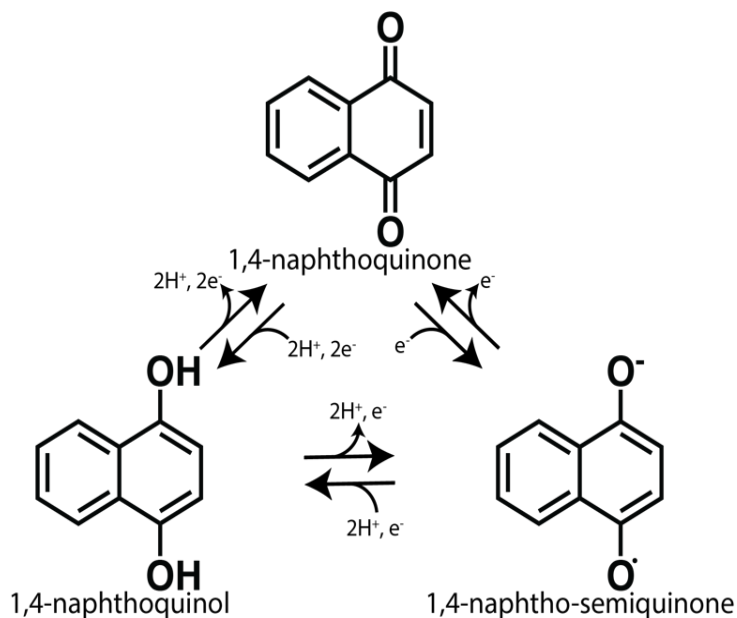


Figure 1.2 Redox states of 1,4-NQs

In photosynthetic organisms, phyloquinone was shown to be a single electron carrier at the A<sub>1</sub> site of Photosystem I (PSI). Phyloquinone at the A<sub>1</sub> site accepts an electron from the chlorophyll at the A<sub>0</sub> site and is reduced to the semiquinone before transferring its electron to the iron-sulfur clusters. More recently, phyloquinone has been implicated in formation of protein disulfide bonds in cyanobacteria<sup>16,17</sup> and plants<sup>18</sup>.

The first evidence for the metabolic origin of the naphthalenoid moiety of vitamin K came from labeling studies with shikimate done in bacteria<sup>19</sup> and *Zea mays*<sup>20</sup>, where all the carbon of shikimate was found to label the benzene ring and a carbonyl carbon of menaquinone and phyloquinone, respectively. Studies in *Impatiens balsamina* investigating the biosynthesis of the specialized 1,4-naphthoquinone lawsone determined that glutamate, through deamination to  $\alpha$ -ketoglutarate, provided the remaining 3 carbons of the naphthalenoid moiety<sup>21</sup>. *o*-succinylbenzoate (OSB) was shown to complement *E. coli* mutants incapable of making menaquinone. Indeed, <sup>14</sup>C-OSB labeled menaquinone in *E. coli*, lawsone in *Impatiens*, and juglone in *J. regia*, suggesting a similar pathway to producing these metabolites. Further studies in *E. coli* using mutants deficient in menaquinone (designated *men* for “menaquinone”) elucidated much of the remainder of the bacterial pathway to menaquinone (reviewed in<sup>22</sup>; Table 1.1).

Table 1.1 Phylloquinone biosynthetic genes in *Arabidopsis* and their *E. coli* menaquinone biosynthetic homologs. Localization is indicated for the *Arabidopsis* proteins.

Reaction	<i>E. coli</i>	<i>Arabidopsis</i>	Localization
Isochorismate synthase	MenF	ICS1 (At1g74710) ICS2 (At1g18870)	Chloroplast <sup>23</sup>
SEPHCHC synthase	MenD	PHYLLO (At1g68890)	Chloroplast <sup>24</sup>
SHCHC synthase	MenH	PHYLLO (At1g68890)	Chloroplast <sup>24</sup>
OSB synthase	MenC	PHYLLO (At1g68890)	Chloroplast <sup>24</sup>
OSB-CoA ligase	MenE	AAE14 (At1g30520)	Chloroplast <sup>25</sup> Peroxisome <sup>26</sup>
DHNA-CoA synthase	MenB	At1g60500?	Peroxisome <sup>26</sup>
DHNA-CoA thioesterase	MenI	DHNAT1 (At1g48320) DHNAT2 (At5g48950)	Peroxisome <sup>27</sup>
DHNA phytyltransferase	MenA	ABC4 (At1g60600)	Chloroplast <sup>28</sup>
Demethylphylloquinone reductase	?	NDC1 (At5g08740)	Chloroplast <sup>29</sup>
Demethylphylloquinol methyltransferase	MenG	MenG (At1g23360)	Chloroplast <sup>30</sup>

Following publication of the genome of the cyanobacteria *Synechocystis* sp. PCC 6803<sup>31</sup>, Johnson et al. saw the genome contained homologs of menA and menB. Knockouts of these genes abolished phylloquinone production and caused plastoquinone to be recruited to the A1 site of photosynthesis instead of phylloquinone<sup>32</sup>. Through homology and genetic approaches, many of the remaining biosynthetic enzymes were identified in *Synechocystis* and then plants.

The OSB pathway begins with the conversion of chorismate to isochorismate by isochorismate synthase<sup>4</sup> (ICS; Figure 1.3; Table 1.1). *Arabidopsis* has two copies of ICS: ICS1 and ICS2. ICS is also the first step in synthesizing the plant hormone salicylic acid<sup>33</sup>. For phylloquinone biosynthesis, isochorismate and  $\alpha$ -ketoglutarate are then combined to 2-succinyl-5-enolpyruvyl-6-hydroxy-3-cyclohexene-2-carboxylate (SEPHCHC) by SEPHCHC synthase. Pyruvate is removed from SEPHCHC to form 2-succinyl-6-hydroxy-2,4-cyclohexadiene-2-carboxylate (SHCHC) by SHCHC synthase, and SHCHC is aromatized to OSB by OSB synthase. In plants, these reactions are catalyzed by a trifunctional enzyme, PHYLLO, with three catalytic sites<sup>24</sup>. PHYLLO also contains a partial isochorismate synthase domain, so it appears to have been a fusion of four bacterial genes<sup>24</sup>. Interestingly, while the partial isochorismate synthase domain is conserved throughout vascular plant PHYLLO, it is non-functional, as double mutants of *ics1/ics2* are devoid of phylloquinone<sup>23</sup>.

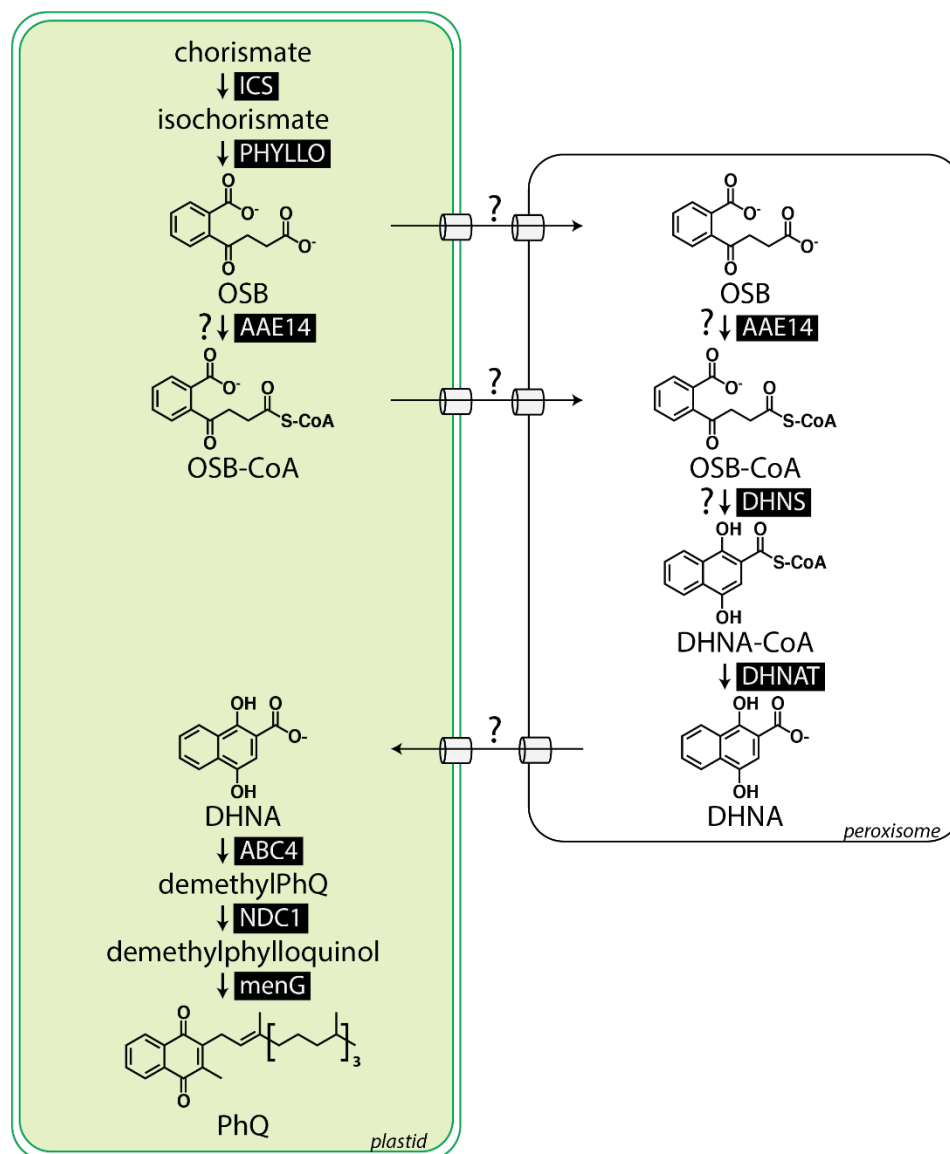


Figure 1.3 The phyloquinone biosynthetic pathway. Question markers indicate areas of uncertainty. See text for abbreviations.

OSB is then ligated to CoA by OSB-CoA ligase<sup>25</sup>, which in *Arabidopsis* is called acyl-activating enzyme 14 (AAE14). OSB-CoA is cyclized by DHNA-CoA synthase (DHNS) to produce DHNA-CoA<sup>34</sup>. No plant DHNS has been identified, but a single, close homolog of the *E. coli* enzyme exists in *Arabidopsis*<sup>25</sup> At1g60550. DHNA-CoA is hydrolyzed to DHNA by DHNA thioesterase<sup>27,35</sup> (DHNAT), providing the naphthoquinone moiety for phyloquinone and menaquinone. *Arabidopsis* contains two DHNATs: DHNAT1 and DHNAT2<sup>27</sup>. The DHNATs are relatively promiscuous and have also been implicated in benzenoid metabolism in petunia<sup>36</sup>.

For phylloquinone biosynthesis, DHNA is then phytylated by DHNA phytyl transferase<sup>28</sup>, called *aberrant chloroplast development 4* (ABC4) in *Arabidopsis*. The quinone moiety is reduced by NAD(P)H dehydrogenase C1<sup>37</sup> and methylated by demethylphylloquinone methyltransferase<sup>38</sup> to form phylloquinol, which can spontaneously oxidize to phylloquinone (Figure 1.3).

Despite phylloquinone's fundamental importance to plants, there are still unanswered questions about the metabolic architecture of the phylloquinone biosynthetic pathway. Interestingly, the phylloquinone pathway is split between plastids and peroxisomes in plants. The first two steps of the pathway, ICS<sup>23,39</sup> and PHYLLO<sup>24</sup>, are known to be localized in the chloroplast. OSB-CoA ligase is presumed to be dual-localized to the chloroplast and the peroxisome<sup>25,26</sup>. DHNA-CoA thioesterase is localized to the peroxisome<sup>27</sup>, and though DHNA-CoA synthase has not been functionally tested in plants, a single, close homolog of the *E. coli* enzyme exists in *Arabidopsis*<sup>25</sup> and is also targeted to the peroxisome<sup>26</sup>. Though the steps to make DHNA are localized to the peroxisome, the phytylation of DHNA by ABC4 occurs in the chloroplast<sup>28</sup>. From DHNA, the remainder of the pathway to phylloquinone continues in the chloroplast<sup>28,37,38</sup> (Figure 1.3), where phylloquinone participates in electron transfer reactions. This split between chloroplasts and peroxisomes implies that transporters are necessary to move intermediates of the pathway between chloroplasts and peroxisomes.

Indeed, it is unclear which intermediates are actually transported. Since AAE14 is thought to be in both organelles, OSB, OSB-CoA, or both could be transported from the chloroplast to the peroxisome. The outer membrane of the chloroplast is thought to be permeable to a wide variety of small metabolites, but the inner membrane is largely impermeable and requires transporters to move metabolites<sup>40</sup>. The peroxisomal membrane is thought to be permeable for molecules up to 300-400 Da<sup>41</sup>. OSB is 222 Da, so presumably free OSB could freely traverse the membrane, while OSB-CoA would have to be transported by a transporter.

While there are many families of transporters represented in the chloroplast envelope, the only known peroxisomal transporters in *Arabidopsis* belong to subfamily D of the ATP binding cassette (ABCD) or the mitochondrial carrier (MC) protein family<sup>42</sup>. The MC proteins mediate transport of cofactors like NAD<sup>+</sup>, ATP, and CoA, while the ABCD proteins transport substrates for  $\beta$ -oxidation of fatty acids. Knockout of the *Arabidopsis* ABCD protein, Comatose (CTS), results in accumulation of acyl-CoAs and deficiency in lipid mobilization from the seed for the growing plant<sup>43</sup>. It was later found that CTS does not recognize free fatty acids, but only acyl CoAs.

Chapter 3 explores the partitioning of the OSB pathway between chloroplasts and peroxisomes by investigating the *in planta* localization of AAE14 and providing genetic evidence for the identity of DHNS. Understanding the partitioning between the pathways will help inform what kind of transporter is involved in phylloquinone metabolism. Fuller knowledge of the architecture of the pathway will help answer why plants are partitioning the pathway between chloroplasts and peroxisomes and help inform engineering strategies to design plants with higher vitamin K content. In addition, there are specialized metabolites thought to branch off the OSB pathway (*i.e.* lawsone and juglone). Understanding the architecture of the OSB pathway will help inform where the enzymes involved in specialized quinone metabolism are localized within the plant cell.

### 1.2.2 Juglone

Beyond phylloquinone, plants make a wide array of natural products by decorating the core 1,4-NQ moiety with different groups, like hydroxyl, carboxy, and prenyl groups. One notorious example is juglone. Juglone (5-hydroxy-1,4-naphthoquinone) is produced by black walnut (*Juglans nigra*) and other members of the Juglandaceae and is used in allelopathy. The responsible metabolite, juglone, was first isolated from shells of the English walnut (*Juglans regia*) in 1856 and identified as 5-hydroxy-1,4-naphthoquinone in 1885. It was not until 1928 that Davis determined that juglone was compound responsible for the allelopathic effects of black walnut<sup>2</sup>.

Juglone is synthesized by many species in the Juglandaceae family, including black (*Juglans nigra*) and English (*Juglans regia*) walnut. Juglone secreted from the roots and/or leaching from fallen hulls, leaves, and other residue is responsible for the well-known phytotoxic effects exhibited by these trees<sup>44</sup> and likely has contributed to their ecological success. Juglone inhibits germination and represses the growth of many weed species<sup>45</sup>. Hydroponically-grown maize and soybean seedlings are sensitive to juglone<sup>46</sup>, but when grown in healthy microbially-active soil were not found to be susceptible<sup>47</sup>. In addition to being metabolized by soil microbes, juglone on the soil surface (such as that leached out of juglone-induced self-mulching cover crop residue) is subject to light degradation. Together, these factors suggest juglone has a low soil residual life<sup>47</sup>.

### ***Mechanism/mode of action***

The mechanism/mode of action of juglone is not fully understood, but there have been many studies detailing its effects in susceptible plants. Spruit and Schuiling found that some 1,4-naphthoquinones, including juglone, decreased luciferase activity in the bioluminescent *Photobacterium phosphoreurn* and hypothesized the phenomenon was due to inhibition of proton transfer<sup>48</sup>. Perry noticed that aqueous juglone decreased the oxygen uptake by leaves of both susceptible tomato (*Lycopersicon esculentum*) and tolerant bean (*Phaseolus vulgaris*) to a similar degree<sup>49</sup>. In 1972, Koeppel found that juglone decreased oxygen uptake by corn roots but increased the amount of O<sub>2</sub> taken up by purified mitochondria<sup>50</sup>. Hejl et al. saw that *Lemna minor* treated with juglone had decreased growth, chlorophyll, and photosynthesis<sup>51</sup>. In addition, oxygen production by chloroplasts from *Pisum sativum* was reduced in the presence of juglone, indicating inhibition of photosynthesis. Hejl and Koster found that juglone relates to decreased H<sup>+</sup>-ATPase activity in the plasma membrane of soybean (*Glycine max*) and corn<sup>52</sup>. Inhibition of H<sup>+</sup>-ATPase represents a mechanism of action unlike any available commercial herbicide<sup>3</sup>.

### ***Biosynthesis of juglone***

Leistner and Zenk used degradation studies of juglone extracted from *J. regia* leaves fed labeled shikimate to establish shikimate as a precursor to juglone. They determined that the benzene ring of juglone is derived from the ring of shikimate, and the carboxyl group of shikimate contributes equally to either the 1- or 4- carbon of the quinone ring. They suggested juglone synthesis from shikimate occurs through a symmetrical intermediate like 1,4-naphthoquinone, which they found is a good precursor to juglone in *J. regia* and the structurally similar lawsone (2-hydroxy-naphthoquinone) in *Impatiens balsamina*<sup>53</sup>. 1,4-naphthoquinone was detected in walnut tissue<sup>54,55</sup> and found to be labeled by *o*-succinylbenzoate<sup>5</sup>. These data, along with knowledge of the OSB pathway, led to the hypothesis that DHNA is decarboxylated to 1,4-naphthoquinone which can then be hydroxylated to juglone for juglone biosynthesis<sup>5,54</sup>. Though OSB and DHNA are intermediates in phylloquinone biosynthesis as well as juglone biosynthesis, the metabolic connection between these two pathways are currently unknown. Chapter 2 addresses the gap in knowledge of juglone biosynthesis in black walnut.

### 1.3 Allelopathy and biotechnology

Allelopathy is a term first used in 1937 to describe production of chemicals (allelochemicals) that are released into the environment that affect the growth and development of competing species<sup>56</sup>. Allelopathy has been implicated in the effectiveness of some invasive plants. One example is Paterson's Curse (*Echium plantagineum* L.), an invasive species affecting large parts of Australia, whose invasion success has been partially attributed to the 1,4-NQ allelochemical shikonin<sup>57</sup>. Allelopathy can be thought of as a plant producing and deploying its own herbicide. Recently, there has been interest in utilizing allelopathic cultivars of crops, including sorghum and rye, as a weed-management strategy less dependent on application of herbicides<sup>58</sup>. Other interest lies in engineering production of an allelochemical in a previously non-allelopathic plant<sup>59</sup>. Finally, allelochemicals, like juglone, have the potential to be utilized as novel, natural product-based herbicides<sup>60</sup>.

New herbicides with novel modes of action are necessary to combat growing resistance to current herbicides. At least 262 weeds have developed resistance to current herbicides<sup>61</sup>. Plant natural products are presently underutilized in this field<sup>3</sup>, including allelochemicals. Juglone is an excellent candidate for a novel, natural product-based herbicide<sup>3</sup>, because it suppresses the growth of many weed species<sup>45</sup> and has a novel mechanism of action<sup>3</sup>. In addition to outstanding questions about the metabolism of juglone, it is not understood what the costs and benefits of introducing synthesis of an allelochemical into crops for weed suppression applications are. This lack of understanding precludes identifying states in which the crop can suppress weeds but not escape and become an invasive species itself.

Production of a novel compound will divert carbon from growth and development, imposing a new cost on the plant, though further work is needed to investigate whether production of an allelochemical imposes a substantial cost. Another concern for engineering production of allelochemicals into crops is whether the engineered species will be able to persist in the environment. If engineered, allelopathic crops are worse competitors than surrounding plants, it could help prevent escape and invasiveness. On the other hand, if the crop is too poor a competitor, it is possible weed species will outcompete it in the field. Therefore, it is important to investigate the circumstances that allow allelopathy to evolve and persist in a population. Chapter 4 addresses this gap in knowledge by describing a game theoretic model of the evolution of allelopathy.

## 1.4 References

1. Rietveld, W. J. Allelopathic effects of juglone on germination and growth of several herbaceous and woody species. *J. Chem. Ecol.* **9**, 295–308 (1983).
2. Davis, E. F. The toxic principle of *Juglans nigra* as identified with synthetic juglone, and its toxic effects on tomato and alfalfa plants. *Am. J. Bot.* **15**, 620 (1928).
3. Dayan, F. E. & Duke, S. O. Natural compounds as next-generation herbicides. *Plant Physiol* **166**, 1090–1105 (2014).
4. Widhalm, J. R. & Rhodes, D. Biosynthesis and molecular actions of specialized 1,4-naphthoquinone natural products produced by horticultural plants. *Hortic. Res.* **3**, 16046 (2016).
5. Chung, D., Maier, U. H., Inouye, H. & Zenk, M. H. Different mode of incorporation of o-succinylbenzoic acid into the naphthoquinones juglone and lawsone in higher plants. *Zeitschrift für Naturforsch. C.* **49**, 885–887 (1994).
6. Müller, W. & Leistner, E. 1,4-Naphthoquinone, an intermediate in juglone (5-hydroxy-1,4-naphthoquinone) biosynthesis. *Phytochemistry* **15**, 407–410 (1976).
7. Basset, G. J., Latimer, S., Fatihi, A., Soubeyrand, E. & Block, A. Phylloquinone (Vitamin K<sub>1</sub>): Occurrence, Biosynthesis and Functions. *Mini-reviews in Medicinal Chemistry* **17**, 1028-1038 (2017). doi:10.2174/1389557516666160623082714
8. Dam, H. The Antihæmorrhagic Vitamin of the Chick. *Biochem. J.* **29**, 1273–1285 (1935).
9. Binkley, S. B., MacCorquodale, D. W., Thayer, S. A. & Doisy, E. A. Isolation of vitamin K<sub>1</sub>. *J. Biol. Chem.* **130**, 219-234 (1939).
10. MacCorquodale, D. W., Binkley, S. B., Thayer, S. A. & Doisy, E. A. On the constitution of vitamin K<sub>1</sub>. *J. Am. Chem. Soc.* **61**, 1928–1929 (1939).
11. McKee, R. W., Binkley, S. B., Thayer, S. A., MacCorquodale, D. W. & Doisy, E. A. Isolation of vitamin K<sub>2</sub>. *J. Biol. Chem.* **131**, 327–344 (1935).
12. Binkley, S. B., McKee, R. W., Thayer, S. A. & Doisy, E. A. Constitution of vitamin K<sub>2</sub>. *J. Am. Chem. Soc.* **61**, 1295 (1939).
13. Almquist, H. J. & Stokstad, E. L. R. Dietary hæmorrhagic disease in chicks. *Nature* **136**, 31 (1935).

14. Matschiner, J. T., Bell, R. G., Amelotti, J. M. & Knauer, T. E. Isolation and characterization of a new metabolite of phylloquinone in the rat. *Biochim. Biophys. Acta* **201**, 309–315 (1970).
15. Furie, B., Bouchard, B. A. & Furie, B. C. Vitamin K-dependent biosynthesis of  $\gamma$ -carboxyglutamic acid. *Blood* **93**, 1798–1808 (1999).
16. Li, W. *et al.* Structure of a bacterial homologue of vitamin K epoxide reductase. *Nature* **463**, 507–512 (2010).
17. Singh, A. K., Bhattacharyya-Pakrasi, M. & Pakrasi, H. B. Identification of an atypical membrane protein involved in the formation of protein disulfide bonds in oxygenic photosynthetic organisms. *J. Biol. Chem.* **283**, 15762–15770 (2008).
18. Furt, F. *et al.* A bimodular oxidoreductase mediates the specific reduction of phylloquinone (vitamin K<sub>1</sub>) in chloroplasts. *Plant J.* **64**, 38–46 (2010).
19. Cox, G. B. & Gibson, F. Biosynthesis of vitamin K and ubiquinone: relation to the shikimic acid pathway in *Escherichia coli*. *Biochim. Biophys. Acta* **93**, 204–206 (1964).
20. Whistance, G. R., Threlfall, D. R. & Goodwin, T. W. Incorporation of [G-<sup>14</sup>C]shikimate and [U-<sup>14</sup>C]para-hydroxybenzoate into phytoquinones and chromanols. *Biochem. Biophys. Res. Commun.* **23**, 849–853 (1966).
21. Campbell, I. M. The roles of alanine, aspartate and glutamate in lawsone biosynthesis in *Impatiens balsamina*. *Tetrahedron Lett.* 4777–4780 (1969).
22. Meganathan, R. & Kwon, O. Biosynthesis of the isoprenoid quinones menaquinone (vitamin K<sub>2</sub>) and ubiquinone (coenzyme Q). *EcoSal Plus* **3**, 1–37 (2009).
23. Garcion, C. *et al.* Characterization and biological function of the ISOCHORISMATE SYNTHASE2 gene of Arabidopsis. *Plant Physiol.* **147**, 1279–1287 (2008).
24. Gross, J. *et al.* A plant locus essential for phylloquinone (vitamin K<sub>1</sub>) biosynthesis originated from a fusion of four eubacterial genes. *J. Biol. Chem.* **281**, 17189–17196 (2006).
25. Kim, H. U., Oostende, C. Van, Basset, G. J. C. & Browse, J. The AAE14 gene encodes the Arabidopsis *o*-succinylbenzoyl-CoA ligase that is essential for phylloquinone synthesis and photosystem-I function. *Plant J.* **54**, 272–283 (2008).
26. Babujee, L. *et al.* The proteome map of spinach leaf peroxisomes indicates partial compartmentalization of phylloquinone (vitamin K<sub>1</sub>) biosynthesis in plant peroxisomes. *J. Exp. Bot.* **61**, 1441–1453 (2010).

27. Widhalm *et al.* Phylloquinone (vitamin K<sub>1</sub>) biosynthesis in plants: two peroxisomal thioesterases of lactobacillales origin hydrolyze 1,4-dihydroxy-2-naphthoyl-CoA. *Plant J.* **71**, 205–215 (2012).
28. Shimada, H. *et al.* Inactivation and deficiency of core proteins of photosystems I and II caused by genetical phylloquinone and plastoquinone deficiency but retained lamellar structure in a T-DNA mutant of Arabidopsis. *Plant J.* **41**, 627–637 (2005).
29. Piller, L. E. *et al.* Chloroplast lipid droplet type II NAD(P)H quinone oxidoreductase is essential for prenylquinone metabolism and vitamin K<sub>1</sub> accumulation. *Proc. Natl. Acad. Sci. U. S. A.* **108**, 14354–14359 (2011).
30. Lohmann, A. *et al.* Deficiency in phylloquinone (vitamin K<sub>1</sub>) methylation affects prenyl quinone distribution, photosystem I abundance, and anthocyanin accumulation in the *Arabidopsis AtmenG* mutant. *J. Biol. Chem.* **281**, 40461–40472 (2006).
31. Kaneko, T. *et al.* Sequence analysis of the genome of the unicellular cyanobacterium *Synechocystis* sp. strain PCC6803. II. Sequence determination of the entire genome and assignment of potential protein-coding regions (supplement). *DNA Res.* **3**, 185–209 (1996).
32. Johnson, T. W. *et al.* Recruitment of a foreign quinone into the A<sub>1</sub> site of Photosystem I. I. Genetic and physiological characterization of phylloquinone biosynthetic pathway mutants in *Synechocystis* sp. PCC 6803. *J. Biol. Chem.* **275**, 8523–8530 (2000).
33. Torrens-Spence, M. P. *et al.* PBS3 and EPS1 complete salicylic acid biosynthesis from isochorismate in Arabidopsis. *Mol. Plant* **12**, 1577–1586 (2019).
34. Sharma, V., Meganathan, R. & Hudspeth, M. E. Menaquinone (vitamin K<sub>2</sub>) biosynthesis: cloning, nucleotide sequence, and expression of the menC gene from *Escherichia coli*. *J. Bacteriol.* **175**, 4917–21 (1993).
35. Widhalm, J. R., van Oostende, C., Furt, F. & Basset, G. J. C. A dedicated thioesterase of the Hotdog-fold family is required for the biosynthesis of the naphthoquinone ring of vitamin K<sub>1</sub>. *Proc. Natl. Acad. Sci.* **106**, 5599–5603 (2009).
36. Adebisin, F., Widhalm, J. R., Lynch, J. H., McCoy, R. M. & Dudareva, N. A peroxisomal thioesterase plays auxiliary roles in plant  $\beta$ -oxidative benzoic acid metabolism. *Plant J.* **93**, (2018).

37. Fatihi, A. *et al.* A dedicated type II NADPH dehydrogenase performs the penultimate step in the biosynthesis of vitamin K<sub>1</sub> in *Synechocystis* and *Arabidopsis*. **27**, 1730–1741 (2015).
38. Lohmann, A. *et al.* Deficiency in phyloquinone (vitamin K<sub>1</sub>) methylation affects prenyl quinone distribution, Photosystem I abundance, and anthocyanin accumulation in the *Arabidopsis AtmenG* Mutant. *J. Biol. Chem.* **281**, 40461–40472 (2006).
39. Strawn, M. A. *et al.* *Arabidopsis* isochorismate synthase functional in pathogen-induced salicylate biosynthesis exhibits properties consistent with a role in diverse stress responses. *J. Biol. Chem.* **282**, 5919–5933 (2007).
40. Heldt, H. W. & Sauer, F. The inner membrane of the chloroplast envelope as the site of specific metabolite transport. *BBA - Bioenerg.* **234**, 83–91 (1971).
41. Antonenkov, V. D. & Hiltunen, J. K. Transfer of metabolites across the peroxisomal membrane. *Biochim. Biophys. Acta - Mol. Basis Dis.* **1822**, 1374–1386 (2012).
42. Linka, N. & Esser, C. Transport proteins regulate the flux of metabolites and cofactors across the membrane of plant peroxisomes. *Front. Plant Sci.* **3**, 1–13 (2012).
43. Footitt, S. *et al.* Control of germination and lipid mobilization by COMATOSE, the *Arabidopsis* homologue of human ALDP. *EMBO J.* **21**, 2912–2922 (2002).
44. Dana, M. & Lerner, B. Black walnut toxicity. *Purdue Univ. Coop. Ext. Serv.* **HO-193-W**, 2 (2001).
45. Dayan, F. E. & Duke, S. O. Biological activity of allelochemicals. in *Plant-derived Natural Products* 361–384 (Springer US, 2009). doi:10.1007/978-0-387-85498-4\_17
46. Jose, S. & Gillespie, A. R. Allelopathy in black walnut (*Juglans nigra* L.) alley cropping. II. Effects of juglone on hydroponically grown corn (*Zea mays* L.) and soybean (*Glycine max* L. Merr.) growth and physiology. *Plant Soil* **203**, 199–205 (1998).
47. von Kiparski, G. R., Lee, L. S. & Gillespie, A. R. Occurrence and fate of the phytotoxin juglone in alley soils under black walnut trees. *J. Environ. Qual.* **36**, 709–717 (2007).
48. Spruit, C. J. P. & Schuiling, A. L. On the influence of naphthoquinones on the respiration and light emission of photobacterium phosphoreum. *Recl. des Trav. Chim. des Pays-Bas* **64**, 219–228 (1945).
49. Perry, S. F. Inhibition of Respiration by Juglone in Phaseolus and Lycopersicon. *Bull. Torrey Bot. Club* **94**, 26–30 (1967).

50. Koeppe, D. E. Some Reactions of Isolated Corn Mitochondria Influenced by Juglone. *Physiol. Plant.* **27**, 89–94 (1972).
51. Hejl, A. A. M., Einhellig, F. A. & Rasmussen, J. A. Effects of juglone on growth, photosynthesis, and respiration. *J. Chem. Ecol.* **19**, 559–568 (1993).
52. Hejl, A. M. & Koster, K. L. Juglone disrupts root plasma membrane H<sup>+</sup>-ATPase activity and impairs water uptake, root respiration, and growth in soybean (*Glycine max*) and corn (*Zea mays*). *J. Chem. Ecol.* **30**, 453–471 (2004).
53. Leistner, E. & Zenk, M. H. Zur Biogenese von 5-Hydroxy-1,4-naphthochinon (Juglon) in *Juglans regia* L. *Z. Naturforsch.* **23**, 259–268 (1968).
54. Müller, W. U. & Leistner, E. 1,4-Naphthoquinone, an intermediate in juglone (5-hydroxy-1,4-naphthoquinone) biosynthesis. *Phytochemistry* **15**, 407–410 (1976).
55. Müller, W. U. & Leistner, E. Aglycones and glycosides of oxygenated naphthalenes and a glycosyltransferase from *Juglans*. *Phytochemistry* **17**, 1739–1742 (1978).
56. Latif, S., Chiapusio, G. & Weston, L. A. *Allelopathy and the Role of Allelochemicals in Plant Defence. Advances in Botanical Research* **82**, (Elsevier Ltd, 2017).
57. Zhu, X. *et al.* Identification and localization of bioactive naphthoquinones in the roots and rhizosphere of Paterson’s curse (*Echium plantagineum*), a noxious invader. *J. Exp. Bot.* **67**, 3777–3788 (2016).
58. Heap, I. Global perspective of herbicide-resistant weeds. *Pest Manag. Sci.* **70**, 1306–1315 (2014).
59. Duke, Dayan, Romagni & Rimando. Natural products as sources of herbicides: current status and future trends. *Weed Res.* **40**, 99–111 (2000).
60. Jabran, K., Mahajan, G., Sardana, V. & Chauhan, B. S. Allelopathy for weed control in agricultural systems. *Crop Prot.* **72**, 57–65 (2015).
61. Heap I. The international survey of herbicide resistant weeds. <http://www.weedscience.org> [accessed Febr. 2020] (2020).

## CHAPTER 2. THE ORIGIN AND BIOSYNTHESIS OF THE NAPHTHALENOID MOIETY OF JUGLONE IN BLACK WALNUT

This chapter is published in full in *Horticulture Research*, Vol. 5, article number 67 (2018).  
DOI: 10.1038/s41438-018-0067-5.

Rachel M McCoy<sup>1,2</sup>, Sagar M Utturkar<sup>3</sup>, Joseph W Crook<sup>1,2</sup>, Jyothi Thimmapuram<sup>3</sup> and Joshua R Widhalm<sup>1,2</sup>

<sup>1</sup>Department of Horticulture and Landscape Architecture, Purdue University, 625 Agriculture Mall Drive., West Lafayette, IN 47907, USA

<sup>2</sup>Purdue Center for Plant Biology, Purdue University, West Lafayette, IN 47907, USA

<sup>3</sup>Bioinformatics Core, Purdue University, 155 South Grant Street, West Lafayette, IN 47907, USA

### 2.1 Abstract

Several members of the Juglandaceae family produce juglone, a specialized 1,4-naphthoquinone (1,4-NQ) natural product that is responsible for the notorious allelopathic effects of black walnut (*Juglans nigra*). Despite its documented ecological roles and potential for being developed as a novel natural product-based herbicide, none of the genes involved in synthesizing juglone have been identified. Based on classical labeling studies, we hypothesized that biosynthesis of juglone's naphthalenoid moiety is shared with biochemical steps of the phylloquinone pathway. Here, using comparative transcriptomics in combination with targeted metabolic profiling of 1,4-NQs in various black walnut organs, we provide evidence that phylloquinone pathway genes involved in 1,4-dihydroxynaphthoic acid (DHNA) formation are expressed in roots for synthesis of a compound other than phylloquinone. Feeding experiments using axenic black walnut root cultures revealed that stable isotopically-labeled L-glutamate incorporates into juglone resulting in the same mass shift as that expected for labeling of the quinone ring in phylloquinone. Taken together, these results indicate that *in planta*, an intermediate from the phylloquinone pathway provides the naphthalenoid moiety of juglone. Moreover, this work shows that juglone can be *de novo* synthesized in roots without the contribution of immediate precursors translocated from aerial tissues. The present study illuminates all genes involved in synthesizing the juglone naphthoquinone ring and provides RNA-sequencing datasets that can be used with functional screening studies to elucidate the remaining juglone pathway genes. Translation of the generated

knowledge is expected to inform future metabolic engineering strategies for harnessing juglone as a novel natural product-based herbicide.

## 2.2 Introduction

The allelopathic effects of black walnut (*Juglans nigra*) on numerous types of plants growing within the span of its canopy and root system have been reported since antiquity<sup>1</sup> and remain a concern of backyard growers today<sup>2</sup>. It is now established that the natural product juglone (5-hydroxy-1,4-naphthoquinone; Figure 2.1), released into the soil through decaying litterfall, root contact, or rain leaching from its drip line, is responsible for the detrimental effects elicited by black walnut on other species. Juglone is also produced in significantly lower quantities by several other members of the Juglandaceae family, including English or Persian walnut (*J. regia*), Japanese walnut (*J. sieboldiana*), butternut (*J. cinerea*), pecan (*Carya illinoensis*), and hickory (*Carya ovata*)<sup>3</sup>. Classically, the effects of juglone toxicity on susceptible species have been characterized as leaf wilting and yellowing eventually resulting in death<sup>4</sup>, but recently juglone was also found to damage roots through induction of reactive oxygen and nitrogen species, as well as through calcium accumulation<sup>5,6</sup>. Though many plants are susceptible to juglone, some commonly grown garden vegetables (*e.g.* squash), fruits (*e.g.* cherry), landscape plants (*e.g.* crabapple), flowers (*e.g.* tulip), and grasses (*e.g.* Kentucky bluegrass) are reportedly tolerant<sup>2</sup>. Together with the fact that juglone inhibits the growth of several common weed species<sup>7</sup>, this raises the prospect of developing juglone as a novel natural product-based herbicide. However, the absence of knowledge about the genes involved in synthesizing juglone precludes designing strategies to metabolically engineer juglone production in economically important crops or in large-scale biological platforms.

Juglone belongs to a class of redox active compounds called the 1,4-naphthoquinones (1,4-NQs). The 1,4-NQs structurally consist of a benzene ring that is linearly fused with a fully conjugated cyclic diketone bearing carbonyl groups arranged in the *para* orientation<sup>8</sup>. All plants synthesize phylloquinone (vitamin K<sub>1</sub>; Figure 2.1), a methylated and phytyl-conjugated 1,4-NQ serving as a one-electron carrier at the A1 site of photosystem I (PSI)<sup>9</sup>. The phylloquinone pathway (Figure 2.1) consists of ten enzymatic reactions starting from chorismate, the final product of the shikimate pathway<sup>10</sup>. Chorismate is isomerized to isochorismate by isochorismate synthase (ICS), an enzyme shared with salicylic acid biosynthesis<sup>11,12</sup>. Next,  $\alpha$ -ketoglutarate is decarboxylated to

form a succinic semialdehyde, which is condensed with isochorismate and the resulting intermediate is converted to *o*-succinylbenzoic acid (OSB) by a trifunctional enzyme called PHYLLLO<sup>11</sup>. The succinyl side chain of OSB is then activated by an OSB-CoA ligase<sup>13</sup> and cyclized by naphthoate synthase to form 1,4-dihydroxy-2-naphthoyl-CoA (DHNA-CoA), which is hydrolyzed to 1,4-dihydroxynaphthoic acid (DHNA) by DHNA-CoA thioesterase<sup>14</sup>. Through a sequential series of phytylation<sup>15</sup>, reduction<sup>16</sup>, and methylation<sup>17</sup> reactions, DHNA is finally converted to phylloquinone (Figure 2.1)<sup>18</sup>.

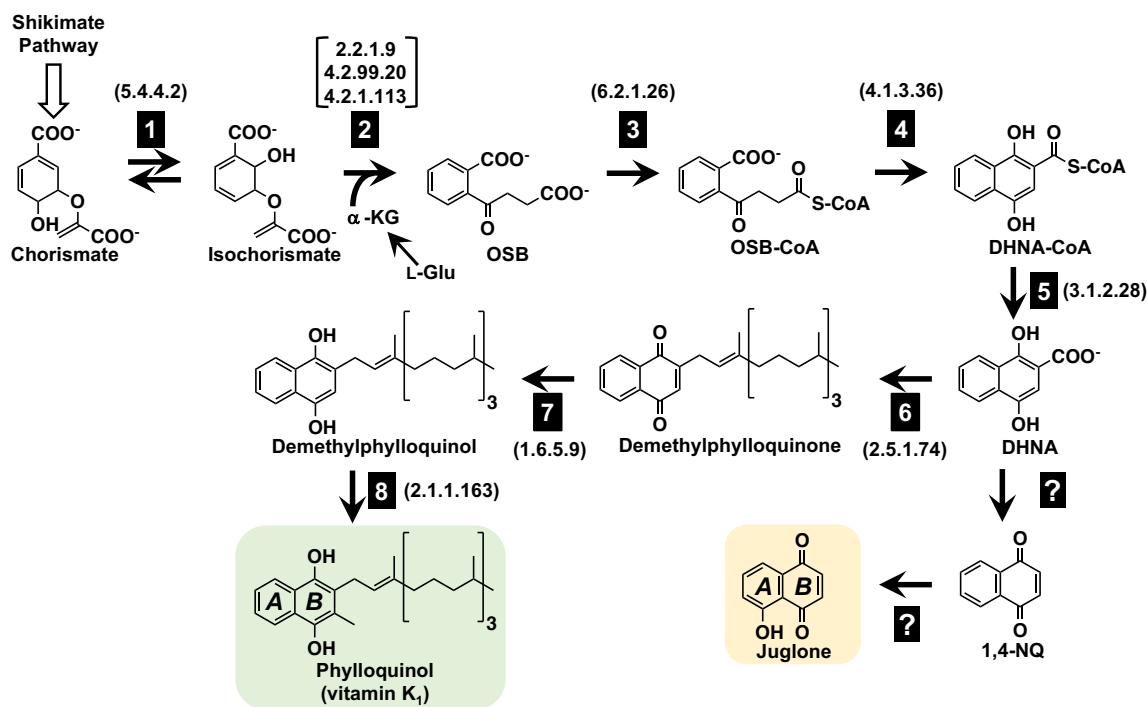


Figure 2.1 The proposed connection between phylloquinone and juglone biosynthesis in *Juglans nigra* (black walnut). Presented is the phylloquinone pathway as elucidated via genetic and biochemical studies in *Arabidopsis thaliana*. The product of the phylloquinone pathway is its reduced form, phylloquinol, which spontaneously re-oxidizes to phylloquinone in the presence of molecular oxygen. We hypothesize that in black walnut, the naphthalenoid moiety of juglone originates from 1,4-dihydroxynaphthoic acid (DHNA) derived from the phylloquinone pathway. Subcellular architecture is not depicted. Boxed numbers next to arrows indicate identified enzymes: 1, isochorismate synthase; 2, PHYLLLO, trifunctional 2-succinyl-5-enolpyruvyl-6-hydroxy-2-cyclohexene-2-carboxylate (SEPHCHC) synthase, 2-succinyl-6-hydroxy-2,4-cyclohexadiene-2-carboxylate (SHCHC) synthase, and *o*-succinylbenzoate (OSB) synthase; 3, OSB-CoA ligase; 4, 1,4-dihydroxy-2-naphthoyl-CoA (DHNA-CoA) synthase; 5, DHNA-CoA thioesterase; 6, DHNA phytyl transferase; 7, NAD(P)H dehydrogenase C1 (NDC1); 8, demethylphyloquinone methyltransferase. Numbers in brackets next to arrows indicate official Enzyme Commission numbers. Open block arrow indicates steps of the shikimate pathway.  $\alpha$ -KG,  $\alpha$ -ketoglutarate; 1,4-NQ, 1,4-naphthoquinone; L-Glu, L-Glutamate.

Early radiotracer studies using English walnut leaves revealed that the benzene ring (ring *A*, Figure 2.1) of juglone is derived from shikimate<sup>19</sup>. Labeling experiments later showed that OSB<sup>20</sup> and DHNA<sup>21</sup> can be incorporated into juglone, suggesting that juglone's quinone ring (ring *B*, Figure 2.1) originates from L-glutamate via  $\alpha$ -ketoglutarate and leading us to hypothesize that juglone biosynthesis branches off the phylloquinone pathway (Figure 2.1). To investigate if the juglone and phylloquinone pathways share common biosynthetic genes to synthesize their naphthalenoid moieties, we used targeted metabolic profiling and comparative RNA sequencing (RNA-seq) to examine the co-occurrence between 1,4-NQ natural product pools and expression of phylloquinone pathway genes in organs of black walnut, the species producing the highest known levels of juglone<sup>3</sup>. We then tested if stable isotopically-labeled glutamate fed to axenic black walnut root cultures is incorporated into juglone with the same mass shift as that expected if juglone is derived from an intermediate of the phylloquinone pathway. The obtained results and generated transcriptomes are expected to serve as useful resources for future studies aimed at elucidating the remainder of the juglone pathway and for uncovering genes involved in its transport and sequestration. These advances in basic knowledge will inform the development of biotechnological approaches for harnessing juglone as a novel natural product-based herbicide.

## **2.3 Materials and Methods**

### **2.3.1 Plant materials and general experimental procedures**

Tissues used in this study were collected from one-year old (leaves, stems, bark, and roots) and mature elite (flowers and hulls) black walnut trees located at Martell Forest (West Lafayette, IN, United States). Naphthoquinone standards of juglone, phylloquinone, menaquinone-4 (MK-4), and plumbagin were from Sigma-Aldrich. Unless otherwise mentioned, all other reagents were from Fisher Scientific. Ultrapure water and high-performance liquid chromatographic (HPLC)- or gas chromatographic (GC)-grade solvents were used for all metabolite extractions. HPLC analyses were carried out on an Agilent 1260 Infinity series instrument (Agilent Technologies) equipped with diode array and fluorometer detection modules employing Chemstation software. An Agilent 7890B GC coupled with a 5977A mass spectrometer (MS) employing Chemstation software was used to perform GC-MS analyses.

### 2.3.2 Metabolic profiling

All steps were conducted in dimmed light to limit photodegradation of naphthoquinones. Approximately 500 mg of flash-frozen ground black walnut organs (young bark, female flowers, pollinated female flowers, male flowers, leaves, roots, and one-year old stems with the bark removed) were extracted in 10 mL methanol containing internal standards (1.8 nmol MK-4 and 200 nmol plumbagin) overnight with moderate shaking. To quantify juglone, 1 mL of the methanolic extract was filtered using a 0.2  $\mu\text{m}$  PTFE syringe filter and 10  $\mu\text{L}$  directly analyzed by HPLC on a Zorbax SB-C18 column (4.6 x 250 mm, Agilent) thermostated at 40°C and eluted in gradient mode at 0.75 mL·min<sup>-1</sup>. The gradient started at 80% A (50 mM sodium acetate in water, pH 5.9) and 20% B (100% methanol) and linearly increased to 45% B over 4 minutes. From 4-17 minutes, the %B linearly increased from 45 to 80%. From 17-20 minutes, the %B linearly increased to 100%, and then returned to 20% B from 20-23 minutes. Finally, the column was washed in 20% B for 3 minutes. Juglone (15.7 minutes) and plumbagin (20.1 minutes) were detected fluorometrically (at 230 nm excitation, 372 nm emission) after reduction in a post-column chemical reactor (1.5 x 70 mm) packed with – 100 mesh zinc (Sigma-Aldrich). Juglone and plumbagin were quantified relative to external calibration standards, and juglone content was corrected according to the recovery of the plumbagin internal standard.

To quantify phylloquinone, 3 mL of the methanolic extract was transferred to a pyrex tube, evaporated to near dryness under gaseous N<sub>2</sub>, resuspended in 2 mL 50% methanol, and partitioned twice with 3 mL hexanes. Upper phases from each partitioning were combined, transferred to new pyrex tubes, dried under gaseous N<sub>2</sub>, resuspended in 1 mL methanol, and 50  $\mu\text{L}$  analyzed by HPLC-fluorescence as described previously<sup>14</sup>.

### 2.3.3 RNA extraction, library construction, and sequencing

For RNA-seq experiments, RNA was extracted from roots and mature leaves of one-year old black walnut trees using the protocol described in Kolosova et al. (2004)<sup>22</sup> except that partitioning was done with phenol/chloroform/isoamyl alcohol (25:24:1 v/v/v). Samples were DNase-treated (NEB) according to manufacturer instructions. A total of six cDNA libraries from three biological replicates, each replicate containing RNA pooled from two unique trees, of *J. nigra* roots and leaves were constructed using an mRNA-seq Kit (Illumina, San Diego, CA), and

101-bp paired-end reads were generated via Illumina HiSeq2500 at the Purdue Genomics Center, with at least 67 million reads per library. Sequence quality was assessed by FastQC (v. 0.10.0; <http://www.bioinformatics.babraham.ac.uk>). The raw data were submitted to the SRA (Sequence Read Archive) (<http://www.ncbi.nlm.nih.gov/sra/>) and are available under the accession number SRP133522.

### 2.3.4 Bioinformatics analysis

Quality based trimming of raw sequence data was performed using FASTX toolkit (version 0.0.14; [http://hannonlab.cshl.edu/fastx\\_toolkit/](http://hannonlab.cshl.edu/fastx_toolkit/)) and reads  $\geq 50$  bp and bases with quality value  $\geq 30$  were retained. Reads mapping to complete chloroplast or mitochondrial genomes of closely related species *J. regia* and *Liriodendron tulipifera* were removed. The overall mapping rate of the six replicates against the *J. regia* genome<sup>23</sup> was in the range of 57-64%, while the rate against transcriptome from *de novo* assembly of clean reads performed using the Trinity<sup>24</sup> (version 2.2.0) transcriptome assembler was 76-85%. Therefore, to include more reads in the analysis, the *de novo* assembly results were used. Redundant transcripts were removed by clustering through CD-HIT tool<sup>25</sup> (version 4.6.5) with default parameter and at least 90% alignment coverage. After clustering, transcripts shorter than 500 bp were excluded from the assembly. These non-redundant transcripts were used for annotation using blastx against the NCBI-NR, *Arabidopsis thaliana* and *J. regia* protein databases.

Clean reads were mapped back to the non-redundant transcripts from the *de novo* assembly and transcript abundance at gene level was estimated using the RSEM package (version 1.2.30)<sup>26</sup> with default parameters. RSEM determines a normalized measure of transcript expression and estimates read counts associated with each gene feature. Counts matrix generated by RSEM was used as input for EBSeq<sup>27</sup> and DESeq2<sup>28</sup> methods to determine Differentially Expressed Genes (DEGs). A false discovery rate (FDR) of 0.05 was selected as cutoff to identify significantly differentially expressed genes.

Gene Ontology (GO) and Kyoto Encyclopedia of Genes and Genomes (KEGG) terms associated with each gene were determined from the *J. regia* and *Arabidopsis* blast hit descriptions, respectively. GO and KEGG enrichment analysis was performed using the Bioconductor package clusterProfiler<sup>29</sup> and terms with adjusted *p-values* of  $\leq 0.05$  were defined as significantly enriched.

### 2.3.5 qPCR analysis

qPCR was used to validate the expression patterns found for the phylloquinone genes in black walnut. Primers were designed using PrimerExpress (ThermoFisher). qPCR reactions were performed using a StepOnePlus (ThermoFisher) in a 20  $\mu$ L reaction as follows: 10  $\mu$ L of 5x Fast SYBR Green PCR master mix (ThermoFisher), 2  $\mu$ L each of the forward and reverse primers (50-900 nM final concentration, Table A.1), 4  $\mu$ L of cDNA diluted from RNA-seq libraries, and 2  $\mu$ L of water. Expression was normalized to the *J. nigra* ubiquitin carrier protein (JnUBC).

### 2.3.6 Stable isotope labeling of juglone by feeding $^{13}\text{C}$ -glutamate

Young, non-woody roots collected from one-year old black walnut trees were excised, rinsed, and cut into 1 cm sections. Roots were sterilized by pre-treatment in 10 mL Murashige and Skoog (MS) containing 5% (v/v) PPM<sup>TM</sup> (Plant Cell Technology) for 1 h. Approximately 150-250 mg of sterilized roots were transferred into 10 mL of half-strength MS media (pH 5.7) containing 3% sucrose, 0.1% PPM, and 25 mM glutamate- $^{13}\text{C}_5^{15}\text{N}_1$  (Cambridge Isotopes). Roots were incubated in darkness at 28°C with moderate shaking (80 rpm). Root tissue and media were separately collected after 1, 6, 12, 24, 48, and 96 h and flash-frozen until analysis by HPLC-FLD and GC-MS. Fed roots were extracted with 10 mL methanol, spiked with 125 nmol  $\alpha$ -aminoadipate and 200 nmol plumbagin internal standards, and incubated overnight at 4°C in the dark. To measure juglone pool sizes, 500  $\mu$ L of the methanolic extract was filtered using a 0.2  $\mu$ m PTFE syringe filter and 10  $\mu$ L was analyzed by HPLC-fluorescence as described above. Isotopic abundance of juglone was measured by directly analyzing 1  $\mu$ L by GC-MS and an Agilent 19091S-433 HP-5MS capillary column (30 m x 0.25 mm; film thickness 0.25  $\mu$ m). 1  $\mu$ L was injected in split mode with a 1:50 split ratio. Injector temperature was 260°C. Column temperature was initially held at 35°C for 3 minutes and then heated 8°C min<sup>-1</sup> to a final temperature of 260°C, where it was held for 1 minute. Helium was used as the carrier gas at a flow rate of 0.8 mL min<sup>-1</sup>. Electron ionization was set to 70 eV. Mass spectrum were obtained in scanning mode from 40 to 400 atomic mass units. Juglone was identified by comparing retention time and mass spectra to an authentic standard.

To determine pool sizes and analyze isotopic abundances of glutamate the remaining 9.5 mL of the original methanolic extract was partitioned with 6 mL water and 5 mL of chloroform.

After vortexing to form an emulsion, the mixture was incubated at least 1 hour at 4°C in the dark to allow phase separation to occur. The aqueous phase was transferred to a new vial and dried to completeness under air. Glutamate was extracted from the aqueous phase in a procedure modified from Rhodes *et al* (1987)<sup>30</sup>. Briefly, the dried samples were resuspended in 1 mL of water and applied to Dowex-1-acetate 200 mesh column. Neutral and basic amino acids were washed off the column with 8 mL water. Acidic amino acids were eluted with 8 mL 0.2 M acetic acid and dried under air. Dried extracts were resuspended in 1 mL of water, applied to Dowex-50-H<sup>+</sup> 200 mesh columns, and eluted with 6 mL of 6 M NH<sub>4</sub>OH. The eluant was then dried, resuspended in 400 µL 60% methanol, and dried again. To derivatize, samples were resuspended in 100 µL 5:1 isobutanol:acetyl chloride and heated at 120°C for 20 minutes. Samples were dried, and 50 µL of heptafluorobutyric anhydride was added, followed by heating at 120°C for 10 minutes. Samples were dried and resuspended in 100 µL 1:1 ethyl acetate:acetic anhydride. Samples were analyzed via GC-MS as previously described<sup>30</sup> using  $\alpha$ -aminoadipate as an internal standard.

To determine isotopic abundances, the percentage of juglone and glutamate labeling was calculated as the sum of the intensities of the shifted molecular ions divided by the sum of intensities for unshifted and shifted molecular ions, after correcting for natural isotope abundance. Labeled glutamate exhibited a shift of +6 atomic mass units (amu), and to capture the interconversion between its amino and keto acid forms, +5 amu was also examined. Labeled juglone exhibited a shift of +3 amu.

## 2.4 Results

### 2.4.1 Spatial accumulation of juglone and phylloquinone in black walnut tissues

When first considering our hypothesis that biosynthesis of the juglone naphthalenoid backbone branches from the phylloquinone pathway, we measured the spatial abundance of these two 1,4-NQ natural products in various black walnut tree tissues (see Materials and Methods for tissue sources) using HPLC coupled with fluorescence detection. This method relies on the property of the 1,4-NQ ring to fluoresce when in its reduced form and allows for sensitive and selective detection without preparation of lipid-enriched fractions prior to analysis. Previously, it was shown that the reduction of phylloquinone needed for detection by HPLC-fluorescence can be achieved using an in-line post-column dry reactor packed with zinc dust<sup>31</sup>. We applied the same

approach to achieve in-line conversion of juglone to its reduced form, hydrojuglone, during HPLC analysis, thereby allowing more sensitive and selective detection and quantification by fluorescence (Figure A.1). The pool size of phylloquinone was found to be highest in black walnut leaves (46.2 pmol mg<sup>-1</sup> FW), below 3.5 pmol mg<sup>-1</sup> FW in all flowers, hulls, peeled stems, and bark, and near the detection limit (less than 0.1 pmol mg<sup>-1</sup> FW) in hulls and roots (Figure 2.2a). At the same time, the free (metabolically active) juglone pool was determined to be highest in roots (64.5 nmol mg<sup>-1</sup> FW), intermediate in bark (21.0 nmol mg<sup>-1</sup> FW), and below 5.5 nmol mg<sup>-1</sup> FW in all other tissues (Figure 2.2b). These results indicate that the relative pool sizes of juglone and phylloquinone are inversely correlated to one another in roots and in leaves. Thus, these tissues were selected for generation of RNA-seq datasets to investigate the spatial expression pattern of phylloquinone pathway genes.

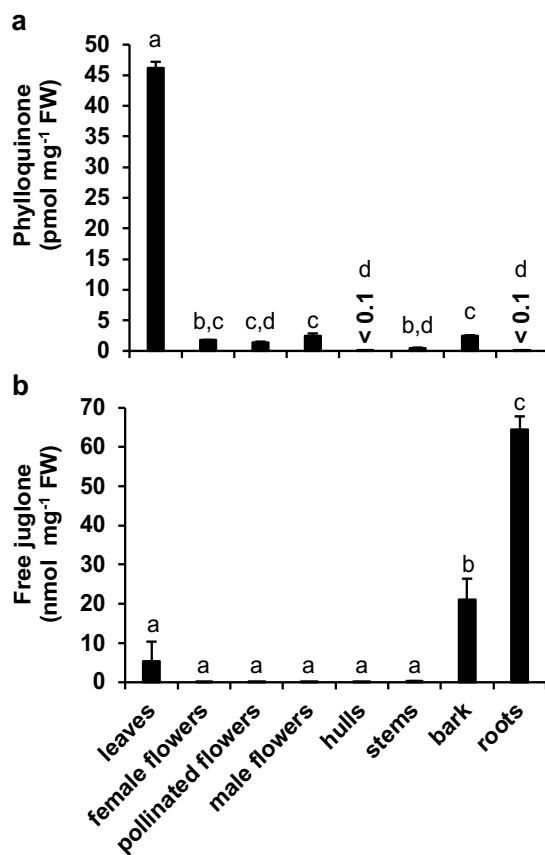


Figure 2.2 Pool sizes of phylloquinone and free juglone in *Juglans nigra* (black walnut) organs. (a) Phylloquinone levels. (b) Free juglone levels. All data are means  $\pm$  SEM ( $n \geq 3$  biological replicates). Different letters indicate significant differences via Analysis of Variance (ANOVA) followed by Post-hoc Tukey test ( $\alpha = 0.05$ ).

### 2.4.2 Transcriptome sequencing, quality control, de novo assembly, and annotation

We generated RNA-seq datasets from *J. nigra* roots and leaves because they were found to be the tissues containing the lowest and highest levels of phyloquinone, respectively, and the highest and lowest levels of free juglone, respectively (Figures 2.2 and A.2). Six cDNA libraries prepared from RNA isolated from roots (RJn1, RJn2, and RJn3) and leaves (LJn1, LJn2, and LJn3) of one-year old *J. nigra* trees were subjected to Illumina 101-bp paired-end sequencing with over 436 million reads produced (Table A.2). After quality control, a total of 290 million clean reads for roots and 292 million clean reads for leaves remained and were assembled into 131,449 non-redundant transcripts ( $\geq 500$  bp; N50 was 1,819 bp). Out of 131,449 transcripts, 106,968 (81%) were found to have blastx hits against the NCBI non-redundant protein database, 105,376 (80%) against the *J. regia* protein database, 96,926 (73%) against the Arabidopsis protein database, and 89,338 (67%) against all three databases. These 131,449 transcripts correspond to 59,254 unique genes, which were used for all subsequent downstream analysis.

### 2.4.3 Summary and GO enrichment analyses of DEGs

A total of 19,415 and 16,208 DEGs were detected in roots compared to leaves ( $FDR \leq 0.05$ ) using EBSseq and DESeq2, respectively. After combining the DEGs from both methods, a total of 21,608 unique DEGs were determined. We next used GO enrichment analysis to examine differences in the functional profiles of the root and leaf transcriptomes. GO terms were assigned to DEGs based on *J. regia* annotation and classified into Cellular Component, Biological Process, and Molecular Function groups (Figure 2.3). In the Cellular Component group, 25, 17, 68, and 239 genes were assigned to the enriched categories photosystem II (PSII), PSII oxygen evolving complex, cell wall, and membrane, respectively. Consistent with the absence of photosynthesis in roots, mRNA levels of all genes represented in the PSII and PSII oxygen evolving complex categories were found to be reduced in roots compared to leaves with DESeq2  $\log_2$  fold-differences ( $\log_2$ FDs) ranging from 2.0-10.9 (Tables A.3 and A.4). Similarly, in the Biological Process group, transcript levels of all 26 genes in the photosynthesis category were observed to be lower in roots compared to leaves with DESeq2  $\log_2$ FDs ranging from 2.4-11.0 (Tables A.5 and A.6). Also, in the Biological Process group, 75, 42, and 224 genes were assigned to the response to oxidative stress, defense response, and regulation of transcription categories, respectively (Figure 2.3).

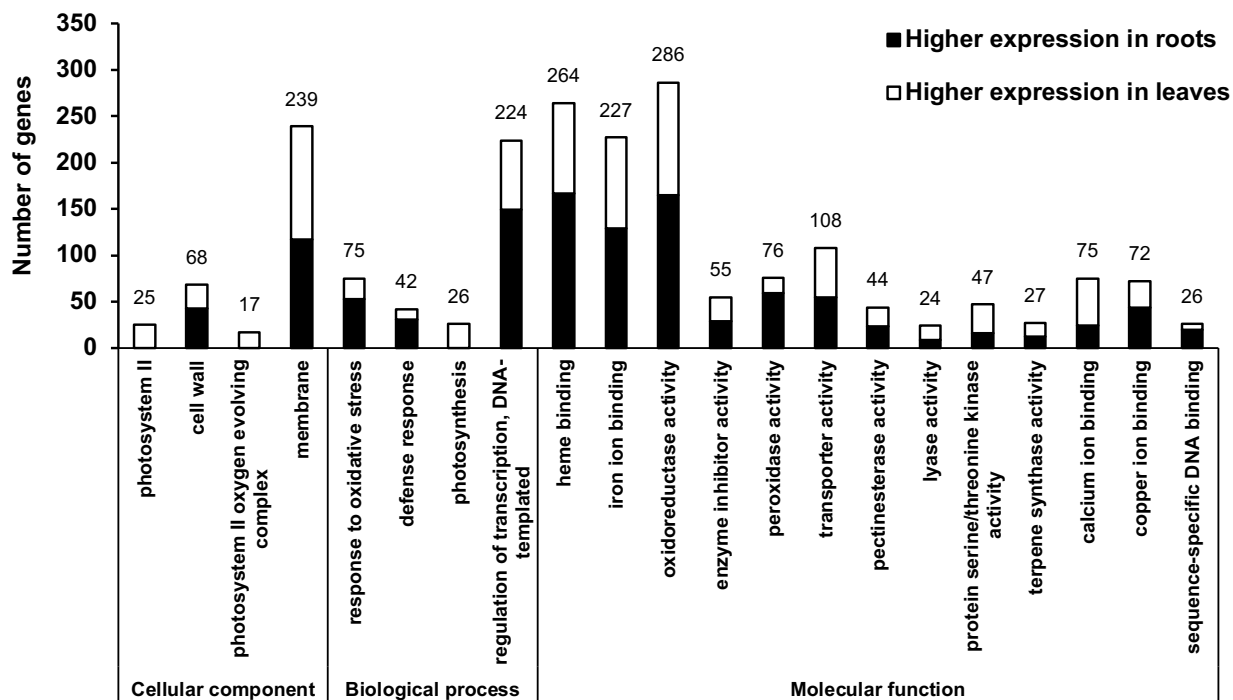


Figure 2.3 GO term enrichment in DEGs between roots and leaves of *Juglans nigra* (black walnut). Black shading in bars indicates higher expression in roots, and white shading indicates higher expression in leaves. Numbers above bars are total DEGs for each GO term.

The most abundant GO terms assigned ( $FDR \leq 0.05$ ) to the Molecular Function group were heme binding, iron binding, and oxidoreductase activity, to which 264, 227, and 286 genes were associated, respectively. The mRNA levels for a majority of the genes in each of these categories were found to be higher in roots compared to leaves (Tables A.7 and A.8). Moreover, many of the genes within the heme binding, iron binding, and oxidoreductase activity categories were assigned to all three categories and were annotated to encode Pigment absorbing at 450 nm (P450) enzymes. P450s share a catalytic center comprised of an iron-coordinated heme, and to be active, P450s must also be coupled with electron-donating proteins, such as P450 reductases<sup>32</sup>. It is suggested that the hydroxylation of 1,4-naphthoquinone to form juglone (Figure 2.1) could be catalyzed by a member of the P450 superfamily<sup>8</sup>. Therefore, P450 genes overrepresented in roots should be considered among candidates for the 1,4-naphthoquinone hydroxylase.

Several of the genes assigned to the heme binding category in the Molecular Function group were also assigned to the peroxidase activity category. Peroxidases are found in all plant organs but are particularly abundant in roots where they function in processes such as root hair

growth and lignin formation<sup>33</sup>. Gene lists for the other significantly enriched categories in the Molecular Function group are provided in Tables A.7 and A.8. Taken together, the GO enrichment analyses revealed typical functional profiles expected from root and leaf transcriptomes.

#### 2.4.4 Phylloquinone pathway gene expression analysis

In *Arabidopsis* and *Zea mays* (maize), there are no known alternative fates of phylloquinone pathway intermediates downstream of isochorismate, which is precursor to certain hydroxybenzoic acids, including salicylic acid, and their cognate catabolites<sup>34</sup>. Accordingly, expression levels of phylloquinone pathway genes are generally much lower in roots compared to leaves in *Arabidopsis* and maize (Figure A.3). In black walnut roots, on the other hand, juglone is present at nanomolar levels compared to sub-picomolar levels of phylloquinone (Figures 2.2 and A.2). We therefore hypothesized that if juglone is *de novo* synthesized in roots using enzymes shared with the phylloquinone pathway, then the relative root versus leaf expression profile for genes involved in forming the naphthalenoid moiety of phylloquinone should be markedly higher in black walnut compared to *Arabidopsis* and maize. Using the amino acid sequences of *Arabidopsis* and English walnut phylloquinone pathway enzymes as query, we first performed a tBlastn search to identify the phylloquinone pathway genes in our black walnut transcriptomes (Table A.9). Then, because RNA-seq is a quantitative approach, gene expression in roots relative to leaves was assessed based on the number of normalized counts corresponding to each gene in the generated datasets. This analysis revealed that expression levels of black walnut genes encoding ICS, the trifunctional enzyme PHYLLLO, OSB-CoA ligase, and DHNA-CoA thioesterase, which together catalyze six of the seven reactions needed to form DHNA, are virtually the same in roots and leaves ( $\log_2$ FD in roots compared to leaves range from -0.22 to 0.29) (Figure 2.4). By comparison, in *Arabidopsis* and maize the  $\log_2$ FD of mRNA levels for the same pathway genes in roots compared to leaves range from -6.10 to -1.03, with the exception of DHNA-CoA thioesterase genes which exhibit  $\log_2$ FDs up to 0.98 (Figure A.3). Similar to its orthologs in *Arabidopsis* and maize, expression of the black walnut DHNA-CoA synthase gene was found to be lower in roots compared to leaves, although to a lesser degree ( $\log_2$ FD of -1.54 in black walnut versus -3.28 and -4.76 in *Arabidopsis* and maize, respectively) (Figures 2.4 and A.3).

The final three enzymes in the phylloquinone pathway catalyze modifications to the naphthoquinone ring of DHNA that are not present in the structure of juglone. We therefore

predicted that unlike genes encoding the enzymes involved in formation of the naphthoquinone ring (reactions 1-5, Figure 2.1), the relative root versus leaf expression profiles of genes encoding enzymes that catalyze phylloquinone specific reactions (reactions 6-8, Figure 2.1) in black walnut would follow the same trend as their orthologs in Arabidopsis and maize. Expression of the gene encoding the black walnut DHNA phytyl transferase was found to have a  $\log_2$ FD in roots versus leaves of -3.56 (Figure 2.4). This value compares with the expression profiles of the Arabidopsis and maize orthologs ( $\log_2$ FDs of -4.49 and -10.94, respectively) (Figure A.3). The  $\log_2$ FDs for the black walnut *NDC1* (-2.67) and *demethylphylloquinone methyltransferase* (-3.14) genes were also found to be within the range of the  $\log_2$ FDs for their cognate orthologs in Arabidopsis and maize (Figure A.3). Thus, the RNA-seq results indicate that the relative root versus leaf expression values for all but one of the genes encoding the enzymes forming the naphthoquinone moiety of phylloquinone are higher in black walnut compared to Arabidopsis and maize. At the same time, the relative root versus leaf expression values for black walnut genes encoding enzymes catalyzing phylloquinone-specific reactions are comparable to those of their Arabidopsis and maize orthologs and to other black walnut photosynthesis-related genes revealed by GO enrichment analysis of DEGs (Tables A.2-6). Similar trends of relative root to leaf gene expression in black walnut were observed by quantitative RT-PCR (qRT-PCR) using gene-specific primers (Figure 2.4). These results support the existence of an alternative fate for DHNA derived from the phylloquinone pathway in black walnut roots.

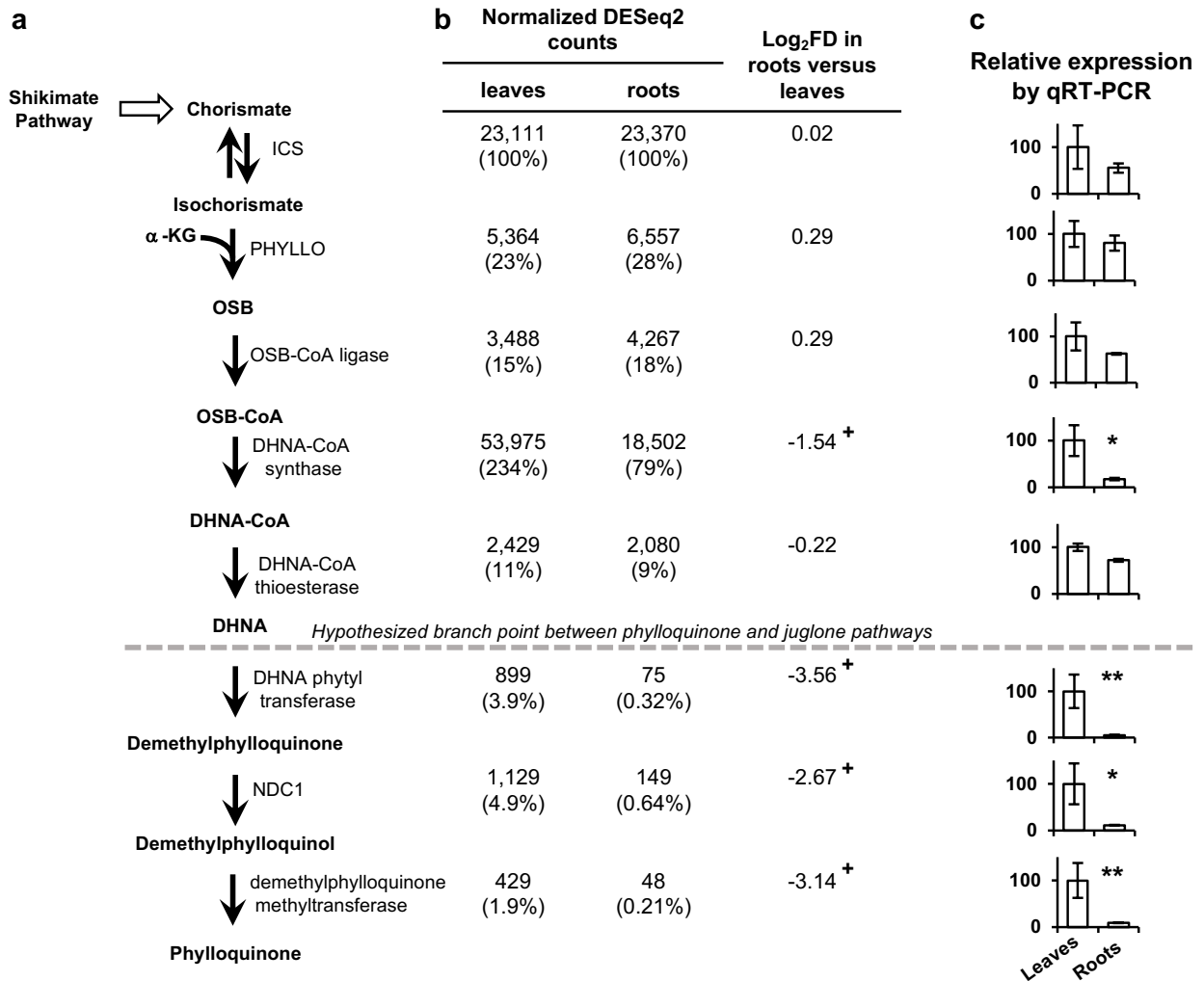


Figure 2.4 Relative expression pattern of phylloquinone pathway genes in *Juglans nigra* (black walnut) roots and leaves. (a) The phylloquinone pathway. See Figure 2.1 legend for abbreviations. (b) Expression pattern of phylloquinone pathway genes based on normalized DESeq2 counts. Log<sub>2</sub> fold-differences (FD) in roots compared to leaves are presented with negative numbers, which indicate lower mRNA accumulation in roots. Numbers in brackets are percent expression relative to ICS expression, based on normalized DESeq2 counts in the cognate organ. + indicates significant differential expression in leaves versus roots as calculated by DESeq2 ( $p < 0.001$ ). (c) Relative gene expression in roots compared to leaves set at 100% as inferred by qPCR. Data are means  $\pm$  SEM ( $n = 3$  biological replicates), \* $p < 0.05$  and \*\* $p < 0.01$  by Student's  $t$ -test relative to leaves.

### 2.4.5 Juglone is de novo synthesized from an intermediate of the phylloquinone pathway in black walnut roots

Given the relative high expression of phylloquinone pathway genes encoding enzymes involved in synthesizing DHNA in black walnut roots, we next sought to determine if stable isotopically-labeled glutamate is incorporated into juglone with the same mass shift as that expected if juglone is derived from an intermediate of the phylloquinone pathway. Because the

quinone ring (ring *B*) of phylloquinone originates from glutamate via  $\alpha$ -ketoglutarate (Figure 2.1)<sup>18</sup>, we therefore assessed the incorporation into juglone of  $^{13}\text{C}_5^{15}\text{N}_1$ -labeled L-glutamate (Glu- $^{13}\text{C}_5^{15}\text{N}_1$ ) fed to axenic black walnut root cultures. We predicted that if the naphthalenoid precursor for juglone is derived from the phylloquinone pathway, then juglone should be labeled by Glu- $^{13}\text{C}_5^{15}\text{N}_1$  with a mass shift of +3 (M3; Figure 2.5a).

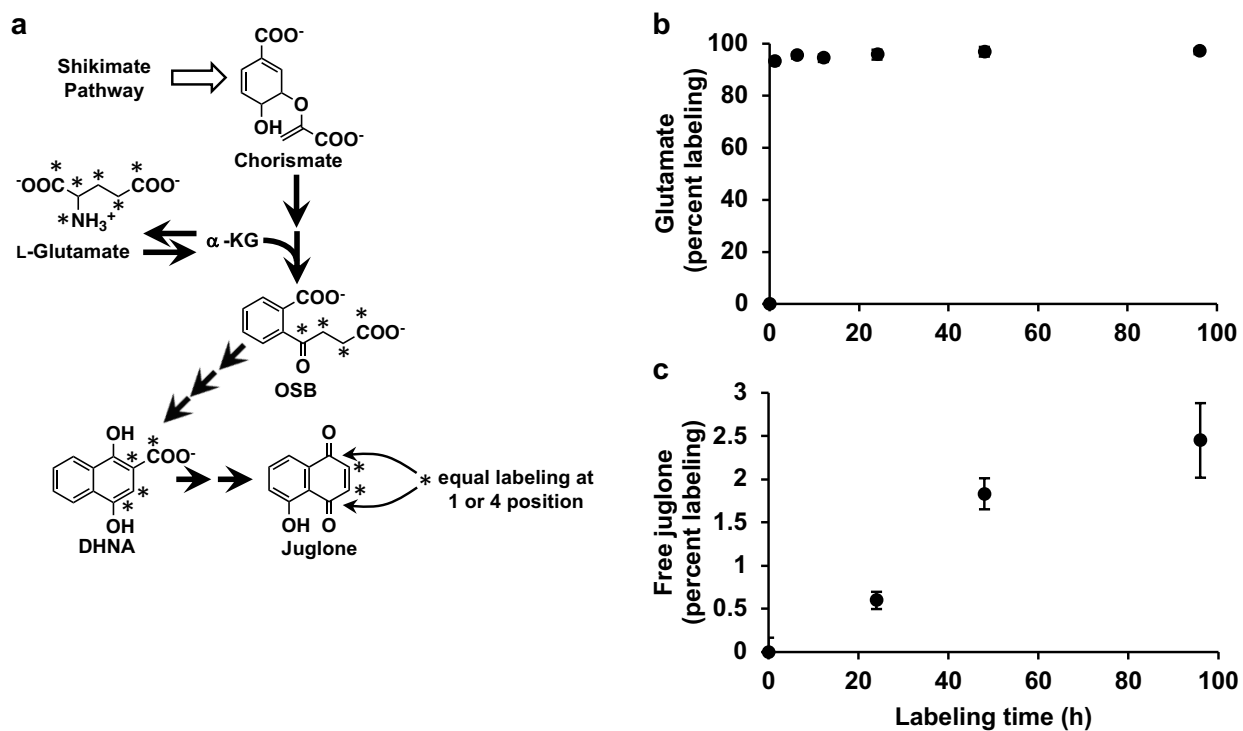


Figure 2.5 Isotopic labeling of juglone from  $^{13}\text{C}_5^{15}\text{N}_1$ -L-glutamate (Glu- $^{13}\text{C}_5^{15}\text{N}_1$ ). (a) Scheme depicting labeling pattern of Glu- $^{13}\text{C}_5^{15}\text{N}_1$  incorporated into the structure of juglone via DHNA derived from the phylloquinone pathway. (b) Time course of percent labeling of the L-glutamate pool in axenically grown *Juglans nigra* (black walnut) roots fed with 25 mM Glu- $^{13}\text{C}_5^{15}\text{N}_1$ . The glutamate pool was labeled by over 90% within 30 min and remained constant over the 96 hr experiment. (c) Time course of percent labeling of the free juglone pool in axenically grown black walnut roots fed with 25 mM Glu- $^{13}\text{C}_5^{15}\text{N}_1$ . Each time point represents the average percent labeling in glutamate or juglone from two independent feeding experiments.

Young roots were detached from one-year-old black walnut trees, washed, surface sterilized, and continuously fed with 25 mM Glu- $^{13}\text{C}_5^{15}\text{N}_1$  for 0, 24, 48, or 96 h in liquid culture. Isotopic abundances of glutamate and free juglone pools were then analyzed by GC-MS. Isotopomers produced from Glu- $^{13}\text{C}_5^{15}\text{N}_1$  fed to roots were distinguished from unlabeled compounds based on mass spectra obtained from GC-MS analyses and natural isotopic abundances

were subtracted. After 0.5 h feeding, the glutamate pool in roots was labeled by over 95% and remained constant in root cultures for the duration of the feeding experiment (Figure 2.5b). The M3  $^{13}\text{C}$  enrichment of the juglone pool from Glu- $^{13}\text{C}_5^{15}\text{N}_1$  increased linearly over 48 h to 1.83% and then began to plateau, reaching 2.45% by 96 h (Figure 2.5c). These results therefore demonstrate that juglone can be *de novo* synthesized in roots and provide additional support that the juglone naphthalenoid moiety originates via the phylloquinone pathway.

## 2.5 Discussion

The ability to synthesize a myriad of 1,4-NQ natural products facilitating plant-plant, plant-microbe, and/or plant-insect interactions has independently evolved across multiple lineages via several different metabolic routes within the flowering plants<sup>8</sup>. Although most pathway genes remain unidentified, biosynthesis of some 1,4-NQ natural products may rely on precursors or intermediates now established to be part of pathways leading to quinones involved in photosynthesis or respiration<sup>8</sup>. Combining comparative transcriptomics with metabolic profiling, we show that phylloquinone pathway genes encoding enzymes involved in forming DHNA are expressed in black walnut roots to support production of a metabolite other than phylloquinone. This result supports the findings of the classical radiotracer study performed by Müller and Leistner (1976)<sup>21</sup>, who demonstrated that  $[1,4-^{14}\text{C}]$ -DHNA fed to English walnut leaves could be incorporated into juglone, but without knowledge of phylloquinone pathway enzymes could not postulate the *in vivo* intermediacy of DHNA. Therefore, to test if DHNA serves as an *in planta* intermediate in juglone biosynthesis, we fed stable isotopically-labeled glutamate to axenic black walnut root cultures and found that Glu- $^{13}\text{C}_5^{15}\text{N}_1$  incorporates into juglone with the same mass shift as that expected for phylloquinone (Figure 2.5). Putting together the transcriptomic, metabolomic, and labeling evidence provided here, with the observations of Müller and Leistner (1976)<sup>21</sup>, thus indicates that juglone is *de novo* synthesized in black walnut roots from DHNA derived via the phylloquinone pathway. By extension of knowledge about the plant phylloquinone pathway, our work has revealed the complete set of genes/enzymes involved in forming the juglone naphthoquinone ring starting from chorismate.

The black walnut DHNA-CoA synthase gene is expressed three times higher in leaves than roots, but it is still highly expressed in both tissues relative to other phylloquinone pathway genes (Figure 2.4). The substrate of DHNA-CoA synthase, OSB-CoA (Figure 2.1), has been shown *in*

*vitro* to be unstable at physiological pH and to spontaneously hydrolyze to its spirodilactone form<sup>35–37</sup>. Recycling of this *a priori* metabolically inactive compound in plants would necessitate the activity of an esterase to convert OSB spirodilactone back to OSB, thereby creating a “futile cycle” within the phylloquinone pathway<sup>18</sup>. It therefore seems reasonable to postulate that in black walnut the DHNA-CoA synthase gene is highly expressed in order to produce enough enzyme to ensure sufficient conversion of OSB-CoA to DHNA-CoA to avoid futile cycling of OSB-CoA back to OSB. Such an expression pattern may have evolved to drive flux toward DHNA to sustain the prolific production of juglone in roots (Figure 2.2). In leaves, high DHNA-CoA synthase levels may ensure sufficient carbon allocation to DHNA to support juglone synthesis without depleting the precursor pool available for phylloquinone, which is a vital component of PSI.

In addition to being transported within or between cells, plant natural products are often translocated from the site of synthesis to other tissues or organs<sup>38</sup>. A classic example of this is translocation of the alkaloid nicotine, produced in roots of some Solanaceous species, to leaves via the xylem<sup>39</sup>. Many other instances of partitioning synthesis and storage of natural products occur throughout flowering plants suggesting this strategy could be a common feature to protect highly metabolically active cells from cytotoxicity or to better utilize resources by centrally localizing synthesis with subsequent deployment to multiple destinations<sup>40</sup>. However, feeding experiments with Glu-[<sup>13</sup>C<sub>5</sub><sup>15</sup>N<sub>1</sub>] supplied to isolated black walnut roots performed in this study (Figure 2.5), combined with previous tracer studies using English walnut leaves<sup>19–21</sup>, demonstrate that juglone can be *de novo* synthesized in both organs. Thus, while the origin of juglone detected in bark and reproductive organs (Figure 2.2) is still unknown, juglone synthesis does not appear to be centrally localized. In addition, the labeling experiment performed in this study demonstrates that *de novo* juglone synthesis can occur in roots without translocation of an immediate precursor from aerial tissues.

Within black walnut roots, juglone accumulates in the periderm (Figure 2.6) from where it is released in large amounts into the rhizosphere to mediate plant-plant and plant-microbe interactions<sup>8</sup>. Because juglone is also present in the root vasculature (Figure 2.6), though, it is possible that a portion of the juglone pool in roots is translocated from aerial parts of the plant and/or that juglone pools in some aerial organs originate via translocation from roots. Moreover, it should be investigated if juglone synthesis in roots occurs in the vascular tissue and is transported to the periderm for secretion into the environment. The identification of juglone pathway genes in

this study now enables future studies to explore the tissue-level distribution of the juglone pathway in roots.

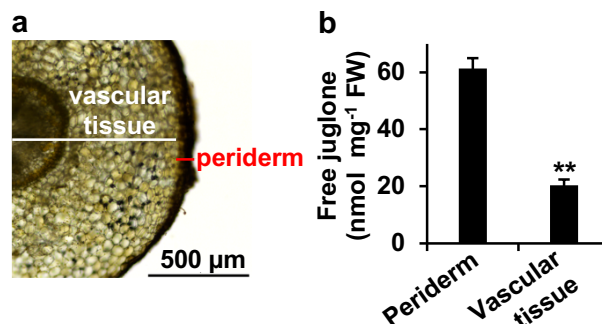


Figure 2.6 Juglone accumulates in *Juglans nigra* (black walnut) root periderm. (a) Black walnut root cross section depicting dissected sections of periderm and vascular tissue. (b) Profiling of free juglone in periderm and vascular tissue. Data are means  $\pm$  SEM ( $n = 3$  biological replicates), \*\* $p < 0.001$  by Students  $t$ -test relative to periderm.

No herbicide with a novel mode of action has been commercialized in over 25 years<sup>41</sup>. Natural products offer a rich source of new chemical structures and modes of action, but compared to other pesticides and pharmaceuticals, they have been vastly underutilized for developing herbicides<sup>42</sup>. Though not yet completely understood, juglone's herbicidal mode(s) of action appears to be distinct from that of any existing synthetic commercial herbicide<sup>41</sup>, making it a prime candidate for developing a novel natural product-based herbicide. The discovery that the naphthalenoid moiety of juglone originates from DHNA derived from the phylloquinone pathway now raises the prospect of developing metabolic engineering strategies in virtually any tolerant crop species or using green algae, cyanobacteria, or certain menaquinone-synthesizing bacteria as a platform for large-scale juglone production. To achieve such goals, however, the next step is to complete the elucidation of juglone biosynthesis from DHNA. We propose this occurs through DHNA decarboxylation followed by hydroxylation of 1,4-naphthoquinone (Figure 2.1), the latter of which may be catalyzed by a member(s) of the cytochrome P450 or 2-oxoglutarate/Fe(II)-dependent dioxygenase families<sup>8</sup>. The transcriptomes generated in this study provide candidate lists (Tables A.10-12) of black walnut genes that may encode the enzymes carrying out the final steps of the juglone pathway. These lists can now be further refined by examining transcriptomes across juglone-producing species and using co-expression analyses with phylloquinone pathway genes to identify target juglone pathway genes for functional testing.

## Acknowledgements

This work was supported by start-up funds and a Showalter Trust Fund award for bioinformatics support from Purdue University to JRW. This material is based upon work supported by the National Science Foundation Graduate Research Fellowship Program under Grant No. DGE-1333468 to JWC. Any opinions, findings, and conclusions or recommendations expressed in this material are those of the authors and do not necessarily reflect the views of the National Science Foundation. We thank Jim McKenna (Hardwood Tree Improvement and Regeneration Center, Purdue University) for providing black walnut seedlings and collecting tissues from mature trees, Elena Yakubova for technical assistance, and Jing Yuan for assistance with microscopy.

## 2.6 References

1. Willis, R. J. *The history of allelopathy. The history of allelopathy* **1542**, (Springer Netherlands, 2008).
2. Dana, M. & Lerner, B. Black walnut toxicity. *Purdue Univ. Coop. Ext. Serv.* **HO-192-W**, 2 (2001).
3. Soderquist, C. J. Juglone and allelopathy. *J. Chem. Educ.* **50**, 782–783 (1973).
4. Massey, A. Antagonism of the walnuts (*Juglans nigra* L. and *J. cinera* L.) in certain plant associations. *Phytopathology* **15**, 773–784 (1925).
5. Babula, P. *et al.* Phytotoxic action of naphthoquinone juglone demonstrated on lettuce seedling roots. *Plant Physiol. Biochem.* **84**, 78–86 (2014).
6. Chi, W. C. *et al.* Identification of transcriptome profiles and signaling pathways for the allelochemical juglone in rice roots. *Plant Mol. Biol.* **77**, 591–607 (2011).
7. Dayan, F. E. & Duke, S. O. Biological Activity of Allelochemicals. in *Plant-derived Natural Products* 361–384 (Springer US, 2009). doi:10.1007/978-0-387-85498-4\_17
8. Widhalm, J. R. & Rhodes, D. Biosynthesis and molecular actions of specialized 1,4-naphthoquinone natural products produced by horticultural plants. *Hortic. Res.* **3**, 16046 (2016).
9. van Oostende, C., Widhalm, J. R., Furt, F., Ducluzeau, A. L. & Basset, G. J. *Vitamin K<sub>1</sub> (Phylloquinone): Function, enzymes and genes. Advances in Botanical Research* **59**, (2011).

10. Maeda, H. & Dudareva, N. The Shikimate Pathway and Aromatic Amino Acid Biosynthesis in Plants. *Annu. Rev. Plant Biol.* **63**, 73–105 (2012).
11. Gross, J. *et al.* A plant locus essential for phylloquinone (vitamin K<sub>1</sub>) biosynthesis originated from a fusion of four eubacterial genes. *J. Biol. Chem.* **281**, 17189–17196 (2006).
12. Garcion, C. *et al.* Characterization and biological function of the ISOCHORISMATE SYNTHASE2 gene of Arabidopsis. *Plant Physiol.* **147**, 1279–87 (2008).
13. Kim, H. U., Oostende, C. Van, Basset, G. J. C. & Browse, J. The AAE14 gene encodes the Arabidopsis o-succinylbenzoyl-CoA ligase that is essential for phylloquinone synthesis and photosystem-I function. *Plant J.* **54**, 272–283 (2008).
14. Widhalm, J. R. *et al.* Phylloquinone (vitamin K<sub>1</sub>) biosynthesis in plants: two peroxisomal thioesterases of lactobacillales origin hydrolyze 1,4-dihydroxy-2-naphthoyl-CoA. *Plant J.* **71**, 205–215 (2012).
15. Shimada, H. *et al.* Inactivation and deficiency of core proteins of photosystems I and II caused by genetical phylloquinone and plastoquinone deficiency but retained lamellar structure in a T-DNA mutant of Arabidopsis. 627–637 (2005). doi:10.1111/j.1365-313X.2004.02326.x
16. Fatihi, A. *et al.* A Dedicated Type II NADPH Dehydrogenase Performs the Penultimate Step in the Biosynthesis of Vitamin K<sub>1</sub> in *Synechocystis* and Arabidopsis. *Plant Cell* **27**, 1730–1741 (2015).
17. Lohmann, A. *et al.* Deficiency in phylloquinone (vitamin K<sub>1</sub>) methylation affects prenyl quinone distribution, photosystem I abundance, and anthocyanin accumulation in the Arabidopsis *AtmenG* mutant. *J. Biol. Chem.* **281**, 40461–40472 (2006).
18. Basset, G. J., Latimer, S., Fatihi, A., Soubeyrand, E. & Block, A. Phylloquinone (vitamin K<sub>1</sub>): occurrence, biosynthesis and functions. *Mini Rev. Med. Chem.* 1–11 (2016). doi:10.2174/13895575166661606230827
19. Leistner, E. & Zenk, M. H. Zur Biogenese von 5-Hydroxy-1.4-naphthochinon (Juglon) in *Juglans regia* L. *Zeitschrift fur Naturforsch. - Sect. B J. Chem. Sci.* **23**, 259–268 (1968).
20. Chung, D., Maier, U. H., Inouye, H. & Zenk, M. H. Different mode of incorporation of o-succinylbenzoic acid into the naphthoquinones juglone and lawsone in higher plants. *Zeitschrift fur Naturforsch.* **49**, 885–887 (1994).

21. Müller, W. & Leistner, E. 1,4-Naphthoquinone, an intermediate in juglone (5-hydroxy-1,4-naphthoquinone) biosynthesis. *Phytochemistry* **15**, 407–410 (1976).
22. Kolosova, N. *et al.* Isolation of high-quality RNA from gymnosperm and angiosperm trees. *Biotechniques* **36**, 821–824 (2004).
23. Martínez-García, P. J. *et al.* The walnut (*Juglans regia*) genome sequence reveals diversity in genes coding for the biosynthesis of non-structural polyphenols. *Plant J.* **87**, 507–532 (2016).
24. Grabherr, M. G. *et al.* Trinity: reconstructing a full-length transcriptome without a genome from RNA-Seq data. *Nat. Biotechnol.* **29**, 644–652 (2013).
25. Fu, L., Niu, B., Zhu, Z., Wu, S. & Li, W. CD-HIT: Accelerated for clustering the next-generation sequencing data. *Bioinformatics* **28**, 3150–3152 (2012).
26. Li, B. & Dewey, C. N. RSEM : accurate transcript quantification from RNA-Seq data with or without a reference genome. *BMC Bioinformatics* **12**, 323 (2011).
27. Leng, N. *et al.* EBSeq: An empirical Bayes hierarchical model for inference in RNA-seq experiments. *Bioinformatics* **29**, 1035–1043 (2013).
28. Love, M. I., Huber, W. & Anders, S. Moderated estimation of fold change and dispersion for RNA-seq data with DESeq2. *Genome Biol.* **15**, 550 (2014).
29. Yu, G., Wang, L.-G., Han, Y. & He, Q.-Y. clusterProfiler: an R Package for Comparing Biological Themes Among Gene Clusters. *Omi. A J. Integr. Biol.* **16**, 284–287 (2012).
30. Rhodes, D. *et al.* Amino Acid Metabolism of *Lemna minor* L: II. Responses to chlorsulfuron. *Plant Physiol.* **84**, 775–780 (1987).
31. Oostende, C. van, Widhalm, J. R. & Basset, G. J. C. Detection and quantification of vitamin K<sub>1</sub> quinol in leaf tissues. *Phytochemistry* **69**, 2457–2462 (2008).
32. Bak, S. *et al.* Cytochromes P450. *Arab. B.* **9**, e0144 (2011).
33. Dunand, C., Crèvecoeur, M. & Penel, C. Distribution of superoxide and hydrogen peroxide in. *New Phytol.* (2006).
34. Widhalm, J. R. & Dudareva, N. A familiar ring to it: biosynthesis of plant benzoic acids. *Mol. Plant* **8**, 83–97 (2015).
35. Dansette, P. & Azerad, R. A new intermediate in naphthoquinone and menaquinone biosynthesis. *Biochem. Biophys. Res. Commun.* **40**, 1090–1095 (1970).

36. Heide, L., Kolkmann, R., Arendt, S. & Leistner, E. Enzymic synthesis of *o*-succinylbenzoyl-CoA in cell-free extracts of anthraquinone producing *Galium mollugo* L. cell suspension cultures. *Plant Cell Rep.* **1**, 180–182 (1982).
37. Meganathan, R. & Bentley, R. Menaquinone (vitamin K<sub>2</sub>) biosynthesis: conversion of *o*-succinylbenzoic acid to 1,4-dihydroxy-2-naphthoic acid by *Mycobacterium phlei* enzymes. *J. Bacteriol.* **140**, 92–8 (1979).
38. Yazaki, K., Sugiyama, A., Morita, M. & Shitan, N. Secondary transport as an efficient membrane transport mechanism for plant secondary metabolites. *Phytochem. Rev.* **7**, 513–524 (2008).
39. Hashimoto, T. & Yamada, Y. New genes in alkaloid metabolism and transport. *Curr. Opin. Biotechnol.* **14**, 163–168 (2003).
40. Jorgensen, M. E., Nour-Eldin, H. H. & Halkier, B. A. Transport of defense compounds from source to sink: Lessons learned from glucosinolates. *Trends Plant Sci.* **20**, 508–514 (2015).
41. Dayan, F. E. & Duke, S. O. Natural Compounds as Next-Generation Herbicides. *Plant Physiol.* **166**, 1090–1105 (2014).
42. Cantrell, C. L., Dayan, F. E. & Duke, S. O. Natural products as sources for new pesticides. *J. Nat. Prod.* **75**, 1231–1242 (2012).
43. Adebesin, F., Widhalm, J. R., Lynch, J. H., McCoy, R. M. & Dudareva, N. A peroxisomal thioesterase plays auxiliary roles in plant  $\beta$ -oxidative benzoic acid metabolism. *Plant J.* (2018). doi:10.1111/tpj.13818
44. Liu, Y. *et al.* RNA-seq analysis reveals MAPKKK family members related to drought tolerance in maize. *PLoS One* **10**, 1–26 (2015).

## CHAPTER 3. INVESTIGATING THE SUBCELLULAR ARCHITECTURE OF THE PHYLLOQUINONE PATHWAY

### 3.1 Abstract

Phylloquinone is a vital metabolite in plants functioning in photosynthetic electron transport and folding of proteins in the thylakoid lumen. Even though all of the steps to synthesize phylloquinone have been identified, there are still unanswered questions about the pathway's subcellular architecture. In this study, we provide genetic evidence that the *Arabidopsis thaliana* At1g60550 gene product, an annotated enoyl-CoA hydratase/isomerase that is targeted to peroxisomes and an ortholog of the *Escherichia coli* 1,4-dihydroxynaphthoyl-CoA (DHNA-CoA) synthase (DHNS, MenB), indeed functions in the phylloquinone pathway. *Arabidopsis At1g60550-RNAi* lines showed up to 85% reduction in phylloquinone. Moreover, using a series of synthetic biology approaches, we reinvestigated the localization of the *Arabidopsis* *o*-succinylbenzoate CoA (OSB-CoA) ligase (AAE14), which provides the substrate for DHNS and was previously shown to be targeted to either chloroplasts or to peroxisomes. Green fluorescent protein (GFP) fusion constructs introduced into tobacco and *Arabidopsis* in which GFP was placed in the middle of *AAE14* and expression was driven under control of the native *aae14* promoter revealed that AAE14 is targeted to both chloroplasts and peroxisomes. In parallel, we demonstrated that OSB-CoA ligase must be targeted to both the chloroplast and peroxisome in order to complement an *Arabidopsis aae14-1* mutant. Taken together, this study suggests a new architecture of the phylloquinone pathway in which OSB-CoA must be formed in chloroplasts and exported to peroxisomes where it is either imported as its free acid and re-ligated with CoA-SH, or where it is imported as an acyl-CoA but requires OSB-CoA ligase activity as part of a metabolic repair mechanism to re-ligate free OSB formed from promiscuous thioesterases. This architecture is reminiscent of the emerging picture for the metabolism of fatty acids and benzenoid/phenylpropanoid products which also involve CoA metabolic steps compartmentalized in peroxisomes.

### 3.2 Introduction

Peroxisomes are small, membrane-bound organelles found across Eukaryota. The peroxisome was one of the last discovered organelles, and understanding of its importance and roles in metabolism is still emerging. Recent studies have shed light on the metabolic enzymes and pathways of the peroxisome. Interestingly, peroxisomes are the sole site of  $\beta$ -oxidation in plant cells and house a variety of oxidative reactions (reviewed in<sup>1,2</sup>). Over the last 10 years, it has been revealed that the CoA-dependent metabolic steps of phylloquinone are localized to the peroxisome, but there are outstanding questions about the architecture of the compartmental split between peroxisomes and chloroplasts.

Phylloquinone (vitamin K<sub>1</sub>) is an essential vitamin for humans, and deficiency leads to blood coagulation disorders. Phylloquinone is also a vital metabolite in photosynthetic plants, green algae, and some cyanobacteria as it serves as an electron carrier in Photosystem I<sup>3</sup>. Recently, it has been implicated for roles beyond photosynthesis, as it has been shown to assist in formation of disulfide bonds in cyanobacteria<sup>4,5</sup> and plants<sup>6</sup> and has been suggested to function in the plasma membrane in parasitic, non-photosynthetic plants<sup>7</sup>. The phylloquinone pathway is largely homologous to the pathway to make menaquinone, a 1,4-naphthoquinone involved in anaerobic respiration in some bacteria, including *Escherichia coli*. Using *E. coli* menaquinone (“men”) genes as query, most of the plant pathway to make phylloquinone has been elucidated through genetic studies (reviewed in<sup>8</sup>).

The phylloquinone pathway begins in the chloroplast with the conversion of chorismate to isochorismate by isochorismate synthase<sup>3</sup> (ICS, Figure 3.1). Isochorismate from ICS is also precursor to the plant hormone salicylic acid and 2,3-dihydroxybenzoic acid. Isochorismate and 2-oxoglutarate are then converted to 2-succinyl-5-enolpyruvyl-6-hydroxy-3-cyclohexene-2-carboxylate (SEPHCHC) by SEPHCHC synthase. Pyruvate is removed from SEPHCHC to form 2-succinyl-6-hydroxy-2,4-cyclohexadiene-2-carboxylate (SHCHC) by SHCHC synthase, and SHCHC is aromatized to *o*-succinylbenzoate (OSB) by OSB synthase. In plants, these three reactions are catalyzed by a trifunctional enzyme, PHYLLO, with three catalytic sites<sup>9</sup>. *o*-Succinylbenzoate is then ligated to CoA by OSB-CoA ligase, called acyl activating enzyme 14 (AAE14) in *Arabidopsis*<sup>10</sup>. OSB-CoA is cyclized by DHNA-CoA synthase (DHNS) to produce DHNA-CoA<sup>11</sup>, which is finally hydrolyzed to DHNA by DHNA thioesterase (DHNAT), providing the naphthoquinone moiety for phylloquinone<sup>12</sup>. DHNA is then phytylated by DHNA phytyl

transferase<sup>13</sup>, called aberrant chloroplast development 4 (ABC4), reduced by NAD(P)H dehydrogenase C1 (NDC1)<sup>14</sup>, and methylated by demethylphyloquinone methyltransferase (menG)<sup>15</sup> to produce phyloquinone. All of the steps in the phyloquinone pathway have been genetically characterized except for the DHNS-catalyzed reaction, although plants contain presumed orthologs of the *E. coli* DHNS (MenB<sup>11</sup>) and *Synechocystis* sp. PCC 6803<sup>16</sup> DHNS.

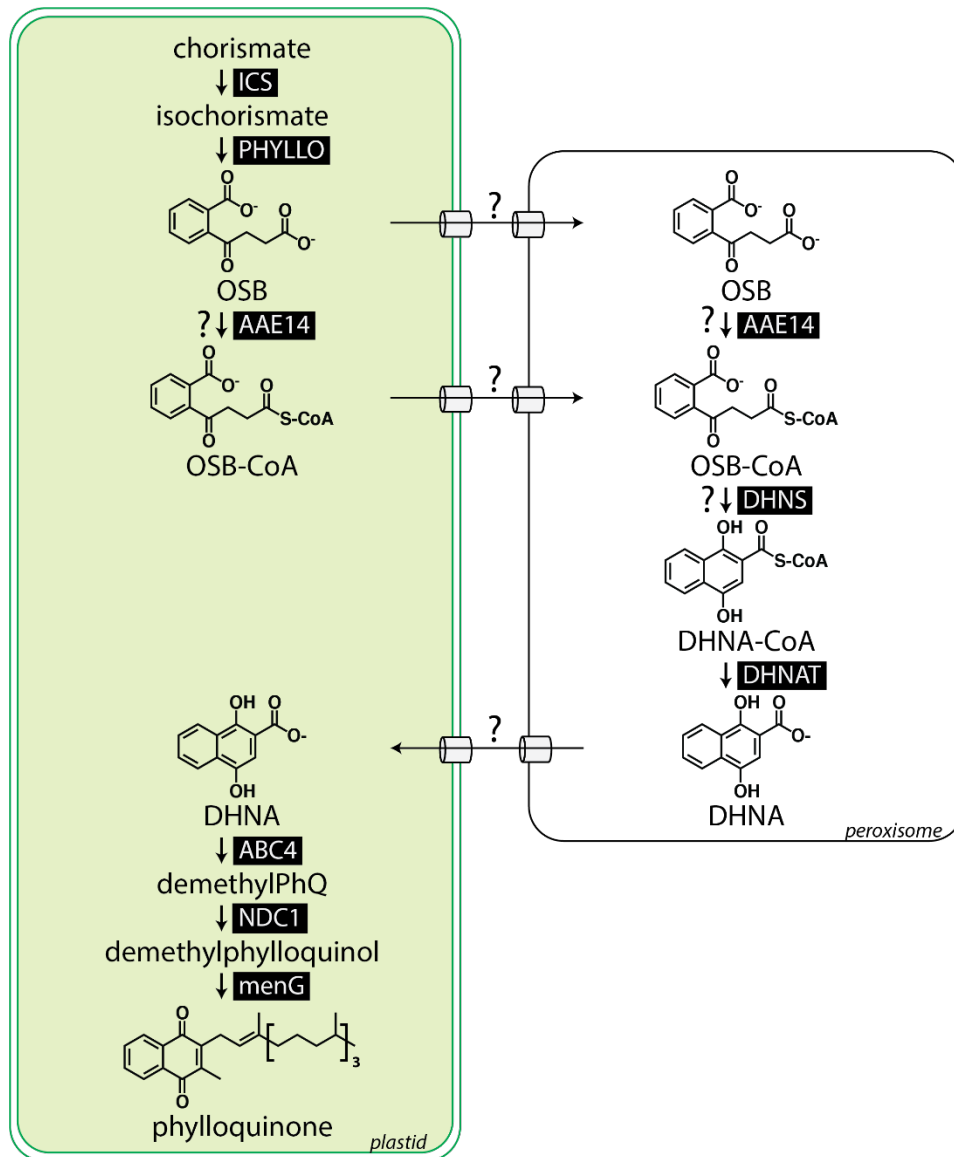


Figure 3.1 The phyloquinone pathway is in both the chloroplast and the peroxisome. See text for abbreviations.

The phyloquinone pathway was long thought to be exclusively localized in the chloroplast until development of methods for purification of peroxisomes allowed for investigation of the

peroxisomal proteome. The first indication came when At1g60550, the presumed ortholog to *E. coli* MenB, was found in the *Arabidopsis* peroxisomal proteome<sup>17</sup>. Subsequently, fusion of yellow fluorescent protein (YFP) or green fluorescent protein (GFP) with the C-terminus of At1g60550<sup>17</sup> or the N-termini of DHNAT1<sup>12</sup> and DHNAT2<sup>12</sup> provided further evidence of the peroxisomal branch. Interestingly, AAE14 bears both a predicted N-terminal chloroplast transit peptide (CTP) and a C-terminal type 1 peroxisomal targeting signal (PTS1). Fluorescent protein fusion experiments have suggested that each of these signals acting alone is sufficient to target AAE14 to chloroplasts<sup>10</sup> or to peroxisomes<sup>17</sup>, but how these signals act in concert to determine the localization of AAE14 is not understood.

Compartmentalization of the phylloquinone pathway implicates the involvement of intermediate transport steps. Although the current model (Figure 3.1) of the phylloquinone pathway reflects an organellar split between chloroplasts and peroxisomes, there is no genetic evidence supporting the involvement of the presumed plant DHNS in the phylloquinone pathway and it remains unknown what pathway intermediate(s) is exported from chloroplasts to peroxisomes. Therefore, to address these gaps in knowledge, we knocked down expression of *At1g60550* to genetically test the involvement of its encoded peroxisomal enzyme it encodes in phylloquinone biosynthesis. We then used two independent synthetic biology strategies to reinvestigate the localization of AAE14 and to test whether AAE14 is required to function in both chloroplasts and peroxisomes. The obtained results provide a new model for the subcellular architecture of the phylloquinone pathway, one which reflects an emerging common theme for the framework of CoA metabolism in plant peroxisomes. Moreover, our study sheds light on what intermediate is transported from chloroplasts to peroxisomes and potentially illuminates an expanded role for AAE14 in the phylloquinone pathway. These advances in understanding of the phylloquinone pathway will guide searches for intermediate transporters involved in shuttling metabolites between chloroplasts and peroxisomes. The findings of this study will also help develop rational engineering strategies to increase vitamin K<sub>1</sub> production in crops and to produce specialized 1,4-naphthoquinones whose synthesis relies on the phylloquinone metabolic framework.

### 3.3 Results

#### 3.3.1 At1g60550 functions as a peroxisomal DHNS

Although no plant DHNS has been genetically characterized, the *Arabidopsis thaliana* genome contains a single, clear homolog of the *E. coli* DHNS, MenB<sup>11</sup>. The protein encoded by *At1g60550* is more than 60% identical to the *Synechocystis* and *E. coli* MenB proteins (Figure B.1). Evaluation of the top co-expressed genes with *At1g60550* using the ATTED-II database<sup>18</sup> (version 9.0) revealed *AAE14* among the top five co-expressed genes (Table B.1). *AAE14* is also involved in the CoA branch of the phylloquinone pathway. GO term analysis of the top 50 co-expressors with Panther<sup>19</sup> (version 15) reveals enriched biological process GO terms related to photosynthesis and chloroplasts, consistent with *At1g60550* being involved in phylloquinone metabolism (Table B.2).

Alignment of *At1g60550* with the *Synechocystis* and *E. coli* MenB proteins (Figure B.1) shows that the *Arabidopsis* protein bears an N-terminal extension. This overhang contains an RLx<sub>5</sub>HL motif, which is a peroxisomal target signal 2 (PTS2) in plants<sup>20</sup>. Previously, it was established that *At1g60550* is in the peroxisomal proteome<sup>17,21</sup> and that a C-terminal fluorescent protein fusion went to peroxisomes in onion epidermal cells<sup>17</sup>. However, given the N-terminal extension on the plant protein and the fact that other phylloquinone pathway genes are localized to chloroplasts, we independently verified the subcellular localization of *At1g60550* in a photosynthetic tissue (*i.e.* a tissue containing chloroplasts). This was achieved by transiently overexpressing *At1g60550* fused with a C-terminal GFP in *Nicotiana benthamiana* leaves. Confocal imaging of infiltrated leaves showed that GFP fluorescence overlapped with that of the peroxisomal marker and was absent in chloroplasts, confirming that it is indeed only localized to peroxisomes (Figure 3.2).

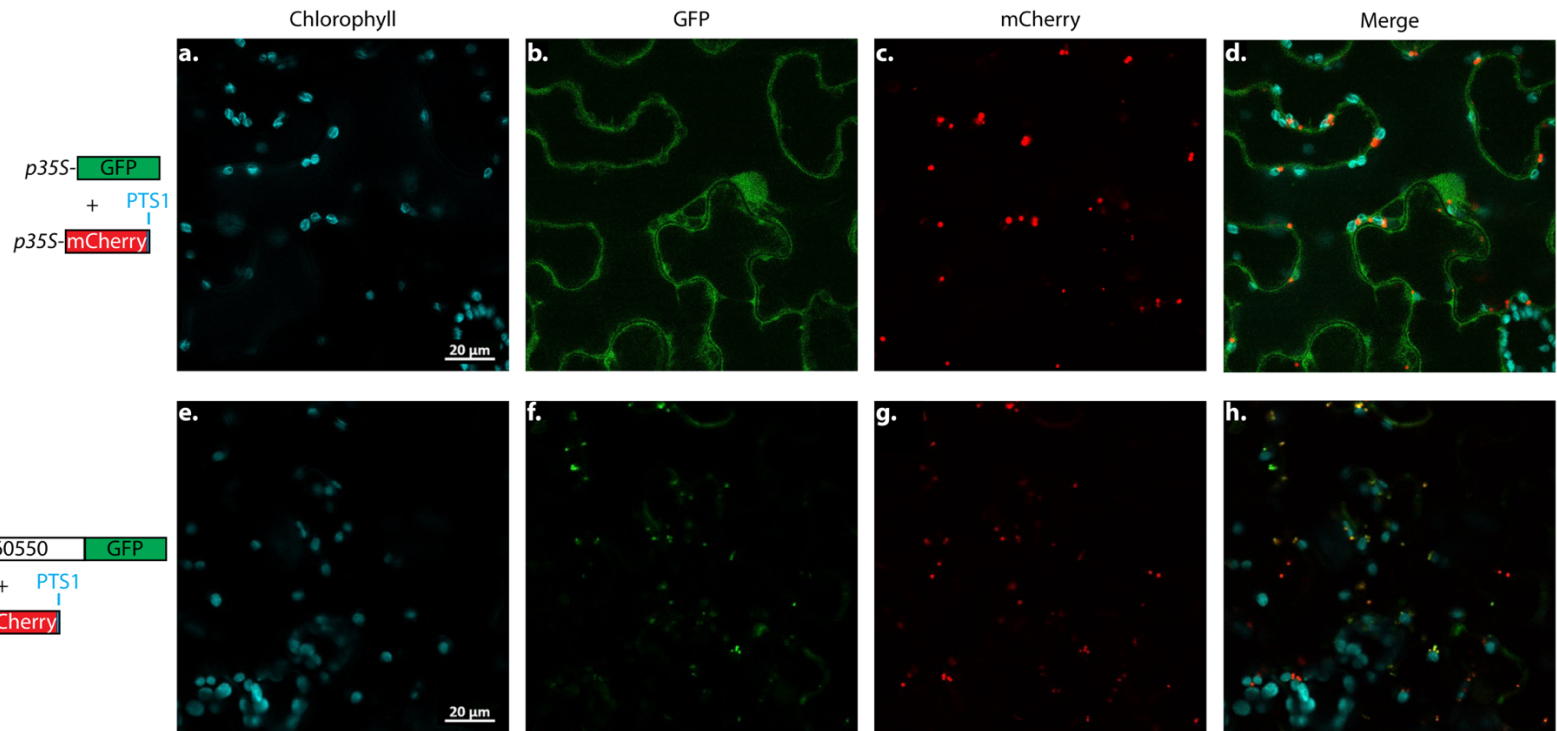


Figure 3.2 Subcellular localization of At1g60550 in *Nicotiana benthamiana* leaves. a.-d. Transient co-expression of GFP-alone and peroxisomal marker: a. autofluorescence of chlorophyll, b. GFP-alone, c. peroxisomal marker with mCherry, d. merged image. e.-h. Transient co-expression of At1g60550-GFP and peroxisomal marker: e. autofluorescence of chlorophyll, f. At1g60550-GFP, g. peroxisomal marker with mCherry, h. merged image.

To functionally test the involvement of *At1g60550* in phylloquinone metabolism, we used an RNAi approach to constitutively knockdown its expression given the lack of commercially available T-DNA insertion mutants. To preliminarily evaluate the involvement of *At1g60550* in phylloquinone synthesis, we measured phylloquinone content in Basta-selected primary transformants using high performance liquid chromatography (HPLC) coupled with fluorescence detection (FLD) (Figure 3.3). Whereas leaves from control plants were found to contain 7.3 pmol mg<sup>-1</sup> fresh weight (FW), the 26 analyzed lines displayed up to 85% reduction in phylloquinone content, ranging from 1.2-8.0 pmol mg<sup>-1</sup> FW. Taken together with the subcellular localization, the apparent orthology to *Synechocystis* and *E. coli* MenB, and the co-expression with *AAE14*, these data provide initial evidence that *At1g60550* indeed functions as a peroxisomal DHNS. Seeds from the primary *At1g60550-RNAi* transformants have been plated on selection media and tissue has been collected to examine *At1g60550* expression by qPCR and to perform additional metabolic profiling with biological replication.

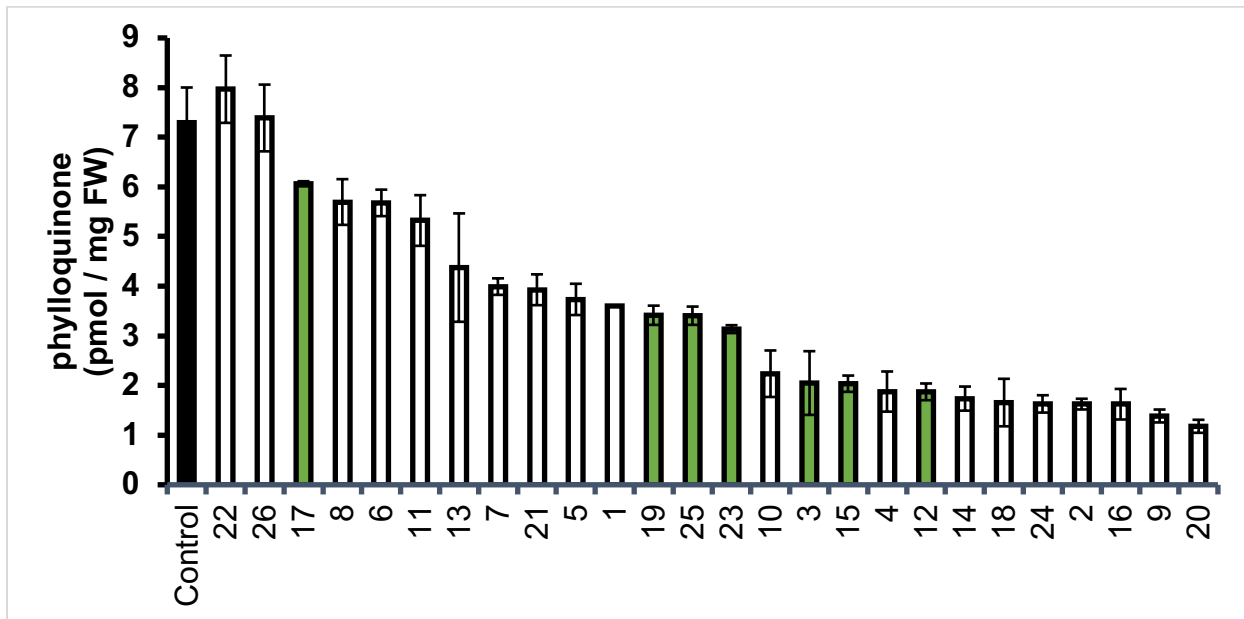


Figure 3.3 Phylloquinone extraction from primary transformants with the *At1g60550-RNAi* construct. Error bars are standard deviation. n=2-3 leaves from an individual plant. Green bars indicate lines taken to the next generation for RNA and phylloquinone profiling.

### 3.3.2 *Arabidopsis* AAE14 is localized to both chloroplasts and peroxisomes

With genetic evidence providing support to indicate that the DHNS-catalyzed reaction occurs in peroxisomes, this reopens the question about the origin of DHNS's substrate, OSB-CoA (Figure 3.1). Fluorescent protein fusion experiments with GFP fused to the C-terminus of AAE14, which catalyzes the ligation of CoA-SH to OSB to form OSB-CoA (Figure 3.1), showed chloroplast localization<sup>10</sup>, while fusion of YFP to the N-terminus resulted in peroxisomal targeting<sup>17</sup>. In these studies, each construct was driven by 35S expression and blocked either the PTS1 or the chloroplast targeting peptide (CTP), thereby preventing the testing of possible dual localization or that one signal overrides the other. Therefore, in order to determine where AAE14 is localized *in planta* without overexpression or interfering with localization signals, we designed a GFP fusion construct with *GFP* coding sequence (CDS) placed in the middle of the *AAE14* CDS under the control of the native *aae14* promoter. This was accomplished by fusing 2.5 kb upstream of the start codon of *AAE14* to the coding sequence of AAE14 with GFP localized between residues 248 and 249 (Figure 3.4).



Figure 3.4 Synthetic construct used to examine subcellular localization of OSB-CoA ligase (AAE14). GFP was placed in-frame in the middle of the *AAE14* cDNA. *pAAE14* is the 2.5 kb native *aae14* promoter used to drive expression.

Transient co-infiltration of the *pAAE14-AAE14-GFP* construct and a peroxisomal marker in *N. benthamiana* resulted in fluorescence localizing to small, punctate structures that overlapped with the fluorescence of the peroxisomal marker (Figure 3.5a-c). Fluorescence from AAE14-GFP also localized to oval structures that overlapped with autofluorescence of chlorophyll (Figure 3.5d-f), indicating AAE14 is targeted to chloroplasts as well. To examine dual localization under native conditions, we stably transformed the *pAAE14-AAE14-GFP* construct into *Arabidopsis* Col-0. Imaging of primary transformants once again revealed small, punctate structures consistent with sizes expected of peroxisomes and larger ovals that overlap with autofluorescence of chlorophyll (Figure 3.5g-i). Thus, these data suggest that AAE14 is indeed present in both chloroplasts and peroxisomes.

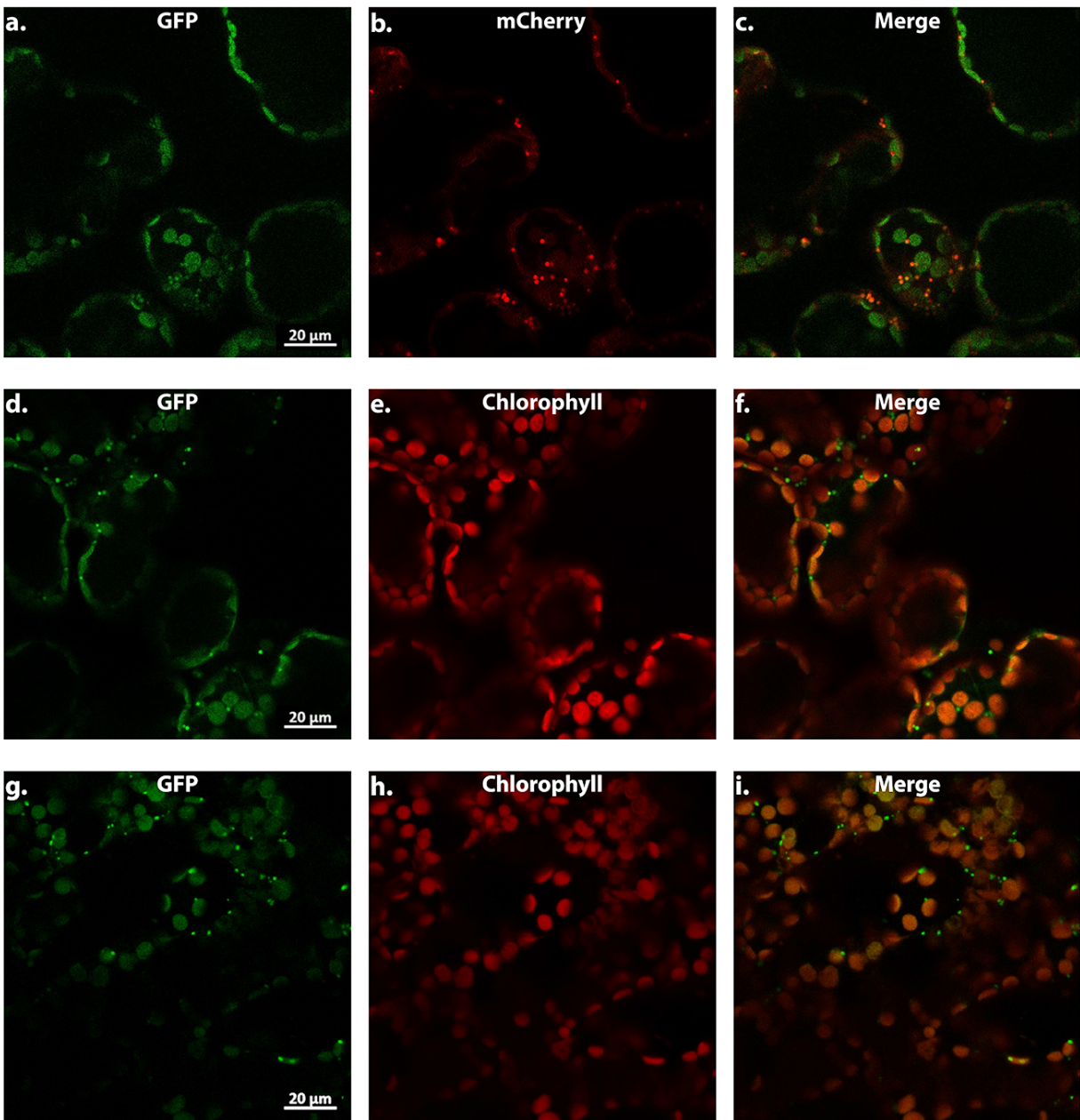


Figure 3.5 AAE14 is localized to the chloroplast and the peroxisome under its native promoter. a.-c. Transient co-expression of AAE14-GFP and a peroxisomal marker in *Nicotiana benthamiana*: a. GFP-tagged AAE14, b. peroxisomal marker tagged with mCherry, c. merged image. d.-f. Transient expression of AAE14 in *N. benthamiana*: d. GFP-tagged AAE14, e. autofluorescence of chlorophyll, f. merged image. g.-i. Stable expression of AAE14-GFP in *Arabidopsis thaliana*: g. GFP-tagged AAE14, h. autofluorescence of chlorophyll, i. merged image.

### 3.3.3 OSB-CoA ligase activity is necessary in both chloroplasts and peroxisomes

Although GFP-fusion experiments demonstrate that AAE14 is localized to both chloroplasts and peroxisomes, they do not provide information on whether the OSB-CoA ligase activity conferred by AAE14 is required in both organelles. To test this, we attempted to functionally complement the Arabidopsis *aae14-1* mutant<sup>10</sup> by overexpressing an OSB-CoA ligase targeted to either chloroplasts or peroxisomes. First, to test if OSB-CoA ligase activity is required in chloroplasts, we fused a PTS1 to the C-terminal end of the *E. coli* OSB-CoA ligase, EcMenE, in order to direct it to peroxisomes in plants. Addition of a PTS1 was indeed sufficient to target EcMenE to peroxisomes based on GFP fusion experiments in *N. benthamiana* (Figure B.2). We also verified that the EcMenE-PTS1 fusion protein was still active by functionally complementing the *E. coli*  $\Delta$ menE mutant (Figure B.3). Next, the *35S-EcMenE-PTS1* construct was transformed into heterozygous *AAE14/aae14* plants given that *aae14/aae14* mutants are seedling lethal. As a positive control, we overexpressed Arabidopsis *35S-AAE14* in heterozygous *AAE14/aae14*, and we were able to retrieve green transformed plants with a homozygous *aae14/aae14* background (Table B.3). After selecting for *35S-EcMenE-PTS1* transformants, we genotyped and phenotyped the hygromycin-resistant plants. Out of 8 selected green plants, all were found to be either heterozygous or WT at the *AAE14* locus (Table B.4). To further evaluate this, we took seeds from the heterozygous plants and evaluated the next generation. Four independent lines followed the expected phenotypic ratio of 3:1 green to white plants seen in progeny of *AAE14/aae14* plants (Table 3.1, n=102-234). No plants with an intermediate green-white phenotype were observed either. We genotyped more than 20 green plants from every line and no green plants were found to be of the *aae14/aae14* background. Instead, the genotyping revealed that the green plants followed a 2:1 ratio of heterozygous to WT (Table 3.2), which suggests that the presence of OSB-CoA ligase activity only in peroxisomes was not sufficient to complement the *aae14/aae14* mutant. Thus, these data suggest that OSB-CoA ligase activity is required in chloroplasts.

Table 3.1 Phenotyping results observed in progeny of heterozygous plants expressing *35S-EcMenE-PTS1*. p-value reported for a  $\chi^2$  test (df=1). The null hypothesis ( $H_0 = 3:1$  ratio of green to white plants) will be rejected at a p-value  $< 0.05$ . Failure to reject the null hypothesis (p-value  $> 0.05$ ) indicates the progeny followed a 3:1 ratio.

Line	green	pale	Ratio	$\chi^2$	p-value
<i>AAE14/aae14</i>	136	48	2.8:1	0.116	0.7335
EcMenE-PTS1 #1	167	43	3.9:1	2.292	0.1300
EcMenE-PTS1 #5	112	25	4.5:1	3.331	0.0680
EcMenE-PTS1 #6	174	60	2.9:1	0.051	0.8208
EcMenE-PTS1 #8	74	28	2.6:1	0.327	0.5676

Table 3.2 Genotyping results from  $>20$  green plants in progeny of heterozygous plants expressing *35S-EcMenE-PTS1*. p-value reported for a  $\chi^2$  test (df=2). The null hypothesis ( $H_0 = 1:2:0$  ratio) will be rejected at a p-value  $< 0.05$ .

Line	AAE14/AAE14	<i>aae14-1</i> /AAE14	<i>aae14-1/aae14-1</i>	Ratio	$\chi^2$	p-value
<i>AAE14/aae14</i>	9	13	0	1:1.4:0	0.568	0.7527
EcMenE-PTS1 #1	6	18	0	1:3:0	0.750	0.6873
EcMenE-PTS1 #5	7	18	0	1:2.6:0	0.320	0.8521
EcMenE-PTS1 #6	10	14	0	1:1.4:0	0.750	0.6873
EcMenE-PTS1 #8	9	15	0	1:1.7:0	0.188	0.9105

Next, to test if OSB-CoA ligase activity is required in peroxisomes, we recoded the Arabidopsis *AAE14* and removed its encoded PTS1, the final 9 base pairs (*35S-AAE14-plastidial*). Recoding was done so the native and introduced *AAE14* construct can be distinguished via qPCR. We then transformed this construct into heterozygous *AAE14/aae14* plants as above. After selecting for *35S-AAE14-plastidial* transformants, we genotyped and phenotyped the Basta-resistant plants. Out of 28 selected green plants expressing *35S-AAE14-plastidial*, all were found to be either heterozygous or WT at the *AAE14* locus (Table 3.3; p-value  $< 0.001$ ), allowing us to reject the null hypothesis that AAE14 is only necessary in the chloroplast. Thus, taken together, the functional complementation experiments indicate that OSB-CoA ligase activity is required in both peroxisomes and chloroplasts.

Table 3.3 Genotyping results from Basta-selected, green primary transformants of *AAE14/aae14* plants transformed with *35S-AAE14-plastidial*

Genotype	Observed	Expected	Chi square test
<i>AAE14/AAE14</i>	14	7	$\chi^2 = 14$
<i>AAE14/aae14</i>	14	14	p-value < 0.001
<i>aae14/aae14</i>	0	7	

### 3.4 Discussion

In this study, we provide genetic evidence for the involvement of the peroxisomal gene product of *Atlg60550* as the plant DHNS. Future work will require further testing of *Atlg60550-RNAi* lines to evaluate correlation of reduced expression of *Atlg60550* with reduction in phylloquinone. Additionally, we showed that OSB-CoA ligase is necessary in both the chloroplast and the peroxisome. Targeting the *E. coli* MenE to the peroxisome only or removing the native PTS1 of AAE14 to target it only to the chloroplast of *aae14* knockouts was not sufficient to complement the mutant. This suggests that OSB-CoA is formed in chloroplasts and is the pathway intermediate exported to peroxisomes.

The required dual localization of identical CoA-ligase activity in the phylloquinone pathway is reminiscent of that involved in synthesis of the 4-hydroxybenzoic acid (4-HBA) moiety of ubiquinone (Figure 3.6a). During 4-HBA biosynthesis, *p*-coumaric acid is ligated with CoA-SH by a 4-coumarate-CoA ligase (4CL) in the cytosol. Next, *p*-coumaroyl-CoA is recognized by the peroxisomal transporter peroxisomal ABC-transporter 1 (PXA1)<sup>22</sup>. PXA1 was shown to have intrinsic thioesterase activity<sup>23</sup> which cleaves the CoA-ester linkage and imports free *p*-coumaric acid into the peroxisome. Once in the peroxisome, other CoA ligases (4CL8 and At4g19010) re-ligate *p*-coumaric acid with CoA-SH and then the acyl-CoA product undergoes side chain shortening<sup>22,24</sup>. Our data suggest that OSB-CoA is exported out of the chloroplast due to the requirement for AAE14 in the chloroplast (Table 3.3). A model similar to the synthesis of 4-HBA from *p*-coumaroyl-CoA can be envisioned: the CoA moiety of OSB-CoA is cleaved upon export from the chloroplast or import into the peroxisome to release free OSB into the peroxisome that must be re-ligated with CoA-SH (Figure 3.6b). Instead of using different members of the acyl activating superfamily, however, the phylloquinone pathway appears to use the same enzyme, AAE14, targeted to both organelles. An alternative model is that OSB-CoA is exported out of

chloroplasts and imported into peroxisomes as OSB-CoA. The promiscuous activity of thioesterases (TEs) in peroxisomes, including DHNAT<sup>12</sup>, might hydrolyze OSB-CoA back to OSB, which would require the activity of AAE14 as part of a “metabolic repair” mechanism<sup>25</sup>. A similar thioesterase/CoA-ligase metabolic repair mechanism has been implicated for driving flux toward production of benzoic acid for synthesis of floral volatiles in petunia flowers<sup>26</sup>.

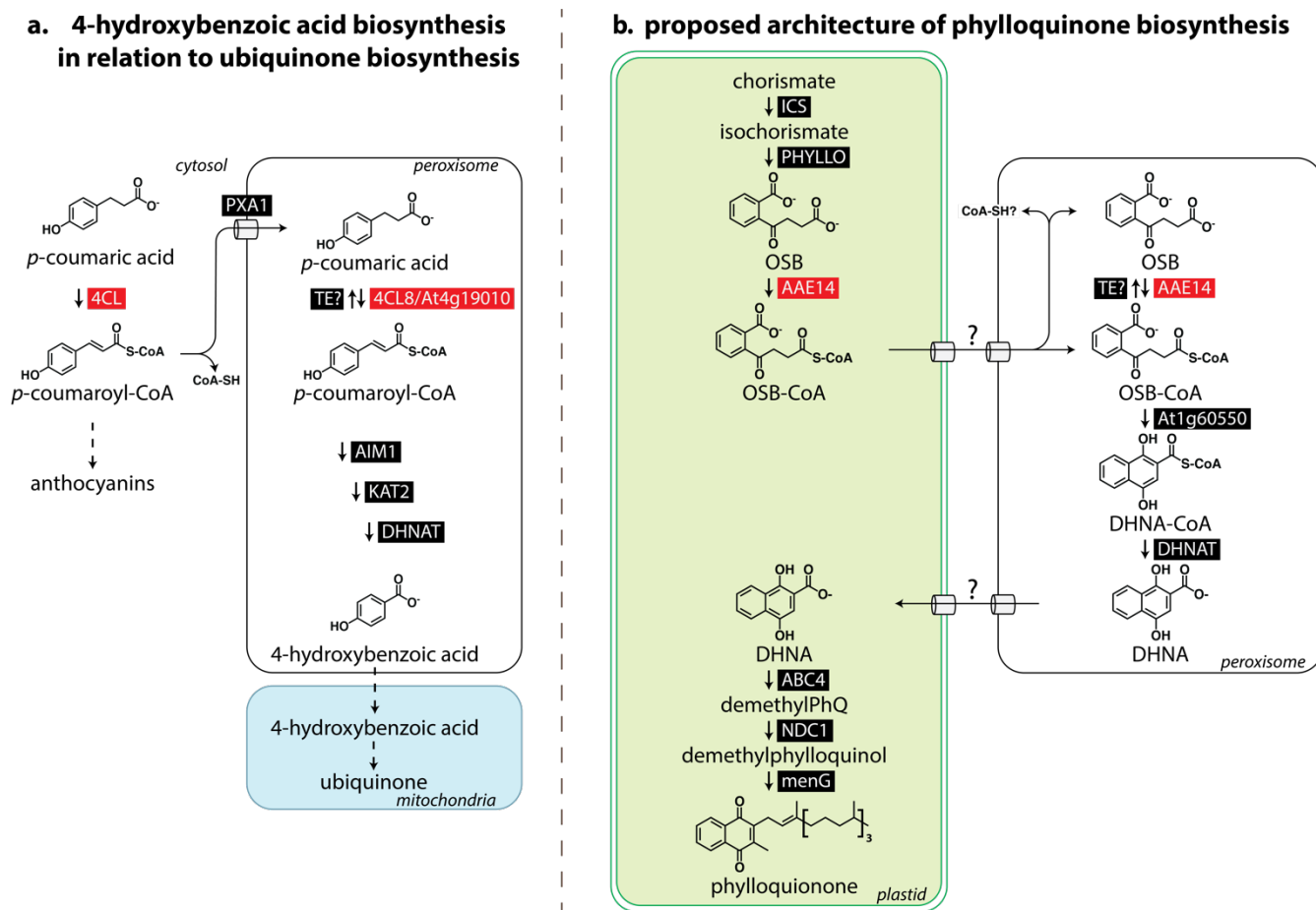


Figure 3.6 a. Established pathway architecture for synthesis of 4-hydroxybenzoic acid in relation to ubiquinone biosynthesis. b. Proposed new model for the subcellular architecture of the phylloquinone pathway.

With the reimagined subcellular architecture of the phylloquinone pathway, this opens the search for the transporters mediating the exchange of intermediates between chloroplasts and peroxisomes. Our findings indicate that OSB-CoA is exported out of the chloroplast. PXA1 is a known peroxisomal transporter acting on several CoA substrates, including other aromatic acyl-CoAs<sup>22</sup>, and would seem like a strong candidate to import OSB-CoA into peroxisomes.

Phylloquinone levels are unchanged in the *pxa1* knockout mutant<sup>22</sup>; however, the involvement of PXA1 in phylloquinone biosynthesis has not been directly tested and may be redundant with another peroxisomal transporter that compensates in the *pxa1* mutant. For transport of DHNA out of the peroxisome, it is unclear whether a transporter is involved or necessary, as the acid (protonated) form of products resulting from peroxisomal  $\beta$ -oxidation could in theory, albeit likely slowly, freely diffuse across the peroxisomal membrane<sup>26</sup>. As transporters are known to co-express with biosynthetic genes<sup>27</sup>, we evaluated the co-expression network of *AAE14* using the ATTED-II database (Table B.5). There are three transporters among the top 50 co-expressors of *AAE14*. The third co-expressor is *At1g78180*, a member of the mitochondrial substrate carrier family. *At1g78180* has been found in plastidial proteomes<sup>28,29</sup> and when using its gene as query against the ATTED-II database, *AAE14* and *ABC4*, the latter of which encodes the enzyme that uses DHNA in chloroplasts as substrate, are its top two co-expressors. Another transporter in the top 50 co-expressors of *AAE14* is a multi-drug and toxic compound extrusion (MATE) gene, *At2g38330*. *At2g38330* has also been found in plastidial proteomes<sup>28</sup> and the encoding gene is expressed in shoots, but shows low expression in roots<sup>30</sup>, consistent with a role in phylloquinone metabolism. The last transporter, *At2g37450*, is not predicted to contain a CTP (TargetP v2.0), PTS1, or PTS2<sup>20</sup>, nor has it been found in any proteome studies. Nonetheless, all of these are excellent candidates to explore as the chloroplast OSB-CoA exporter and/or DHNA importer. Once the responsible transport steps are identified, this will then allow investigation of whether transport limits flux through the pathway, which is important for metabolic engineering attempts aimed at increasing the phylloquinone (vitamin K<sub>1</sub>) content of food or production of other specialized 1,4-naphthoquinone metabolites.

The compartmental split of the phylloquinone pathway between chloroplasts and peroxisomes likely predates the evolution of land plants as the same subcellular architecture is apparent in modern green algae<sup>31</sup>. Given that the phylloquinone pathway was acquired during the plastid endosymbiosis event and that in some modern red algae the phylloquinone (menaquinone) pathway is encoded in the plastid genome<sup>32</sup>, the ancestral state was probably an all-chloroplast pathway. What physiological consequences led green algae to evolve the compartmental split between chloroplasts and peroxisomes is an open question. One potential hypothesis is that the susceptibility of DHNA-CoA to oxidation<sup>33</sup> would lead to the production of a metabolically “dead-end” intermediate in the chloroplast. As a result of the light reactions of photosynthesis, the

chloroplast is full of potent oxidizing agents like superoxide anions, hydrogen peroxide, hydroxyl radicals, and singlet oxygen<sup>34</sup>. While peroxisomes contain high levels of hydrogen peroxide derived from  $\beta$ -oxidation, they are also the site with highest activity of catalase used to convert hydrogen peroxide to water and oxygen<sup>35</sup>. Thus, it can be envisioned that it became advantageous in the green lineage to compartmentally separate the vital, yet susceptible, intermediate DHNA-CoA away from the chloroplast environment. Perhaps another driving force for the compartmental split of the phylloquinone pathway has to do with the redox nature of DHNA and its lack of a tethering membrane anchor. It can be imagined that soluble DHNA produced in the chloroplast would be free to interrupt electron transport or otherwise inhibit photosynthesis. Consistent with the idea of controlling the pool of free DHNA in chloroplasts is that upon its import from peroxisomes into chloroplasts, DHNA is conjugated with a phytyl side chain by ABC4, a chloroplast membrane protein<sup>13</sup>. Nonetheless, if DHNA-CoA oxidation and/or freely soluble DHNA in chloroplasts posed existential or deleterious metabolic consequences, they would have *a priori* been solved by cyanobacteria prior to the evolution of chloroplasts.

Free CoA-SH levels in the chloroplast are known to be low, with most of the CoA (>88%) in the chloroplast existing as acetyl-CoA<sup>36</sup>, presumably for fatty acid biosynthesis. The fact that the peroxisomal steps of the phylloquinone pathway are connected with CoA metabolism could suggest that the selective pressure to move these reactions out of chloroplasts was connected to fatty acid synthesis. Given the relatively small pool size of phylloquinone compared to fatty acids, however, this was unlikely a contributing factor, especially considering that a CoA molecule is anyway exported with every model of OSB-CoA. Interestingly, phylloquinone and ubiquinone biosynthesis are not the only pathways that localize their CoA-dependent steps to the peroxisome. Fatty acid  $\beta$ -oxidation, auxin biosynthesis, jasmonate biosynthesis, and benzoic acid metabolism also localize CoA-dependent parts of their pathway to the peroxisome (reviewed in<sup>1,2</sup>). This may point to peroxisomes having evolved an environment better suited to carry out such reactions or better able to manage the byproducts of  $\beta$ -oxidative metabolism. An intriguing way to test this hypothesis would be to attempt complementation of the *Atlg60550-RNAi* lines with an all-chloroplast phylloquinone pathway, in which the DHNS and DHNAT enzymes are expressed in the chloroplast. Combined with future investigations to identify OSB-CoA and DHNA transporters, using the same strategy to design an all-chloroplast pathway but done in a wild-type background

would allow testing the control that transport of intermediates exerts on control of flux through the phylloquinone pathway.

### **3.5 Materials and methods**

#### **3.5.1 Chemical reagents and general experimental procedures**

Standards of phylloquinone and menaquinone-4 were purchased from Sigma-Aldrich. Murashige and Skoog media was purchased from PhytoTech laboratories. Basta (1% solution), timentin, and plant agar were from plantmedia.com. Unless otherwise specified, all other reagents and materials were purchased from Fisher Scientific. Ultra-pure water and chromatography-grade solvents were used for all metabolic profiling. HPLC analyses were carried out on an Agilent 1260 Infinity series instrument (Agilent Technologies) equipped with diode array and fluorometer detection modules employing Chemstation software.

#### **3.5.2 Plant materials and growth conditions**

*Arabidopsis thaliana* (ecotype Col-0) was used as genetic background for all experiments. *aae14-1* (SALK\_060226) was obtained from the Arabidopsis Biological Resource Center at Ohio State University (<https://abrc.osu.edu/researchers>). Seeds were germinated on half-strength Murashige-Skoog (MS) media containing 1% sucrose, 2.2 g/L Gelzan™ CM (plantmedia.com), and appropriate selectable marker(s). Timentin was included at 200 mg/L when selecting seeds from a floral dip to reduce growth of *Agrobacterium*. Basta was used at 10 mg/L, hygromycin at 20 mg/L, and kanamycin at 100 mg/L for selection of transformed plants. When kanamycin was the selectable marker, 3 g/L Plant Agar was substituted for Gelzan.

#### **3.5.3 Plant genotyping and quantitative expression analysis**

*aae14/aae14* is seedling-lethal, so seed stocks were maintained from heterozygous plants, determined by genotyping. Genotyping of *aae14* was done using the gene-specific primers (P1 and P2) identified in Kim et al.<sup>10</sup> and LBa1 (P3) (see Table B.6 for a list of primers used in this study). Total RNA was extracted from leaves following the manufacturer protocol with the RNeasy Plant Mini Kit (Qiagen). DNase treatment and clean up were done following

manufacturer instructions with the RNA Clean and Concentrator-5 Kit (Zymo). cDNA synthesis was performed by 5X All-In-One RT MasterMix (abm) according to manufacturer instructions using 150 ng of total RNA.

#### **3.5.4 Generation of *At1g60550-RNAi* lines**

For the *At1g60550-RNAi* construct, DNA containing two spliced *At1g60550* cDNA fragments of the coding region corresponding to nucleotides 110-502 and 110-465, the latter in antisense orientation to create a hairpin structure, was synthesized (Genscript, Piscataway, NJ). 5'-CACC was added for subcloning into pENTR/D-TOPO (Invitrogen), sequence verified, and transferred into the destination vector, pB2GW7 by recombination using LR Clonase II (Invitrogen).

#### **3.5.5 Generation of transgenic *Arabidopsis* with a single organellar OSB-CoA ligase**

The coding sequence of *E. coli* menE was codon-optimized for expression in plants and synthesized by GenScript. The recoded sequence was amplified without its stop codon and a PTS1 (amino acids SRL) and stop codon were added with the reverse primer (P4 and P5). The EcMenE-PTS1 construct was cloned using pENTR/D-TOPO (Invitrogen) and sequence verified. The overexpression construct was generated by transferring EcMenE-PTS1 to pB2GW7 (overexpression) with LR Clonase II (Invitrogen).

The full-length coding sequence of AAE14 was recoded by Twist Biosciences for use as a positive control in the Gateway-compatible pTwistENTR. Recoding was done to be able to distinguish native gene expression from the complementation construct. For the full-length construct, recoded AAE14 was transferred to pB2GW7 (overexpression) with LR Clonase II (Invitrogen). To generate the plastid-only AAE14, the recoded *AAE14* was amplified with a CACC for cloning into pENTR/D-TOPO (Invitrogen) without its native PTS1 with primers P6 and P7. After cloning into pENTR/D-TOPO and sequence verification, *AAE14-plastidial* was transferred to pB2GW7 with LR Clonase II.

The constructs were transformed into *Agrobacterium tumefaciens* (strain GV3101) with the freeze-thaw method described previously<sup>37</sup>. Heterozygous *AAE14/aae14* plants were

transformed with the EcMenE-PTS1, full-length *AAE14*, and *AAE14-plastidial* constructs, as well as pB2GW7 and pH2GW7 alone, using the floral dip procedure described by Zhang et al<sup>38</sup>.

### 3.5.6 Functional complementation of *E. coli* and menaquinone analysis

In order to determine whether addition of a peroxisomal targeting signal or codon optimization affects activity of the *E. coli* MenE, a complementation experiment was performed using the *E. coli* *AmenE* knockout strain JW2255-1<sup>39</sup>. The native *E. coli* menE was amplified as a positive control from *E. coli* genomic DNA using gene-specific primers (P8 and P9) that added a 5'-KpnI site and a 3'-SalI site. Recoded *E. coli* menE with a peroxisomal targeting signal was amplified from the pENTR/D-TOPO: EcMenE-PTS1 generated above with primers adding a 5'-KpnI and a 3'-SalI (P10 and P11). Polymerase chain reaction (PCR) products were digested with KpnI/SalI and cloned into pBad33 (Novagen). Competent JW2255-1 and ME9062 (WT) were generated by the method described by Chung et al.<sup>40</sup>.

For complementation, 3 JW2255-1 colonies transformed with pBad33 (empty vector), pBad33-EcMenE (native gene), and pBad33-EcMenE-PTS1 were selected. 3 colonies of WT transformed with pBad33 were used as a positive control. Starter cultures were grown in LB with appropriate antibiotics overnight at 37°C. 1 mL starter culture was pelleted, washed twice with 1 mL of sterile water, and diluted to OD<sub>600</sub>=2. 500 µL of the diluted culture was added to approximately 12 mL of 1X M9 salts with 2 mM MgSO<sub>4</sub> and 0.1 mM CaCl<sub>2</sub> with 40 mM sodium fumarate and 40 mM lactate to promote anaerobic growth. 0.2% (w/v) arabinose was added to induce the promoter of pBad33. Complementation cultures were grown in glass tubes with as little headspace as possible to support anaerobic growth. The cultures were grown for 6 days at 37°C with 50 rpm shaking. Cells were pelleted by centrifugation, washed with sterile water twice, and resuspended in 650 µL water. 100 µL was used to take an OD and 500 µL was used for menaquinone extraction in a procedure similar to Kim et al<sup>10</sup>.

Briefly, 500 µL of cells were moved to a pyrex tube with 1 mL of 95% ethanol. 133 pmol of phyloquinone was added as internal standard. After mixing, the samples were incubated at 70°C for 1 hour. 500 µL water was added and quinones were extracted twice with 2.5 mL hexanes. The hexane layers were dried and the samples were resuspended in 500 µL methanol. 25 µL was analyzed by HPLC with fluorescence detection on a 5 µm Zorbax SB-C18 column (4.6 mm x 250 mm) held at 30°C. Samples were eluted in isocratic mode at a flow rate of 1 mL min<sup>-1</sup> for 50

minutes with methanol: ethanol (80:20, v/v) containing 1 mM sodium acetate, 2 mM acetic acid and 2 mM ZnCl<sub>2</sub>. Phylloquinone and menaquinone were detected by fluorescence (excitation 238 nm, emission 426 nm) following post-column chemical reduction as described previously<sup>41</sup>.

### 3.5.7 Subcellular localization

For the native promoter construct, 2.5 kb upstream of the start codon and the *Atlg60550* coding sequence was synthesized with codon-optimization of the first exon for GC content and the coding sequence of GFP in the middle of the 6<sup>th</sup> exon by Twist Bioscience with a 5'-SbfI and a 3'-SacI site. The promoter was dropped out of the vector pBI121 with SbfI/SacI and the native promoter construct was ligated in using NEB T4 Ligase (NEB).

EcMenE-PTS1 was transferred from pENTR/D-TOPO to pK7WGF2 to generate a GFP-EcMenE-PTS1 fusion as described above. The coding sequence of the recoded AAE14 was amplified, with a 5'-CACC and without its peroxisomal targeting signal or stop codon, with primers P6 and P12, cloned into pENTR/D-TOPO (Invitrogen) and sequence verified, and recombined into pK7FWG2 to generate a AAE14 without its PTS1 – GFP fusion as described above.

cDNA for *Atlg60550* (U90655) was obtained from the Arabidopsis Biological Resource Center (ABRC). The coding sequence of *Atlg60550* was amplified with a 5'-CACC for Gateway cloning and without its stop codon (primers P13 and P14) and cloned into pENTR/D-TOPO. After sequence verification, *Atlg60550* was recombined into pK7FWG2 to generate a C-terminal GFP fusion construct.

Localization constructs were transformed into *A. tumefaciens* and dipped into WT *Arabidopsis* as described above or transiently expressed in *Nicotiana benthamiana* as described previously<sup>42</sup>. The px-rb (CD3-984) construct, containing mCherry fused to a PTS1<sup>43</sup>, was used as a peroxisomal marker. Images were acquired using a Zeiss Axio Examiner.Z1 upright microscope with Zen Blue analysis software (Zeiss).

### 3.5.8 Phylloquinone analysis

All steps were performed in reduced light to reduced photodegradation of quinones. To quantify phylloquinone, 100-200 mg of ground leaf tissue was extracted at 4°C overnight with

shaking in 5 mL methanol containing 900 pmol menaquinone-4 (MK-4) as internal standard. The methanol was moved to a clean tube and dried before resuspending the sample in 1.6 mL of 62.5% methanol. Phylloquinone was extracted with 5 mL hexane twice. The hexane layers were combined and dried. Samples were resuspended in 500  $\mu$ L methanol and 25  $\mu$ L was analyzed by HPLC-fluorescence as described previously<sup>41</sup>.

### 3.6 References

1. Pan, R., Liu, J., Wang, S. & Hu, J. Peroxisomes: versatile organelles with diverse roles in plants. *New Phytol.* **225**, 1410–1427 (2020).
2. Kao, Y. T., Gonzalez, K. L. & Bartel, B. Peroxisome function, biogenesis, and dynamics in plants. *Plant Physiol.* **176**, 162–177 (2018).
3. Widhalm, J. R. & Rhodes, D. Biosynthesis and molecular actions of specialized 1,4-naphthoquinone natural products produced by horticultural plants. *Hortic. Res.* **3**, 16046 (2016).
4. Li, W. *et al.* Structure of a bacterial homologue of vitamin K epoxide reductase. *Nature* **463**, 507–512 (2010).
5. Singh, A. K., Bhattacharyya-Pakrasi, M. & Pakrasi, H. B. Identification of an atypical membrane protein involved in the formation of protein disulfide bonds in oxygenic photosynthetic organisms. *J. Biol. Chem.* **283**, 15762–15770 (2008).
6. Furt, F. *et al.* A bimodular oxidoreductase mediates the specific reduction of phylloquinone (vitamin K1) in chloroplasts. *Plant J.* **64**, 38–46 (2010).
7. Gu, X., Harding, S. A., Nyamdari, B., Aulakh, K. B. & Clermont, K. A role for phylloquinone biosynthesis in the plasma membrane as revealed in a non-photosynthetic parasitic plant. *bioRxiv* (2018). doi:10.1101/257519
8. van Oostende, C., Widhalm, J. R., Furt, F., Ducluzeau, A. L. & Basset, G. J. Vitamin K1 (Phylloquinone): Function, enzymes and genes. *Advances in Botanical Research* **59**, (2011).
9. Gross, J. *et al.* A plant locus essential for phylloquinone (vitamin K1) biosynthesis originated from a fusion of four eubacterial genes. *J. Biol. Chem.* **281**, 17189–17196 (2006).
10. Kim, H. U., Oostende, C. Van, Basset, G. J. C. & Browse, J. The AAE14 gene encodes the Arabidopsis *o*-succinylbenzoyl-CoA ligase that is essential for phylloquinone synthesis and photosystem-I function. *Plant J.* **54**, 272–283 (2008).

11. Sharma, V., Suvarna, K., Meganathan, R. & Hudspeth, M. E. S. Menaquinone (vitamin K<sub>2</sub>) biosynthesis: Nucleotide sequence and expression of the menB gene from *Escherichia coli*. *J. Bacteriol.* **174**, 5057–5062 (1992).
12. Widhalm, J. R. *et al.* Phylloquinone (vitamin K<sub>1</sub>) biosynthesis in plants: two peroxisomal thioesterases of lactobacillales origin hydrolyze 1,4-dihydroxy-2-naphthoyl-CoA. *Plant J.* **71**, 205–215 (2012).
13. Shimada, H. *et al.* Inactivation and deficiency of core proteins of photosystems I and II caused by genetical phylloquinone and plastoquinone deficiency but retained lamellar structure in a T-DNA mutant of Arabidopsis. *Plant J.* **41**, 627–637 (2005). doi:10.1111/j.1365-313X.2004.02326.x
14. Fatihi, A. *et al.* A dedicated Type II NADPH dehydrogenase performs the penultimate step in the biosynthesis of vitamin K<sub>1</sub> in *Synechocystis* and Arabidopsis. *Plant Cell* **27**, 1730–1741 (2015).
15. Lohmann, A. *et al.* Deficiency in phylloquinone (vitamin K<sub>1</sub>) methylation affects prenyl quinone distribution, photosystem I abundance, and anthocyanin accumulation in the *Arabidopsis AtmenG* mutant. *J. Biol. Chem.* **281**, 40461–40472 (2006).
16. Song, H. & Guo, Z. Characterization of 1,4-dihydroxy-2-naphthoyl-coenzyme A synthase (MenB) in phylloquinone biosynthesis of *Synechocystis* sp. PCC 6803. *Sci. China Chem.* **55**, 98–105 (2012).
17. Babujee, L. *et al.* The proteome map of spinach leaf peroxisomes indicates partial compartmentalization of phylloquinone (vitamin K<sub>1</sub>) biosynthesis in plant peroxisomes. *J. Biol. Chem.* **61**, 1441–1453 (2010).
18. Obayashi, T. *et al.* ATTED-II: A database of co-expressed genes and cis elements for identifying co-regulated gene groups in Arabidopsis. *Nucleic Acids Res.* **35**, 4–6 (2007).
19. Mi, H. *et al.* Protocol Update for large-scale genome and gene function analysis with the PANTHER classification system (v.14.0). *Nat. Protoc.* **14**, 703–721 (2019).
20. Reumann, S. Specification of the peroxisome targeting signals type 1 and type 2 of plant peroxisomes by bioinformatics analyses. *Plant Physiol.* **135**, 783–800 (2004).
21. Reumann, S. *et al.* Proteome analysis of Arabidopsis leaf peroxisomes reveals novel targeting peptides, metabolic pathways, and defense mechanisms. *Plant Cell Online* **19**, 3170–3193 (2007).

22. Block, A. *et al.* The origin and biosynthesis of the benzenoid moiety of ubiquinone (Coenzyme Q) in Arabidopsis. *Plant Cell* **26**, 1938–1948 (2014).
23. De Marcos Lousa, C. *et al.* Intrinsic acyl-CoA thioesterase activity of a peroxisomal ATP binding cassette transporter is required for transport and metabolism of fatty acids. *Proc. Natl. Acad. Sci. U. S. A.* **110**, 1279–1284 (2013).
24. Soubeyrand, E. *et al.* Arabidopsis 4-COUMAROYL-COA LIGASE 8 contributes to the biosynthesis of the benzenoid ring of coenzyme Q in peroxisomes. *Biochem. J.* **476**, 3521–3532 (2019). doi:<https://doi.org/10.1042/BCJ20190688>
25. Hanson, A. D., Henry, C. S., Fiehn, O. & de Crécy-Lagard, V. Metabolite damage and metabolite damage control in plants. *Annu. Rev. Plant Biol.* **67**, annurev-arplant-043015-111648 (2016).
26. Adebessin, F., Widhalm, J. R., Lynch, J. H., McCoy, R. M. & Dudareva, N. A peroxisomal thioesterase plays auxiliary roles in plant  $\beta$ -Oxidative benzoic acid metabolism. *Plant J.* **93**, (2018).
27. Widhalm, J. R. *et al.* Identification of a plastidial phenylalanine exporter that influences flux distribution through the phenylalanine biosynthetic network. *Nat. Commun.* **6**, (2015).
28. Tomizioli, M. *et al.* Deciphering thylakoid sub-compartments using a mass spectrometry-based approach. *Mol. Cell. Proteomics* **13**, 2147–2167 (2014).
29. Ferro, M. *et al.* Integral membrane proteins of the chloroplast envelope: identification and subcellular localization of new transporters. *Proc. Natl. Acad. Sci. U. S. A.* **99**, 11487–11492 (2002).
30. Liu, J., Magalhaes, J. V., Shaff, J. & Kochian, L. V. Aluminum-activated citrate and malate transporters from the MATE and ALMT families function independently to confer Arabidopsis aluminum tolerance. *Plant J.* **57**, 389–399 (2009).
31. Emonds-Alt, B., Coosemans, N., Gerards, T., Remacle, C. & Cardol, P. Isolation and characterization of mutants corresponding to the MENA, MENB, MENC and MENE enzymatic steps of 5'-monohydroxyphyllquinone biosynthesis in *Chlamydomonas reinhardtii*. *Plant J.* **89**, 141–154 (2017).
32. Gross, J., Meurer, J. & Bhattacharya, D. Evidence of a chimeric genome in the cyanobacterial ancestor of plastids. *BMC Evol. Biol.* **8**, 1–12 (2008).

33. Chen, M., Jiang, M., Sun, Y., Guo, Z. F. & Guo, Z. Stabilization of the second oxyanion intermediate by 1,4-dihydroxy-2-naphthoyl-coenzyme a synthase of the menaquinone pathway: Spectroscopic evidence of the involvement of a conserved aspartic acid. *Biochemistry* **50**, 5893–5904 (2011).
34. Kim, C. ROS-Driven Oxidative Modification: Its Impact on Chloroplasts-Nucleus Communication. *Front. Plant Sci.* **10**, 1–6 (2020).
35. Neill, S., Desikan, R. & Hancock, J. Hydrogen peroxide signalling. *Curr. Opin. Plant Biol.* **5**, 388–395 (2002).
36. Post-Beittenmiller, D., Roughan, G. & Ohlrogge, J. B. Regulation of Plant Fatty Acid Biosynthesis. *Plant Physiol.* **100**, 923–930 (1992).
37. Cui, W., Liu, W. & Wu, G. A simple method for the transformation of *Agrobacterium tumefaciens* by foreign DNA. *Chin. J. Biotechnol.* **11**, 267–274 (1995).
38. Zhang, X., Henriques, R., Lin, S. S., Niu, Q. W. & Chua, N. H. Agrobacterium-mediated transformation of *Arabidopsis thaliana* using the floral dip method. *Nat. Protoc.* **1**, 641–646 (2006).
39. Baba, T. *et al.* Construction of *Escherichia coli* K-12 in-frame, single-gene knockout mutants: The Keio collection. *Mol. Syst. Biol.* **2**, 2006.0008 (2006).
40. Chung, C. T., Niemela, S. L. & Miller, R. H. One-step preparation of competent *Escherichia coli*: transformation and storage of bacterial cells in the same solution. *Proc. Natl. Acad. Sci. U. S. A.* **86**, 2172–2175 (1989).
41. McCoy, R. M., Utturkar, S. M., Crook, J. W., Thimmapuram, J. & Widhalm, J. R. The origin and biosynthesis of the naphthalenoid moiety of juglone in black walnut. *Hortic. Res.* **5**, 67 (2018).
42. Sparkes, I. A., Runions, J., Kearns, A. & Hawes, C. Rapid, transient expression of fluorescent fusion proteins in tobacco plants and generation of stably transformed plants. *Nat. Protoc.* **1**, 2019–2025 (2006).
43. Nelson, B. K., Cai, X. & Nebenfu, A. A multicolored set of in vivo organelle markers for co-localization studies in *Arabidopsis* and other plants. *Plant J.* **51**, 1126–1136 (2007). doi:10.1111/j.1365-313X.2007.03212.x

## CHAPTER 4. ALLELOPATHY AS AN EVOLUTIONARILY STABLE STRATEGY

### 4.1 Abstract

Plants compete for the finite resources available in an area with surrounding organisms. Plants can increase their competitive ability through allelopathy, which is the release of a toxic chemical, an allelochemical, into the environment by a plant to inhibit the growth and development of competing organisms. Plant allelochemicals offer promising candidates for developing novel herbicides (e.g. juglone) and some have been implicated in the invasion success of invasive species, like Paterson's curse (*Echium plantagineum* L.). Despite the importance of allelochemicals, the circumstances and conditions that favor the development and maintenance of allelochemicals is not well understood. In order to gain insight into the cost and benefit of allelopathy, we have developed a 2-by-2 matrix game to model the interaction between plants that produce allelochemicals and plants that do not. Production of an allelochemical introduces novel cost to a plant, both in terms of synthesis and in detoxifying a toxic chemical but may also convey a competitive advantage. A plant that does not produce an allelochemical will suffer the cost of encountering one. Our model predicts three cases, in which the evolutionarily stable strategies are different. In the first, the non-allelopathic plant is a stronger competitor, and not producing allelochemicals is the evolutionarily stable strategy. In the second, the allelopathic plant is the better competitor and production of allelochemicals is the more beneficial strategy. In the last case, neither is the evolutionarily stable strategy. Instead, there are alternating stable states, depending on whether the allelopathic or non-allelopathic plant arrived first. Our model sheds light on the circumstances leading to the evolution of allelochemicals. One potential application of this model is in the engineering of crops that produce allelochemicals for weed control. In this case, the cost of production and detoxification of the allelochemical should remain low enough that the crop is able to grow while suppressing weed species.

### 4.2 Introduction

Competition is ubiquitous in the natural world, as there are a finite number of resources available in a given space<sup>1-3</sup>. Thus, competition generally reduces plant fitness when resources,

such as light, space, and water are limiting<sup>4,5</sup>. This type of competition for finite resources is broadly named resource competition and occurs when organisms compete by simply reducing the availability of resources to other organisms<sup>6</sup>. Alternatively, interference competition occurs when one organism interferes with, and therefore reduces, the ability of the other to obtain a shared resource while not necessarily drawing down resource concentrations<sup>6</sup>. Animals routinely face interference competition as they can physically fight over resources<sup>7</sup>. Sessile plants primarily compete via resource competition. However, one of the major mechanisms of interference competition in plants is mediated chemically through allelopathy<sup>8</sup>.

Allelopathy is production of chemicals (often called allelochemicals) that are released into the environment and negatively affect the growth and development of competing individuals<sup>9</sup>. Although the term was first used in 1937, the effect has been described for thousands of years<sup>9</sup>. There have been difficulties in studying the competitive effects of allelopathy because of methodological difficulties (e.g.<sup>10,11</sup>). However, one of the best documented examples is allelopathy by walnut trees (*Juglans* spp.), mediated by the allelochemical juglone, which is toxic to a variety of crop and horticultural species, including corn and soybean<sup>12</sup> and tomato and cucumber<sup>13</sup>.

Allelopathy has been implicated in the success of some invasive plants, highlighting the advantage of interference competition as a strategy<sup>14</sup>. Invasion by non-native species is ranked the second strongest risk to natural diversity<sup>15</sup>. For example, Paterson's curse (*Echium plantagineum* L.) is an invasive weed in Australia, affecting up to 30 Mha, whose invasion success is partially attributed to production of the allelochemical shikonin and its derivatives<sup>16</sup>. One commonly invoked mechanism for invasion by non-native species is the novel weapons hypothesis, which suggests invasive species are successful through use of competitive strategies for which native species have not co-evolved counter strategies<sup>17,18</sup>. This mechanism has been linked to the invasion success of Policeman's helmet (*Impatiens glandulifera*)<sup>19</sup>. It releases a compound structurally similar to shikonin called 2-methoxy-1,4-naphthoquinone (2-MNQ) that elicits negative effects on herb germination and mycelium growth and is otherwise absent in soils without *I. glandulifera*, thus suggesting 2-MNQ may function as a "novel weapon."<sup>19-21</sup>.

Despite the potential advantages of allelochemicals as a tool for interference competition, they seem to have only rarely evolved. Here, we develop an evolutionary game theoretic model to probe the benefits and circumstances that might favor the evolution of allelochemicals.

Specifically, we ask: 1) What circumstances favor the production of allelochemicals? 2) How does the cost of producing an allelochemical affect fitness of the plant producing the allelochemical and plants competing with that plant? 3) When will allelopathic plants be stable in a population?

### 4.3 Model

In what follows, we develop a two-by-two matrix game of interactions among a plant player with (+A) and without (-A) allelopathy. The proportion of plants in a population producing or not producing allelochemicals is represented by  $p$  and  $(1 - p)$ , respectively. We envision that competition is for the benefits of available resources ( $B$ ), that the cost ( $C$ ) to the player of producing allelochemicals is the sum of the costs of production of the allelochemical and detoxification to prevent autotoxicity, and that allelochemicals impose some different cost to the opponent in the form of toxicity and/or detoxification ( $T$ ). These parameters of the model should adhere to the following:  $0 < B, C, T$  and  $\frac{1}{2} < a \leq 1$ ,  $0 \leq p \leq 1$  (see appendix C). Combining these parameters, we can derive the payoff,  $G_{v,u}$ , across several competitive contexts where  $v$  is the focal plant strategy (+A or -A), and  $u$  is the neighboring plant strategy (+A or -A). Finally, we also assume that there are two plants competing in something like a pot experiment, because we imagine this is the most likely way to empirically test our model in the future. However, the equations below can be extended to any number of competing plants by simply replacing 2 with  $N$ , where  $N$  is the number of competing plants.

First, when both plants produce allelochemicals, we argue that they will, on average, share the total benefit of the soil volume equally,  $\frac{B}{2}$ , but will also pay the cost of producing and detoxifying allelochemicals,  $C$ . Thus, the fitness pay-off to a plant in a population of pure +A plants is:

$$G_{+A,+A} = \frac{B}{2} - C \quad (\text{equation 1})$$

Second, in a mixed population of +A and -A plants, the +A plant will pay the cost  $C$ , but will share the benefits  $B$  differently. Instead of equally sharing the benefits, the player will get a proportion of benefits,  $a$ , that takes into account the competitive advantage of production of allelochemicals according to:

$$G_{+A,-A} = aB - C \quad (\text{equation 2})$$

Inversely, in the mixed population, the  $-A$  plant obtains the remaining benefit, represented by  $(1-a)B$ , and pays the cost of toxicity,  $T$ , according to:

$$G_{-A,+A} = (1 - a)B - T \quad (\text{equation 3})$$

Finally, in a pure population of  $-A$  plants, because no plant produces allelochemicals, they merely share the benefits as  $\frac{B}{2}$  and have no costs associated with allelochemicals, according to:

$$G_{-A,-A} = \frac{B}{2} \quad (\text{equation 4})$$

Combined, equations 1-4 yield the pay-off matrix shown as Figure 4.1.

		Opponent	
		$+A$	$-A$
Player	$+A$	$\frac{B}{2} - C$	$aB - C$
	$-A$	$(1 - a)B$ $- T$	$\frac{B}{2}$

Figure 4.1 Symmetric pay-off matrix for competition between plants that either produce allelochemicals ( $+A$ ) or not ( $-A$ ). See text for parameter definitions.

### 4.3.1 Evolutionarily stable strategy definition

In a matrix game, an evolutionarily stable strategy (ESS) is identical to a Nash equilibrium<sup>22,23</sup>. A pure ESS is defined as the strategy which once adopted by members of a population cannot be invaded by any alternative strategy. Mixed ESSs are also permissible where multiple strategies either ecologically coexist through evolutionary time or form non-coexisting alternative stable states (sometimes also called priority effects). Here, in a two-by-two matrix game, if  $G_{v,u}$  is the fitness payoff of a focal plant species using strategy ‘ $v$ ’ against a competing plant species using strategy ‘ $u$ ’ such that  $v \neq u$ , then  $v$  is a pure ESS if and only if:  $G_{v,v} > G_{u,v}$  and  $G_{v,u} > G_{u,u}$ . Alternatively,  $u$  is a pure ESS when  $G_{u,v} > G_{v,v}$  and  $G_{u,u} > G_{v,u}$  (*i.e.* under the opposite inequalities). Most interestingly, under this definition mixed ESS solutions are possible where the two strategies may coexist or for a system of alternative stable states<sup>2</sup>. A mixed ESS occurs when:  $G_{u,v} > G_{v,v}$  and  $G_{v,u} > G_{u,u}$ . Alternative stable states occur when:  $G_{v,v} > G_{u,v}$  and  $G_{u,u} > G_{v,u}$ .

Together, a keen observer will note that these four inequalities form all possible pairs of inequalities within each column of a two-by-two payoff matrix (Figure 4.1).

## 4.4 Results

### 4.4.1 Pure evolutionarily stable strategies

For  $+A$  to be a pure ESS,  $+A$  needs to be able to (i) invade a population of  $-A$  and (ii) resist invasion from  $-A$ . According to the ESS definition, this occurs when:

$$aB - C > \frac{B}{2} \text{ and } \frac{B}{2} - C > B(1 - a) - T \quad (\text{equations 5a})$$

Equations 5a can be rearranged into isoclines in  $B$  and  $C$  space to find:

$$B > \frac{2C}{2a-1} \text{ and } B > \frac{2(C-T)}{2a-1} \quad (\text{equations 5b})$$

Alternatively, for  $-A$  to be ESS,  $-A$  needs to be able to (i) invade a population of  $+A$  and (ii) resist invasion from  $+A$ .

$$\frac{B}{2} > aB - C \text{ and } (1 - a)B - T > \frac{B}{2} - C \quad (\text{equations 6a})$$

Equations 6a can be rearranged to find:

$$B < \frac{2C}{2a-1} \text{ and } B < \frac{2(C-T)}{2a-1} \quad (\text{equations 6b})$$

Notice that equations 5 and 6 are simply opposite inequalities.

### 4.4.2 Mixed evolutionarily stable strategies

The mixed strategy, where there are alternating stable states such that either  $-A$  or  $+A$  can resist invasion from the other strategy occurs when,

$$\frac{B}{2} < aB - C \text{ and } (1 - a)B - T > \frac{B}{2} - C \quad (\text{equations 7a})$$

Equations 7a can be rearranged to find:

$$B < \frac{2C}{2a-1} \text{ and } B > \frac{2(C-T)}{2a-1} \quad (\text{equations 7b})$$

The isoclines in equations 5-7 create two parallel lines, each with slope  $\frac{2}{2a-1}$ , but that either intercept the y-axis at 0 or at  $\frac{-2T}{2a-1}$ . Thus, depending on the values of  $a$  and  $T$ , we can plot the entire solution space graphically in  $B$  and  $C$  phase space (Figure 4.2). For  $+A$  to be the ESS, the parameters need to be above both isoclines. For  $-A$  to be the ESS, the parameters need to be below

both isoclines. Between the two lines, which will never cross as they have the same slope, there is a region of alternative stable states (*i.e.* priority effect). In our model, coexistence is never possible. For it to be so, would require;

$$\frac{2C}{2a-1} < B < \frac{2(C-T)}{2a-1}. \quad (\text{equation 8})$$

Because  $T > 0$  by definition, these conditions can never be met. This suggests that within a population, all plants of a species will either produce or not produce allelochemicals.

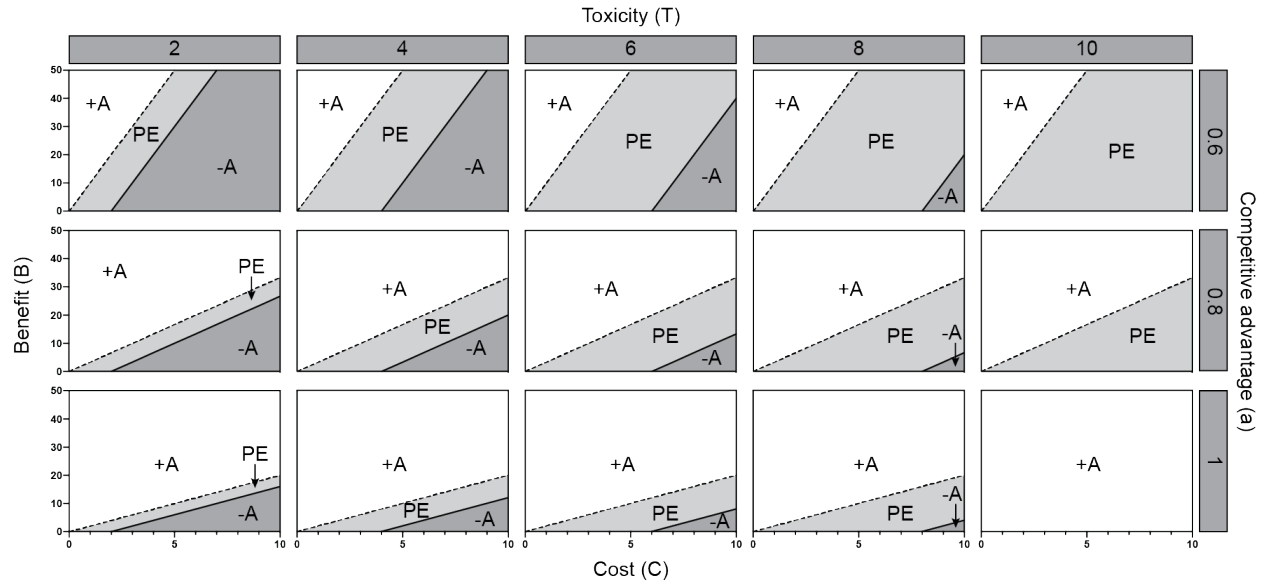


Figure 4.2 Isoclines that depict ESS states in  $B$  and  $C$  phase space depending on the value of  $T$  (columns) or  $a$  (rows). The dashed line represents the isocline  $B = \frac{2C}{2a-1}$ . The solid line represents the isocline  $B = \frac{2(C-T)}{2a-1}$ . White space is the area of parameter space where production of allelochemicals (+A) is the ESS. Dark grey is where not producing allelochemicals is the ESS (-A). The space in between (light grey) is where priority effect (PE) occurs.

Allelopathic plants gain a competitive advantage only when  $B > \frac{2C}{2a-1}$  which can offset the cost of producing allelochemicals beyond just the cost of toxicity on the neighboring plant (Figure 4.2). However, if  $B < \frac{2(C-T)}{2a-1}$  then non-allelopathic -A plants gain the competitive advantage because the benefits of allelopathy do not outweigh the costs to the allelopathic plant, or the allelopathic chemical is simply not that toxic (*i.e.* low  $T$ ). This region of pure +A as the ESS expands as  $a$  increases (Figure 4.2). When  $a > 0.5$ , but  $\frac{2(C-T)}{2a-1} < B < \frac{2C}{2a-1}$ , there is an interesting region between the two isoclines of alternative stable states where only one strategy can exist at a time, but which one occurs depends on the initial conditions (*i.e.* on this history of colonization

and/or mutation). This area of alternative stable states also expands with increasing  $T$  but decreasing  $a$ .

## 4.5 Discussion

In this study, we developed and analyzed a model of the evolution of allelopathy between two competing plants as an evolutionary game to examine the conditions under which the production and deployment of allelochemicals becomes a favorable competitive strategy. The model has four parameters that describe costs and benefits among different players. Somewhat intuitively, allelopathy can only evolve when the benefits outweigh the costs, but the model outlines these precise conditions in 4-dimensional phase space (Figure 4.2). For example, in the case of an extremely toxic allelochemical (i.e. large  $T$ ) that also happens to be metabolically costly to produce (i.e. large  $C$ ), the model makes it clear that there must be relatively high benefits (e.g. high  $B$ , very fertile environments) and confer a very large competitive advantage (large  $a$ ). Indeed, except where  $a$  approaches 1 and  $T$  is large, we see large regions of alternative stable states, and relatively small regions where  $+A$  is the pure ESS. Assuming that  $-A$  is the ancestral condition, this could help explain why allelopathy has been relatively rare to evolve, despite the obvious advantage. That is, in the region of alternative stable states, any  $+A$  mutants would simply not be able to invade the ancestral  $-A$  population. The relative rarity of allelopathy in nature might mean we live in a world closer to the top left of Figure 4.2, though future work should investigate whether the cost of production and the cost of detoxification are substantial energetic costs to plants. There may be some biochemical constraints that place the plant kingdom in this part of the phase space, and this would be an important area to explore further. It is also possible that allelopathy is more common than current knowledge suggests.

One way of reducing the cost of producing novel allelochemicals is to harness existing metabolic frameworks. Many species producing naphthoquinone-based compounds, for example, have independently evolved to do so from 1,4-dihydroxy-2-naphthoic acid (DHNA), an intermediate of the phyloquinone (vitamin K<sub>1</sub>) pathway<sup>25</sup>. Examples include juglone in black walnut trees<sup>26</sup>, lawsone and 2-MNQ in the Balsaminaceae (e.g. *Impatiens* species)<sup>27</sup>, lawsone and lapachol in the Bignoniaceae<sup>28</sup>, anthraquinones like alizarin made by Rubiaceae species<sup>29</sup>, and anthrasesamones produced by sesame (*Sesamum indicum*, Pedaliaceae)<sup>30</sup>. Interestingly, juglone, lawsone, and 2-MNQ are all implicated as allelochemicals<sup>19,31,32</sup>. This indicates that DHNA

derived from the phylloquinone pathway, which is present in all plants, likely provides a lower cost path for plants to synthesize allelochemicals.

Over time, the cost allelochemical toxicity,  $T$ , to  $-A$  plants could be mitigated by evolution of mechanisms to tolerate or detoxify the allelochemical. Therefore, the competitive disadvantage of not producing the allelochemical to  $-A$  plants would dissipate; however, the cost of detoxification, which is also part of  $T$ , would likely remain non-zero. We can draw inferences from evolution of herbicide resistances, which occur via mutations in herbicide target sites (target-site resistance) or non-target sites (non-target-site resistance)<sup>33</sup>. In an analogous scenario of non-target-site resistance, the allelochemical itself or the toxicity arising from the allelochemical could be metabolically counteracted through biochemical modification and/or compartmentalization of the allelochemical or its modified product. Thus, non-target-site resistance is referred to as “metabolism-based resistance”<sup>34</sup>. Metabolism-based resistance to herbicides is primarily achieved via four gene families: cytochrome P450 monooxygenases, glutathione transferases (GSTs), glycosyltransferases, and/or ABC transporters<sup>33</sup>. It is likely that plants that evolve in proximity to an allelopathic plant use similar methods to tolerate allelochemicals. GSTs function by covalently linking glutathione (GSH) with compounds that are hydrophobic and electrophilic<sup>35</sup>; some also function as carriers that transport GSH-conjugates to vacuoles for detoxification<sup>36</sup>. Black-grass (*Alopecurus myosuroides*) is a weed species that has evolved resistance to multiple herbicides. It appears that GSTs play a role in this. Along with being highly expressed in black-grass, heterologous overexpression of a black-grass GST, AmGSTF1, in Arabidopsis was previously shown to confer resistance to multiple herbicides<sup>37</sup>. Beyond glutathione, glycosylation appears to be a major mechanism of detoxification of specialized metabolites<sup>38</sup>. Indeed, much of the juglone found in black walnut is glycosylated<sup>39</sup>, suggesting that one of the mechanisms black walnut uses to tolerate producing and storing an autotoxic compound is through glycosylation. Reduced uptake or increased export could also confer some tolerance to allelopathic exposure. Mutations in transport proteins have been shown to confer resistance to herbicides through decreased uptake (reviewed in<sup>40</sup>). Additionally, fungi and bacteria have been shown to be able to degrade structurally diverse, toxic chemicals from a variety of plant families<sup>41–43</sup>. Studies from microorganisms may provide more insight into mechanisms plants use to tolerate allelochemicals or provide guidance for transgenic strategies to convey resistance to allelochemicals.

Investigating the methods plants use to reduce cost and increase fitness will allow engineering of novel cropping systems. For example, intercropping is a common agricultural practice used in many parts of the world to improve land use efficiency, to mitigate the risk of a single crop failing, and to diversify farming income. Often, intercropping involves co-cultivation of two or more cash crops, but in some cases a cash crop is grown alongside a non-cash crop to provide benefits, such as weed suppression, to the primary crop<sup>41</sup>. In either case, intercropped species are grown in close enough proximity to allow biological interaction. Therefore, the allelopathic potential of each species should be considered when designing mixed cropping systems<sup>42</sup>. For example, a study by Iqbal *et al.*<sup>43</sup> showed that intercropping cotton (*Gossypium hirsutum* L., cv FH901) with allelopathic crops, including sorghum (*Sorghum bicolor* L.), soybean (*Glycine max* L.), or sesame (*Sesamum indicum* L.), was an effective strategy to control purple nutsedge (*Cyperus rotundus* L.), a common aggressive weed found in parts of South Asia. According to the matrix game presented here, the fitness pay-off to both cotton and purple nutsedge (the  $-A$  species) would be expected to decrease as the toxicity,  $T$ , of allelochemicals produced by sorghum, soybean, or sesame (the  $+A$  species) increased. Indeed, seed cotton yield was found to decrease between 8-23% in all intercropping systems, compared to unmanaged cotton alone. Similarly, the presence of allelopathic species led to 70-96% reduced purple nutsedge density<sup>43</sup>. That control of purple nutsedge was found to be more effective in the second year of the study compared to the first year, which was suggested to be the result of residual allelochemicals leftover in the soil in year two<sup>43</sup>. This is consistent with purple nutsedge paying an increased penalty,  $T$ , to detoxify higher levels of allelochemicals.

Herbicide applications have increased over the last 25 years in many major cropping systems<sup>44</sup>. With this trend, so too has the number of weeds that have developed resistance to commonly used pesticides<sup>45</sup>. To address the lack of new herbicidal modes of action needed to combat resistant weeds<sup>46</sup>, allelochemicals, which offer a wide diversity of new chemical structures, have been suggested as sources for developing novel herbicides<sup>47</sup>. One attractive strategy is to engineer or breed production of allelochemicals into non-allelopathic cash crops, although autotoxicity and the metabolic cost of biosynthesis must remain low enough to not significantly impact its agricultural performance<sup>48</sup>. If the cost,  $C$ , to the crop engineered to be  $+A$  is too high then it would not be an ESS and could be invaded by  $-A$  species (*i.e.* weeds) (equations 5a and 5b). At the same time, if the cost,  $C$ , to the  $+A$  crop is too low then it may allow it to become too

easily capable of escaping and invading native populations of  $-A$  species (Figure 4.2). If the crop were engineered such that it was in the realm of alternative stable states, the allelopathic crop would be able to resist invasion from  $-A$  weeds, without the possibility of escape and invasion. Thus, an alternative use of allelochemicals in agricultural systems that should be considered is for crops that are dependent on termination by synthetic herbicides, such as with certain cover crops. For example, a  $-A$  cover crop could be engineered, with inducible production of an autotoxic allelochemical that comes at a very high metabolic cost. Induced production of the autotoxic allelochemical, whether it be by an external cue like temperature, day length or application of a cheap and benign chemical, would create a cost,  $C$ , to the engineered  $+A$  cover crop so high that it could be easily overtaken by a subsequently planted cash crop. By purposefully engineering a less fit cover crop to fall *outside* the region where  $+A$  is ESS (Figure 4.2), it would also provide a mechanism by which to prevent escape of the transgenic species.

Another interesting consideration in the evolution of allelopathy is the presence of allelobiosis. Allelobiosis is a relatively new term that describes communication between plants via non-toxic compounds<sup>49</sup>. For example, planting tomato (*Lycopersicon esculentum*) in proximity with sagebrush (*Artemisia tridentata*) resulted in increased production of proteinase inhibitors in tomato due to methyl jasmonate released by the sagebrush<sup>50</sup>. Though allelobiosis has been most often demonstrated with volatile compounds, there are examples of this kind of plant-plant communication through the rhizosphere. Indeed, Li *et al.* (2016) found that allelobiosis and allelopathy coexist in interactions of weeds with allelopathic wheat. Root exudates from weed species were sufficient to induce allelopathy in the wheat, suggesting a chemical signal sensed by the wheat. Further work is necessary to detangle the effects of allelobiosis and allelopathy, especially in the case of inducible production of allelochemicals.

Allelopathy may also have indirect effects on neighboring plants by modifying the soil microbiome. The soil microbiome has been shown to have diverse effects on plant fitness (reviewed in<sup>51</sup>). In addition to directly harming nearby plants, allelopathy may also play a role in altering the microbial soil community to the benefit of the allelopathic plant. For example, invasive garlic mustard has been shown to inhibit the interaction between seedlings of competitors and their mutualistic fungi<sup>52</sup>. Similarly, *I. glandulifera* invasion disrupts symbiotic associations between arbuscular mycorrhiza and native saplings<sup>20</sup>, likely via the release of 2-MNQ, which was also shown to inhibit mycelium growth of ectomycorrhiza fungi<sup>19</sup>. Conversely, some studies have

suggested that the plant microbiome reduces the effect of allelochemicals on the plant<sup>56</sup>, in effect lowering the cost of toxicity/detoxification,  $T$ , to opponents. *Paxillus involutus*, a mycorrhizal fungi of black spruce (*Picea mariana*), has been shown to be able to degrade allelopathic compounds produced by *Kalmia angustifolia*, perhaps conveying some tolerance to black spruce<sup>57</sup>. These examples demonstrate the complexity of studying allelopathy in field conditions.

#### 4.6 Conclusion

Our model predicts three cases, differing in the benefit to the allelopathic plant, in which the evolutionarily stable strategies are different. In the first, the non-allelopathic plant is a stronger competitor, and not producing allelochemicals is the evolutionarily stable strategy. In the second, the allelopathic plant is the better competitor and production of allelochemicals is the more beneficial strategy. In the last case, the allelopathic and non-allelopathic plants are equal competitors, but pay different costs resulting in alternative stable states depending on the history of the system. We find that despite the obvious benefits of allelopathy, there are relatively few conditions that lead to  $+A$  as a pure ESS. We argue that these results potentially help explain the relative rarity of allelopathy in nature. Further empirical exploration of this model could lead to useful agricultural tools.

#### Acknowledgements

This work was supported by the USDA National Institute of Food and Agriculture Predoctoral Grant 2018-67011-28032 to R.M.M. and start-up funds from Purdue University to G.G.M. and J.R.W. This work was also supported by the USDA National Institute of Food and Agriculture Hatch Projects number 1010722 to G.G.M. and number 177845 to J.R.W.

#### 4.7 References

1. Schoener, T. W. Field Experiments on Interspecific Competition. *Am. Nat.* **122**, 240–285 (1983).
2. Connell, J. H. On the Prevalence and Relative Importance of Interspecific Competition : Evidence from Field Experiments. *Am. Nat.* **122**, 661–696 (1983).

3. Fowler, N. The role of competition in studies of spatial pattern. *Annu. Rev. Ecol. Syst.* **17**, 89–110 (1986).
4. Wilson, J. B. Shoot Competition and Root Competition. *J. Appl. Ecol.* **25**, 279–296 (1988).
5. Friedman, J. The effect of competition by adult *Zygophyllum dumosum* Boiss. on seedlings of *Artemisia herba-alba* Asso in the Negev Desert of Israel. *J. Ecol.* **59**, 775 (1971).
6. Carothers, J. H. & Jaksić, F. M. Time as a Niche Difference: The Role of Interference Competition. *Oikos* **42**, 403–406 (1984).
7. Ford, H. A. Interspecific competition in Australian honeyeaters—depletion of common resources. *Aust. J. Ecol.* **4**, 145–164 (1979).
8. Fuerst, E. P. & Putnam, A. R. Separating the competitive and allelopathic components of interference - Theoretical principles. *J. Chem. Ecol.* **9**, 937–944 (1983).
9. Latif, S., Chiapusio, G. & Weston, L. A. *Allelopathy and the Role of Allelochemicals in Plant Defence. Advances in Botanical Research* **82**, (Elsevier Ltd, 2017).
10. Inderjit & Callaway, R. M. Experimental designs for the study of allelopathy. *Plant Soil* **256**, 1–11 (2003).
11. Lau, J. A. *et al.* Inference of allelopathy is complicated by effects of activated carbon on plant growth. *New Phytol.* **178**, 412–423 (2008).
12. Jose, S. & Gillespie, A. R. Allelopathy in black walnut (*Juglans nigra* L.) alley cropping. II. Effects of juglone on hydroponically grown corn (*Zea mays* L.) and soybean (*Glycine max* L. Merr.) growth and physiology. *Plant Soil* **203**, 199–205 (1998).
13. Wilcove, D. S., Rothstein, D., Dubow, J., Phillips, A. & Losos, E. Quantifying Threats to Imperiled Species in the United States. *Bioscience* **48**, 607–615 (1998).
14. Callaway, R. M. & Aschehoug, E. T. Invasive Plants Versus Their New and Old Neighbors: A Mechanism for Exotic Invasion. *Science* **290**, 521–523 (2000).
15. Keane, R. M. & Crawley, M. J. Exotic plant invasions and the enemy release hypothesis. *Trends Ecol. Evol.* **17**, 164–170 (2002).
16. Zhu, X. *et al.* Identification and localization of bioactive naphthoquinones in the roots and rhizosphere of Paterson's curse (*Echium plantagineum*), a noxious invader. *J. Exp. Bot.* **67**, 3777–3788 (2016).
17. Callaway, R. M. & Ridenour, W. M. Novel weapons: Invasive success and the evolution of increased competitive ability. *Front. Ecol. Environ.* **2**, 436–443 (2004).

18. Prati, D. & Bossdorf, O. Allelopathic inhibition of germination by *Alliaria petiolata* (Brassicaceae). *Am. J. Bot.* **91**, 285–288 (2004).
19. Ruckli, R., Hesse, K., Glauser, G., Rusterholz, H.-P. & Baur, B. Inhibitory potential of naphthoquinones leached from leaves and exuded from roots of the invasive plant *Impatiens glandulifera*. *J. Chem. Ecol.* **40**, 371–8 (2014).
20. Ruckli, R., Rusterholz, H. P. & Baur, B. Invasion of an annual exotic plant into deciduous forests suppresses arbuscular mycorrhiza symbiosis and reduces performance of sycamore maple saplings. *For. Ecol. Manage.* **318**, 285–293 (2014).
21. Gruntman, M., Pehl, A. K., Joshi, S. & Tielbörger, K. Competitive dominance of the invasive plant *Impatiens glandulifera*: Using competitive effect and response with a vigorous neighbour. *Biol. Invasions* **16**, 141–151 (2014).
22. Maynard Smith, J. & Price, G. R. The Logic of Animal Conflict. *Nature* **246**, 47–49 (1973).
23. Apaloo, J., Brown, J. S., McNickle, G. G., Vincent, T. L. S. & Vincent, T. L. ESS versus Nash: Solving evolutionary games. *Evol. Ecol. Res.* **16**, 293–314 (2014).
24. Maynard Smith, J. *Evolution and the Theory of Games*. (Cambridge University Press, 1982).
25. Widhalm, J. R. & Rhodes, D. Biosynthesis and molecular actions of specialized 1,4-naphthoquinone natural products produced by horticultural plants. *Hortic. Res.* **3**, 16046 (2016).
26. McCoy, R. M., Utturkar, S. M., Crook, J. W., Thimmapuram, J. & Widhalm, J. R. The origin and biosynthesis of the naphthalenoid moiety of juglone in black walnut. *Hortic. Res.* **5**, 67 (2018).
27. Zenk, M. H. & Leistner, E. On the mode of incorporation of shikimic acid into 2-hydroxy-1, 4-naphthoquinone (lawsone). *Zeitschrift für Naturforsch. - Sect. B J. Chem. Sci.* **22**, 460 (1967).
28. Hussain, H., Krohn, K., Ahmad, V. U., Miana, G. A. & Green, I. R. Lapachol: An overview. *Arkivoc* **2007**, 145 (2007).
29. Yamazaki, M. *et al.* Coupling deep transcriptome analysis with untargeted metabolic profiling in ophiorrhiza pumila to further the understanding of the biosynthesis of the anti-cancer alkaloid camptothecin and anthraquinones. *Plant Cell Physiol.* **54**, 686–696 (2013).

30. Furumoto, T. & Hoshikuma, A. Biosynthetic origin of 2-geranyl-1,4-naphthoquinone and its related anthraquinone in a *Sesamum indicum* hairy root culture. *Phytochemistry* **72**, 871–4 (2011).
31. Dana, M. & Lerner, B. Black walnut toxicity. *Purdue Univ. Coop. Ext. Serv.* **HO-193-W**, 2 (2001).
32. Block, A. K., Yakubova, E. & Widhalm, J. R. Specialized naphthoquinones present in *Impatiens glandulifera* nectaries inhibit the growth of fungal nectar microbes. *Plant Direct* **3**, e00132 (2019).
33. Yuan, J. S., Tranel, P. J. & Stewart, C. N. Non-target-site herbicide resistance: a family business. *Trends Plant Sci.* **12**, 6–13 (2007).
34. Hatzios, K. & Burgos, N. Metabolism-based herbicide resistance : regulation by safeners. *Weed Science* **52**, 454–467 (2004).
35. Cummins, I., Dixon, D. P., Freitag-Pohl, S., Skipsey, M. & Edwards, R. Multiple roles for plant glutathione transferases in xenobiotic detoxification. *Drug Metab. Rev.* **43**, 266–280 (2011).
36. Sun, Y., Li, H. & Huang, J. R. Arabidopsis TT19 functions as a carrier to transport anthocyanin from the cytosol to tonoplasts. *Mol. Plant* **5**, 387–400 (2012).
37. Cummins, I. *et al.* Key role for a glutathione transferase in multiple-herbicide resistance in grass weeds. *Proc. Natl. Acad. Sci. U. S. A.* **110**, 5812–5817 (2013).
38. Le Roy, J., Huss, B., Creach, A., Hawkins, S. & Neutelings, G. Glycosylation is a major regulator of phenylpropanoid availability and biological activity in plants. *Front. Plant Sci.* **7**, 735 (2016).
39. Müller, W. U. & Leistner, E. Aglycones and glycosides of oxygenated naphthalenes and a glycosyltransferase from *Juglans*. *Phytochemistry* **17**, 1739–1742 (1978).
40. Conte, S. S. & Lloyd, A. M. Exploring multiple drug and herbicide resistance in plants- Spotlight on transporter proteins. *Plant Sci.* **180**, 196–203 (2011).
41. Pedras, M. S. C. & Ahiahonu, P. W. K. Metabolism and detoxification of phytoalexins and analogs by phytopathogenic fungi. *Phytochemistry* **66**, 391–411 (2005).
42. Yu, R.-Q., Kurt, Z., He, F. & Spain, J. C. Biodegradation of the allelopathic chemical pterostilbene by a *Sphingobium* sp. strain from the peanut rhizosphere. *Appl. Environ. Microbiol.* **85**, 1–12 (2019).

43. Rettenmaier, H., Kupas, U. & Lingens, F. Degradation of juglone by *Pseudomonas putida* J 1. *FEMS Microbiol. Lett.* **19**, 193–195 (1983).
44. Mohler, C. L. & Stoner, K. A. Guidelines for Intercropping. in *Crop Rotation on Organic Farms* (eds. Mohler, C. L. & Johnson, S. E.) 95–100 (NRAES, 2009).
45. Cheng, F. & Cheng, Z. Research progress on the use of plant allelopathy in agriculture and the physiological and ecological mechanisms of allelopathy. *Front. Plant Sci.* **6**, 1020 (2015).
46. Iqbal, J., Cheema, Z. A. & An, M. Intercropping of field crops in cotton for the management of purple nutsedge (*Cyperus rotundus* L.). *Plant Soil* **300**, 163–171 (2007).
47. Kniss, A. R. Long-term trends in the intensity and relative toxicity of herbicide use. *Nat. Commun.* **8**, 1–7 (2017).
48. Heap, I. The international survey of herbicide resistant weeds. (2020).
49. Dayan, F. E., Owens, D. K. & Duke, S. O. Rationale for a natural products approach to herbicide discovery. *Pest Manag. Sci.* **68**, 519–528 (2012).
50. Cantrell, C. L., Dayan, F. E. & Duke, S. O. Natural products as sources for new pesticides. *J. Nat. Prod.* **75**, 1231–1242 (2012).
51. Duke, S. O. Weeding with transgenes. *Trends Biotechnol.* **21**, 192–195 (2003).
52. Ninkovic, V., Glinwood, R. & Pettersson, J. Communication between undamaged plants by volatiles: the role of allelobiosis. in *Communication in Plants: Neuronal Aspects of Plant Life* 421–434 (2010). doi:10.1007/978-3-540-28516-8
53. Farmer, E. E. & Ryan, C. A. Interplant communication: Airborne methyl jasmonate induces synthesis of proteinase inhibitors in plant leaves. *Proc. Natl. Acad. Sci. U. S. A.* **87**, 7713–7716 (1990).
54. Lakshmanan, V., Selvaraj, G. & Bais, H. P. Functional soil microbiome: Belowground solutions to an aboveground problem. *Plant Physiol.* **166**, 689–700 (2014).
55. Stinson, K. A. *et al.* Invasive plant suppresses the growth of native tree seedlings by disrupting belowground mutualisms. *PLoS Biol.* **4**, 727–731 (2006).
56. Mishra, S., Upadhyay, R. S. & Nautiyal, C. S. Unravelling the beneficial role of microbial contributors in reducing the allelopathic effects of weeds. *Appl. Microbiol. Biotechnol.* **97**, 5659–5668 (2013).

57. Zeng, R. Sen & Mallik, A. U. Selected ectomycorrhizal fungi of black spruce (*Picea mariana*) can detoxify phenolic compounds of *Kalmia angustifolia*. *J. Chem. Ecol.* **32**, 1473–1489 (2006).

## CHAPTER 5. CONCLUSIONS AND FUTURE DIRECTIONS

### 5.1 Conclusion

The findings presented here contribute knowledge of the connection between phylloquinone and juglone biosynthesis and present a model that explores the evolutionary circumstances that favor the production of allelochemicals. Chapter 2 showed that juglone biosynthesis in black walnut (*Juglans nigra*) branches off a pathway to make phylloquinone, a vital compound used in photosynthesis in all plants, and effectively identified the first five biosynthetic enzymes to make juglone. Chapter 3 presents the first genetic evidence for a plant 1,4-dihydroxy-2-naphthoyl-CoA synthase (DHNS), the last remaining enzyme in phylloquinone biosynthesis. In addition, chapter 3 demonstrated that the OSB-CoA ligase step is necessary in both the chloroplast and the peroxisome. Chapter 4 produced a game theoretic model describing the costs and benefits of producing allelochemicals.

### 5.2 Remaining questions

Though in chapter 2 we established the first five biosynthetic steps to make juglone in black walnut, the enzymes responsible for converting DHNA to juglone remain unknown. We hypothesize that a DHNA decarboxylase and a 1,4-naphthoquinone (1,4-NQ) hydroxylase, likely a cytochrome P450 monooxygenase (P450) or a 2-oxoglutarate-dependent oxygenase (2-ODD), are required. We identified candidate genes from our black walnut RNA-seq dataset including six decarboxylase, 14 P450, and six ODD candidate genes as priority candidates for functional testing based on (i) higher expression in roots versus leaves ( $\log_2$  fold difference  $> 0$ ), (ii) absence of an ortholog in *Arabidopsis* (does not produce juglone) as defined by OrthoMCL<sup>3</sup> analysis, and (iii) relative expression levels, based on normalized RNA-seq counts, similar to those of phylloquinone genes involved in DHNA synthesis (Figure 5.1).

Cumulative Filters for Genes	Decarboxylase	P450	2-ODD
# Annotated	68	302	161
# Upregulated in roots	40	180	87
# without <i>Arabidopsis</i> ortholog	28	68	34
# with counts > 1000	6	14	5

Figure 5.1 Bioinformatics strategy to identify and prioritize candidates for functional testing of involvement in juglone biosynthesis. Genes highlighted in gray will be screened first.

Because black walnut is not genetically amenable, candidates were screened by transiently expressing them in *Nicotiana benthamiana*. The substrate for the decarboxylases, DHNA, should already be present in *N. benthamiana* because it is an intermediate in phylloquinone biosynthesis, but 1,4-NQ, the predicted substrate of the hydroxylase reaction, was infiltrated into *N. benthamiana* leaves. Candidates tested so far – three decarboxylases, five P450s, and 3 2-ODDs, – do not have DHNA decarboxylase or 1,4-NQ hydroxylase activity. There are still other candidates to screen for activity, but we may not have identified the right candidate in our filtering process described in Figure 5.1.

In addition, it is possible that juglone biosynthesis goes through a conjugated intermediate. For example, there were longstanding questions about the biosynthesis of the plant hormone salicylic acid. Recently, it was shown that isochorismate is conjugated to a glutamate before being converted to salicylic acid<sup>4,5</sup>. It is possible that due to the toxic nature of juglone and even 1,4-NQ (Figure 5.2), juglone synthesis also proceeds through a conjugated intermediate. Juglone is known to occur as a glucose conjugate<sup>6</sup>, likely for reduced toxicity and increased solubility. Indeed, glycosyltransferases are among the most highly expressed genes in our black walnut RNAseq data<sup>7</sup>.



Figure 5.2 1,4-naphthoquinone is toxic. 100  $\mu$ M 1,4-NQ or DHNA were infiltrated into tobacco leaves and imaged 5 days later.

In chapter 3, we showed the first genetic evidence for a plant DHNS. Further work is needed to achieve biological replication in independent lines and to correlate expression of DHNS with phylloquinone levels. Additionally, we showed that AAE14 is required in both the chloroplast and the peroxisome. It remains an open question why plants have partitioned the phylloquinone pathway in this way.

In chapter 4, we presented a game theoretic model of the evolution of allelochemicals. As it stands, the model is purely theoretical. One way to functionally test the model is to engineer production of an allelochemical into a naturally non-allelopathic plant. For example, once we identify the juglone biosynthetic genes discussed previously, we could transform them in the model plant *Arabidopsis*. We would also need to engineer a tolerance mechanism into the *Arabidopsis* to prevent it from dying from producing a toxic chemical. Once we could engineer production and tolerance of juglone into *Arabidopsis*, we could perform competition experiments in pots to functionally test the model.

### 5.3 Future applications

Once we identify the genes that make juglone from DHNA, it will be possible to engineer juglone production in any plant. All plants have the phylloquinone pathway and, therefore, have

the metabolic framework to make juglone. Knowledge from chapter 3 will increase understanding of the subcellular architecture of the phyloquinone pathway, which will inform where in the cell we should target the juglone-specific genes. The model in chapter 4 can help engineer a plant that is fit enough to survive, but not fit enough to overtake natural populations and become invasive.

One impactful application of the knowledge gained from this dissertation could be the development of a “self-mulching” cover crop: a cover crop that could terminate itself by producing juglone at certain stage in development. Major cover crops used in the Midwest, like Crimson Clover (*Trifolium incarnatum*), are sprayed with herbicides to prepare for planting the cash crop. A juglone-induced, self-mulching cover crop could be designed to respond to developmental or environmental cues through an inducible promoter to turn on production of juglone that would kill the cover crop. This would eliminate the need to apply synthetic herbicides, resulting in reduced herbicide applications (and hence reduced selective pressure for herbicide-resistant weeds), lack of emission from the actual application of herbicides, and reduction in labor by farmers.

#### 5.4 References

1. Dayan, F. E., Owens, D. K. & Duke, S. O. Rationale for a natural products approach to herbicide discovery. *Pest Manag. Sci.* **68**, 519–528 (2012).
2. Maynard Smith, J. *Evolution and the Theory of Games*. (Cambridge University Press, 1982).
3. Li, L., Stoeckert, C. J. J. & Roos, D. S. OrthoMCL: Identification of Ortholog Groups for Eukaryotic Genomes. *Genome Res.* **13**, 2178–2189 (2003).
4. Torrens-Spence, M. P. *et al.* PBS3 and EPS1 Complete Salicylic Acid Biosynthesis from Isochorismate in Arabidopsis. *Mol. Plant* **12**, 1577–1586 (2019).
5. Rekhter, D. *et al.* Isochorismate-derived biosynthesis of the plant stress hormone salicylic acid. *Science* **365**, 498–502 (2019).
6. Daghish, C. The isolation and identification of a hydrojuglone glycoside occurring in the walnut. *Biochem. J* **47**, 452–457 (1950).
7. McCoy, R. M., Utturkar, S. M., Crook, J. W., Thimmapuram, J. & Widhalm, J. R. The origin and biosynthesis of the naphthalenoid moiety of juglone in black walnut. *Hortic. Res.* **5**, 67 (2018).

**APPENDIX A. SUPPLEMENTAL INFORMATION FROM  
MCCOY ET AL. 2018 (CHAPTER 2)**

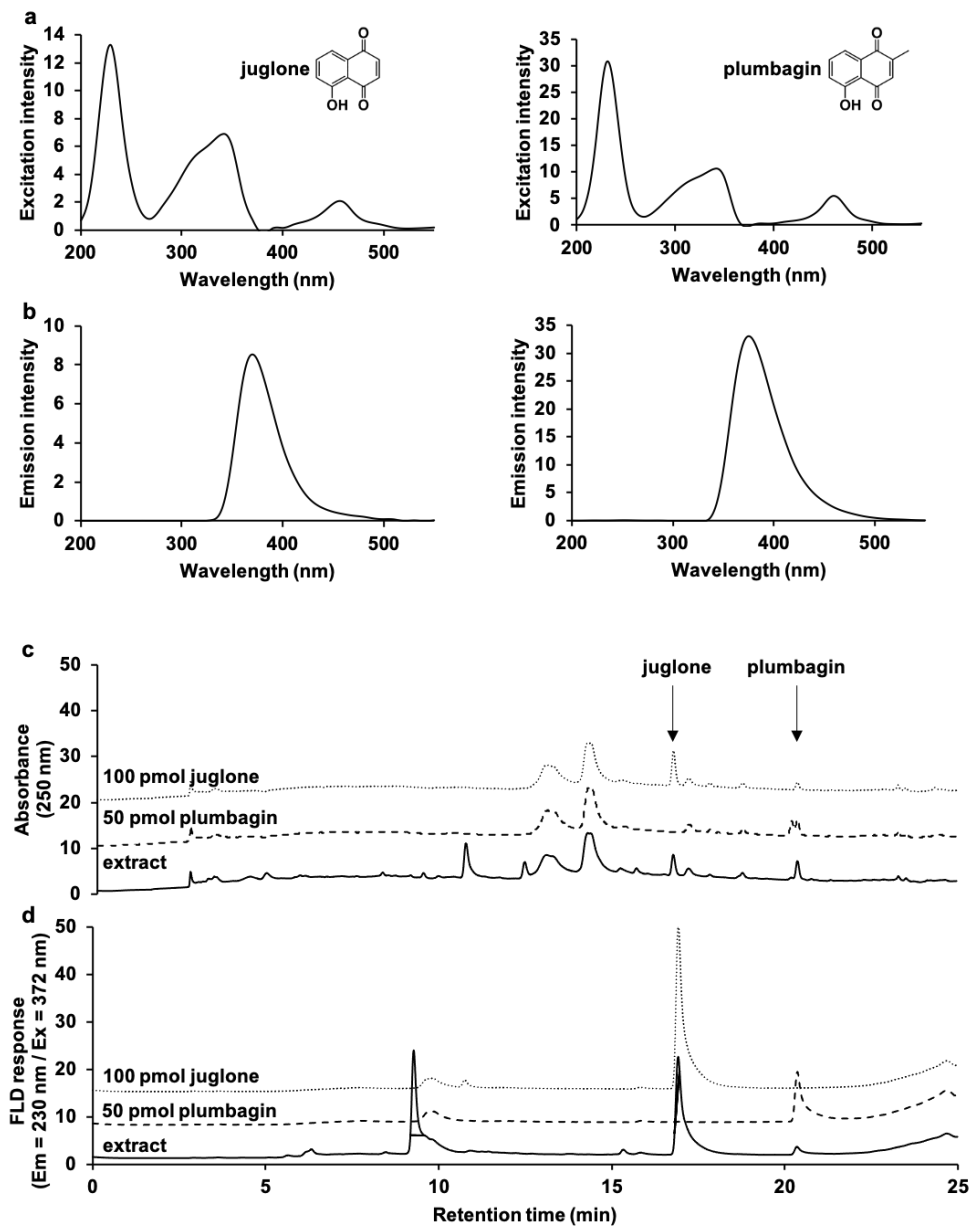


Figure A.1 Detection of free juglone in plant tissue by HPLC fluorescence. (a) On-line excitation scans for juglone and plumbagin with the emission wavelength set at 372 nm. (b) On-line emission scans for juglone and plumbagin with the excitation wavelength set at 230 nm. (c) HPLC diode array spectrophotometric traces of a juglone standard, a plumbagin standard, and a *Juglans nigra* (black walnut) leaf extract. Juglone elutes at 17.1 minutes and plumbagin elutes at 20.1 minutes. (d) HPLC fluorescence traces of the same samples in (c) using the optimized excitation and emission wavelengths determined from the scans presented in (a) and (b).

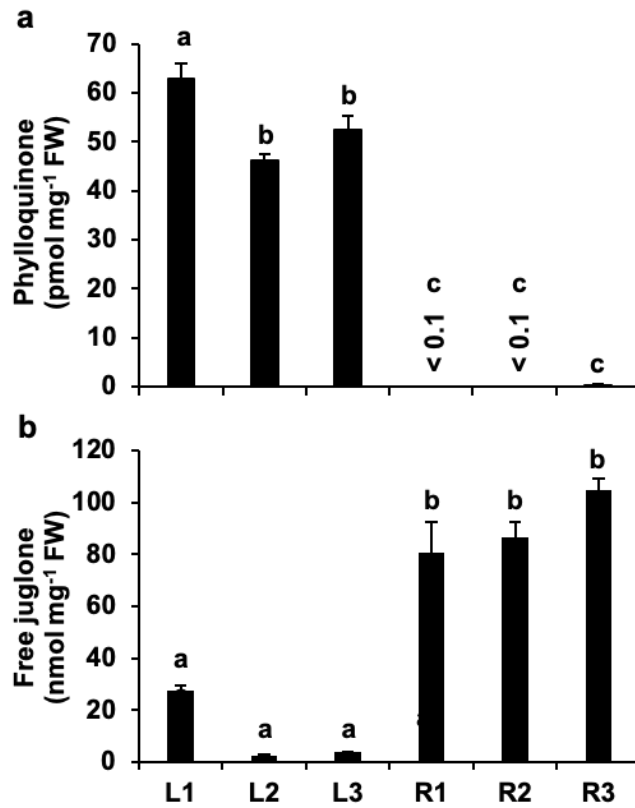


Figure A.2 Pool sizes of phylloquinone and free juglone in *Juglans nigra* (black walnut) organs used to generate RNA-seq datasets. **(a)** Phylloquinone levels. **(b)** Free juglone levels. Data are means  $\pm$  SEM ( $n = 3$  technical replicates). Different letters indicate significant differences via Analysis of Variance (ANOVA) followed by Post-hoc Tukey test ( $\alpha = 0.05$ ).

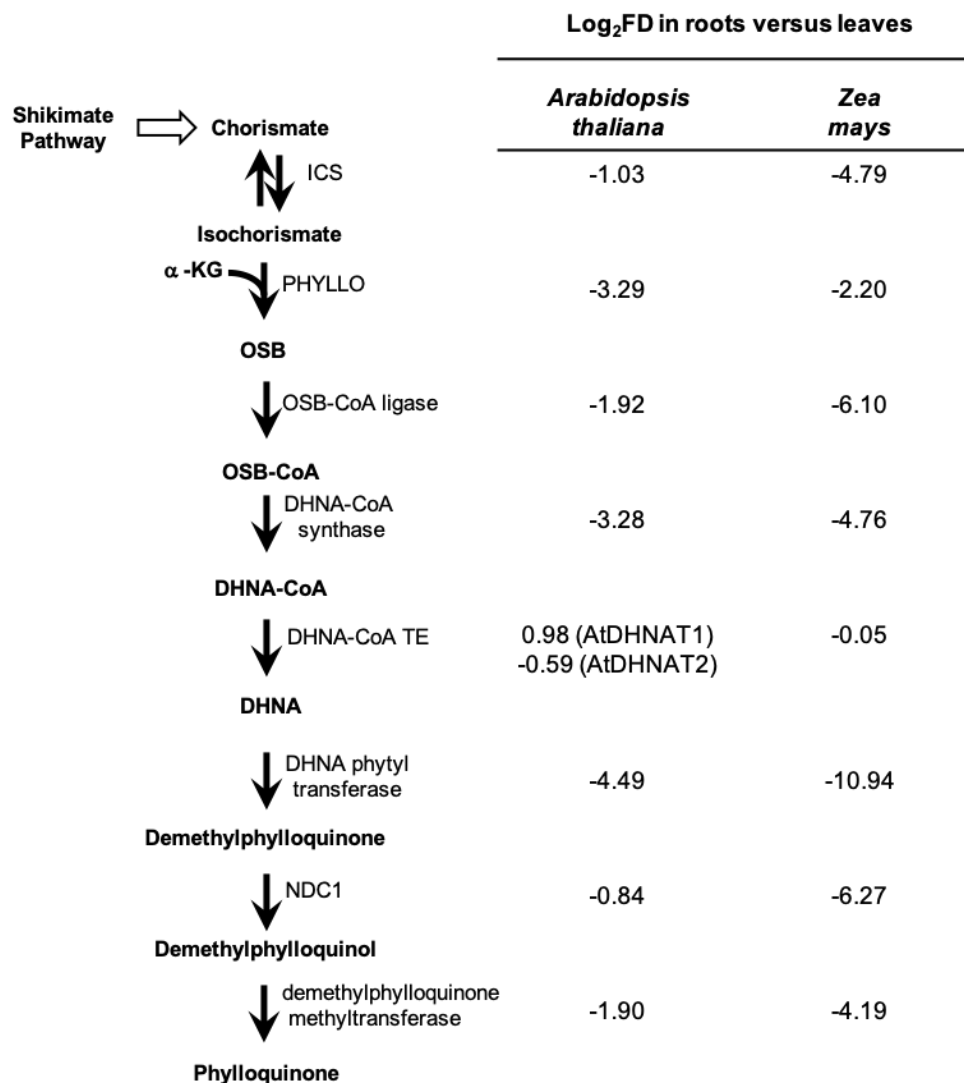


Figure A.3 Relative expression of phyloquinone pathway genes in *Arabidopsis thaliana* and *Zea mays* (maize) roots versus leaves. Unlike *Juglans nigra* (black walnut) roots, all phyloquinone pathway genes involved in synthesizing 1,4-dihydroxynaphthoic acid (DHNA) in *Arabidopsis* and maize, except those encoding 1,4-dihydroxy-2-naphthoyl-CoA (DHNA-CoA) thioesterases, which are known to be promiscuous enzymes<sup>14,43</sup>, have more than two-fold lower expression in roots. Log<sub>2</sub> fold-differences (FD) were calculated based on expression of phyloquinone pathway genes in *Arabidopsis* and maize using publicly available Gene Expression Omnibus datasets. The corresponding accession numbers are GSE87760 (unpublished) and GSE71377<sup>44</sup>. Count data were accessed from control wild-type samples for leaves and roots. AtDHNAT1, *Arabidopsis thaliana* DHNA-CoA thioesterase 1; AtDHNAT2, *Arabidopsis thaliana* DHNA-CoA thioesterase 2. See Figure 2.1 legend for other abbreviations.

Table A.1 Primers used for qPCR analysis in this study. F and R refer to forward and reverse.

<b>ID</b>	<b>Sequence (5'-&gt;3')</b>	<b>Working concentration (nM)</b>
qRT-JnUBC-F	TCAAGGGCCCGTCAGAGA	200
qRT-JnUBC-R	CAGGAACAGCAAAGCAAGCT	200
qRT-JnICS-F	AGGCACGGGTTTTTATTGCA	200
qRT-JnICS-R	TCCTCCGCTAAACCAACCAA	200
qRT-JnPHYLLO-F	CGCCCACCCGTACTIONACTTT	900
qRT-JnPHYLLO-R	CCACCGGACCGTCATATCTC	900
qRT-JnMenE-F	CGCCATCTCTGCTTTCAACA	50
qRT-JnMenE-R	GCAGCTATTCTCCAACAACG	50
qRT-JnMenB-F	GTGTGCGGAGATCGTGAGAA	900
qRT-JnMenB-R	TGAAGCCCAGCATGACCAT	300
qRT-JnDHNAT-F	GGAGGTGCAGTTCTGGAAGGT	200
qRT-JnDHNAT-R	TCCGGCACAGGCATGTTAC	200
qRT-JnMenA-F	GCCCCCATTTCGATTAAG	300
qRT-JnMenA-R	AAATGGACCAAATGCTGCAA	300
qRT-JnNDC1-F	TGCCCCCCTGGAAATAG	300
qRT-JnNDC1-R	ACAGCGGACAAAATAACCCAAT	300
qRT-JnPMT-F	AGCATCGAGTGTGGAAAAGGA	300
qRT-JnPMT-R	CGATAAATCCCCACTTCCACAA	300

Table A.2 Summary of RNA-seq data statistics and mapping results.

<b>Sample ID</b>	<b>Raw Reads (millions)</b>	<b>Clean Reads (millions)</b>	<b>Q30 nucleotide (%)</b>	<b>Unique Mapped Reads (millions)</b>	<b>Multiple Mapped Reads (millions)</b>	<b>Total Mapped Reads (millions)</b>	<b>Percentage of total mapped reads</b>
RJn1	72.33	71.43	97.77	21.81	35.47	57.28	80.18
RJn2	69.74	67.72	95.98	20.12	32.7	52.81	77.99
RJn3	72.92	71.55	96.98	20.81	33.9	54.71	76.47
LJn1	83.02	82.12	98	24.42	44.84	69.26	84.34
LJn2	65.62	64.42	97.06	19.5	31.48	50.98	79.14
LJn3	72.51	71.15	97.06	20.48	36.98	57.46	80.76

Tables A.3-12 are included as an Excel spreadsheet. Table legends are below.

Table A.3 Enriched Molecular Function GO categories among differentially expressed genes in *Juglans nigra* (black walnut) roots versus leaves (adjusted  $p < 0.05$ ).

Table A.4 Log<sub>2</sub> fold-difference for genes involved in the 15 enriched Molecular Function GO categories among differentially expressed genes in *Juglans nigra* (black walnut) roots versus leaves (adjusted  $p < 0.05$ ). Note that log<sub>2</sub>FD value 'inf' denotes the genes that are not differentially expressed by specific method.

Table A.5 Enriched Cellular Component GO categories among differentially expressed genes in *Juglans nigra* (black walnut) roots versus leaves (adjusted  $p < 0.05$ ).

Table A.6 Log<sub>2</sub> fold-difference for genes involved in the four enriched Cellular Component GO categories among differentially expressed genes in *Juglans nigra* (black walnut) roots versus leaves (adjusted  $p < 0.05$ ). Note that log<sub>2</sub>FD value 'inf' denotes the genes that are not differentially expressed by specific method.

Table A.7 Enriched Biological Process GO categories among differentially expressed genes in *Juglans nigra* (black walnut) roots versus leaves (adjusted  $p < 0.05$ ).

Table A.8 Log<sub>2</sub> fold-difference for genes involved in the four enriched Biological Process GO categories among differentially expressed genes in *Juglans nigra* (black walnut) roots versus leaves (adjusted  $p < 0.05$ ). Note that log<sub>2</sub>FD value 'inf' denotes the genes that are not differentially expressed by specific method.

Table A.9 Phylloquinone biosynthetic genes in *Arabidopsis thaliana* and *Juglans regia* (English walnut) used to identify orthologs in *J. nigra* (black walnut).

Table A.10 Candidate *Juglans nigra* (black walnut) decarboxylase genes encoding the putative 1,4-dihydroxynaphthoic acid (DHNA) decarboxylase. Candidate genes were identified from the transcriptomic datasets generated in this study based on functional annotation, DESeq2 log<sub>2</sub>FD  $\geq 1$  in roots versus leaves, and normalized DESeq2 root counts  $\geq 100$ .

Table A.11 Candidate *Juglans nigra* (black walnut) P450 genes encoding the putative 1,4-naphthoquinone hydroxylase. Candidates were identified from the transcriptomic datasets generated in this study based on functional annotation, DESeq2 log<sub>2</sub>FD  $\geq 1$  in roots versus leaves, and normalized DESeq2 root counts  $\geq 100$ .

Table A.12 Candidate *Juglans nigra* (black walnut) 2-oxoglutarate/Fe(II)-dependent dioxygenase genes encoding the putative 1,4-naphthoquinone hydroxylase. Candidates were identified from the transcriptomic datasets generated in this study based on functional annotation, DESeq2 log<sub>2</sub>FD  $\geq 1$  in roots versus leaves, and normalized DESeq2 root counts  $\geq 100$ .

## APPENDIX B. SUPPLEMENTAL INFORMATION FROM CHAPTER 3

```

At1g60550      MADSNELGSASRRLSVVTNHLIPIGFSPARADSVELCSASSMDDRFHKVHGEVPTHEVVW
E. coli DHNS   -----MIYPDEAMLY
Synechocystis DHNS -----

At1g60550      KKTDFFGEGDNKEFVDIIYEKALDEGIAKITINRPERRNAFRPQTVKELMRAFNDARDDS
E. coli DHNS   APVEWH--DCSEGFEDIRYEKS-TDGIAKITINRPQVRNAFRPLTVKEMIQALADARYDD
Synechocystis DHNS --MDWH--IAK-HYDDLILYY-K-AGGIAKIVINRPHKRNAFRPQTVFELYDAFCNAREDN
                ::. . : ** * *****.****. ***** ** *: *: :** *.

At1g60550      SVGVIILTQK-----TKAFCSGGDQALRTQ-DGYADPNDVGRNLNVLDLQVQIRRLPKPV
E. coli DHNS   NIGVIILTGAG-----DKAFCSGGDQKVRGDYGGYKDDSGVHHLNVLDFQRQIRTCPKV
Synechocystis DHNS RIGVLLTGAGPHSDGKYAFCSGGDQSVRGE-GGYIDDQGTPLNLVLDLQRLIRSMKPVV
                :*:*** * ***** :* : .** * ... :*****:* ** ** *

At1g60550      IAMVAGYAVGGGHI LHMVCDLTIAADNAIFGQTGPKVGSFDAGYGSSIMSRLVGPKKARE
E. coli DHNS   VAMVAGYSIGGGHVLHMMCDLTIAADNAIFGQTGPKVGSFDGGWGASYMARIVGQKKARE
Synechocystis DHNS IALVAGYAI GGGHVLHLVCDLTIAADNAIFGQTGPKVGSFDGGFGSSYLARIVGQKKARE
                :*:****:****:*:*****:*****:*****:*****:*****:*****:*****

At1g60550      MWFMTFRFYTASEAEKMGLINTVVPLEDLEKETVKWCREILRNSPTAIRVLKAAALNAVDDG
E. coli DHNS   IWFLCROYDAKQALDMGLVNTVVPVLDLEKETVVRWCREMLQNSPMALRCLKAAALNADCDG
Synechocystis DHNS IWYLCROYSAQEAERMGMVNTVVPVDRLEEEGIQWAKEILSKSPLAIRCLKAAFNAADCDG
                :*: * * *.* **:******: **.* :*.*:* ** *.* *****:** **

At1g60550      HAGLQGLGGDATLLFYGTEEATEGRTAYMHRPPDFSKFHRRP
E. coli DHNS   QAGLQELAGNATMLFYMTEEGQEGRNFAFNQKRPDFSKFKRNP
Synechocystis DHNS QAGLQELAGNATLLYMTTEEGSEGKQAFLEKRPPDFSQYPWLP
                :**** *.*:*:*:* **.* **.* :*.* **.*: *

```

Figure B.1 Alignment of At1g60550 with the *E. coli* and *Synechocystis* DHNSs. Highlighting indicates level of conservation: red indicates conserved amino acids, orange is highly similar amino acids, yellow is slightly similar amino acids. The purple box indicates the predicted PTS2.

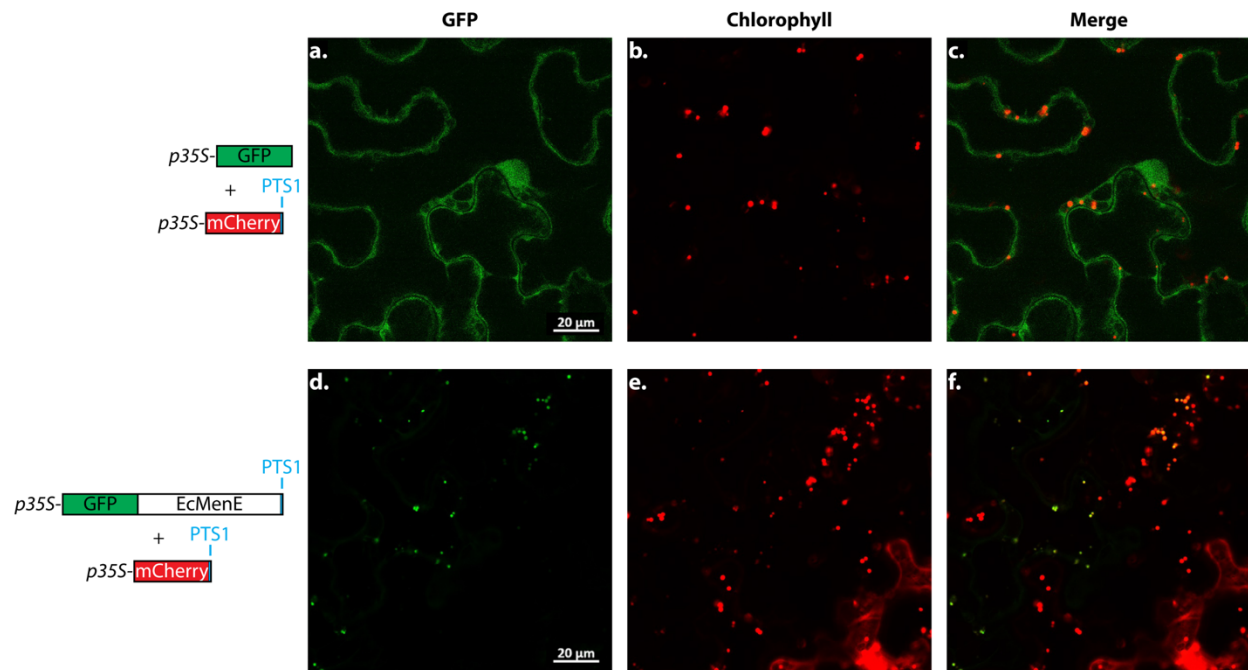


Figure B.2 Subcellular localization of EcMenE-PTS1 in *Nicotiana benthamiana* leaves. a.-c. Transient co-expression of GFP-alone and peroxisomal marker: a. GFP-alone, b. peroxisomal marker with mCherry, c. merged image. d.-f. Transient co-expression of GFP-EcMenE-PTS1 and peroxisomal marker: d. GFP-EcMenE-PTS1, e. peroxisomal marker with mCherry, f. merged image.

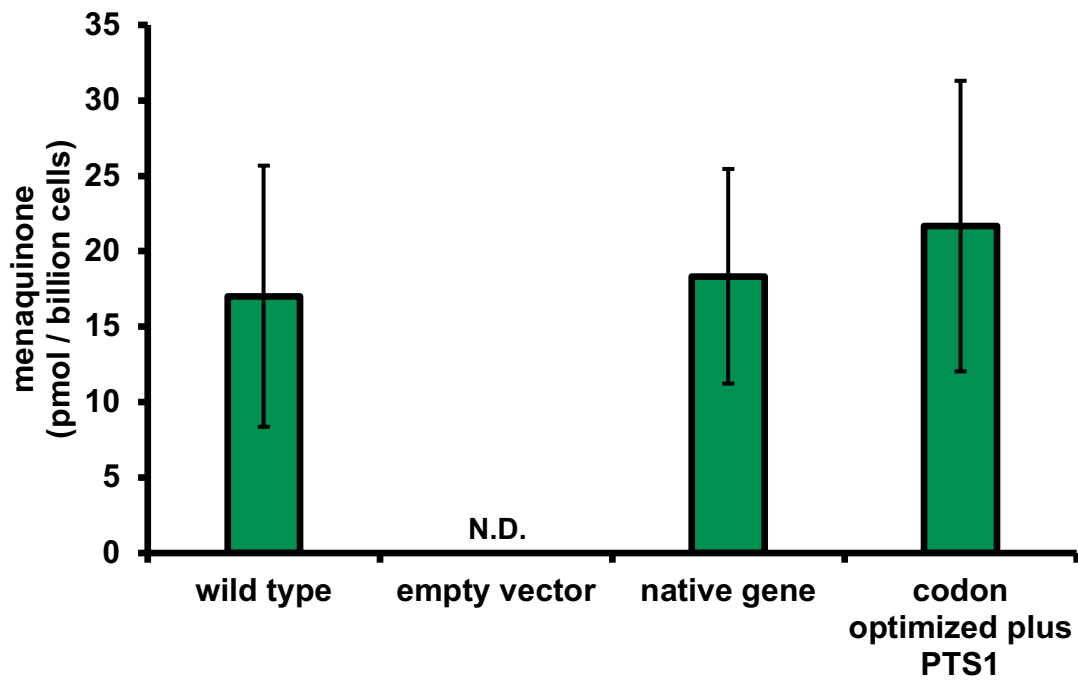


Figure B.3 Functional complementation of an *E. coli* OSB-CoA ligase mutant by *EcMenE-PTS1*. Error bars are standard deviation. n=3 independent colonies for each transformant.

Table B.1 The top 50 co-expressed genes with At1g60550 retrieved from Atted-II database<sup>18</sup> (version 9.0)

#	Locus	Alias	Function
1	At1g60000	RNA-binding	RNA-binding (RRM/RBD/RNP motifs) family protein
2	At4g25080	CHLM	magnesium-protoporphyrin IX methyltransferase
3	At4g16410		
4	<b>At1g30520</b>	<b>AAE14</b>	<b>acyl-activating enzyme 14</b>
5	At1g44000		
6	At2g47450	CPSRP43	chloroplast signal recognition particle component (CAO)
7	At2g36000	EMB3114	Mitochondrial transcription termination factor family protein
8	At3g59400	GUN4	enzyme binding;tetrapyrrole binding
9	At3g15850	JB67	fatty acid desaturase 5
10	At5g51110	dehydratase	Transcriptional coactivator/pterin dehydratase
11	At4g01050	TROL	thylakoid rhodanese-like
12	At5g35790	G6PD1	glucose-6-phosphate dehydrogenase 1
13	At5g47110	LIL3:2	Chlorophyll A-B binding family protein
14	At5g23060	CaS	calcium sensing receptor
15	At5g22340		
16	At1g03600	PSB27	photosystem II family protein
17	At1g12900	GAPA-2	glyceraldehyde 3-phosphate dehydrogenase A subunit 2
18	At3g56940	CRD1	dicarboxylate diiron protein, putative (Crd1)
19	At3g01480	CYP 38.00	cyclophilin 38
20	At1g14345	oxidoreductase	NAD(P)-linked oxidoreductase superfamily protein
21	At4g21280	PSBQA	photosystem II subunit QA
22	At5g02120	PDE335	one helix protein
23	At5g38520	alpha/beta-Hydrolases	alpha/beta-Hydrolases superfamily protein
24	At5g01920	STN 8.00	Protein kinase superfamily protein
25	At3g26710	CCB1	cofactor assembly of complex C
26	At4g25050	ACP4	acyl carrier protein 4
27	At1g74070	isomerase	Cyclophilin-like peptidyl-prolyl cis-trans isomerase family protein
28	At3g56910	PSRP5	plastid-specific 50S ribosomal protein 5
29	At1g74730	DUF1118	Protein of unknown function (DUF1118)
30	At2g03750	hydrolase	P-loop containing nucleoside triphosphate hydrolases superfamily protein

Table B.1 continued

#	Locus	Alias	Function
31	At2g34620	transcription	Mitochondrial transcription termination factor family protein
32	At5g17670	alpha/beta-Hydrolases	alpha/beta-Hydrolases superfamily protein
33	At5g08050	DUF1118	Protein of unknown function (DUF1118)
34	At3g17040	HCF107	high chlorophyll fluorescent 107
35	At1g19150	Lhca6	photosystem I light harvesting complex gene 6
36	At3g55800	SBPASE	sedoheptulose-bisphosphatase
37	At5g56850		
38	At4g12970	STOMAGEN	stomagen
39	At1g74970	TWN3	ribosomal protein S9
40	At1g72030	NAT	Acyl-CoA N-acyltransferases (NAT) superfamily protein
41	At1g31920	Tetratricopeptide repeat (TPR)-like	Tetratricopeptide repeat (TPR)-like superfamily protein
42	At4g09650	PDE332	ATP synthase delta-subunit gene
43	At1g75690	LQY1	DnaJ/Hsp40 cysteine-rich domain superfamily protein
44	At2g33180		
45	At4g25910	NFU3	NFU domain protein 3
46	At1g22430	dehydrogenase	GroES-like zinc-binding dehydrogenase family protein
47	At3g55330	PPL1	PsbP-like protein 1
48	At5g53580	PLR1	NAD(P)-linked oxidoreductase superfamily protein
49	At1g07320	RPL4	ribosomal protein L4
50	At2g39470	PPL2	PsbP-like protein 2

Table B.2 GO term enrichment analysis of the top 50 coexpressors of At1g60550 from Table B.1. GO term analysis was performed using Panther<sup>19</sup> (version 15)

<b>GO term (biological processes)</b>	<b>Genes in top 50</b>	<b>False discovery rate (FDR)</b>
chloroplast ribulose biphosphate carboxylase complex assembly (GO:0110102)	2	2.24E-02
photosynthetic electron transport in photosystem II (GO:0009772)	2	2.44E-02
chlorophyll metabolic process (GO:0015994)	5	9.37E-05
chlorophyll biosynthetic process (GO:0015995)	3	2.00E-02
photosynthetic electron transport chain (GO:0009767)	3	2.05E-02
porphyrin-containing compound metabolic process (GO:0006778)	5	1.64E-04
tetrapyrrole metabolic process (GO:0033013)	5	1.75E-04
glucose metabolic process (GO:0006006)	3	2.28E-02
photosynthesis, light harvesting (GO:0009765)	3	2.17E-02
photosynthesis, light reaction (GO:0019684)	8	1.93E-07
porphyrin-containing compound biosynthetic process (GO:0006779)	3	2.25E-02
photosynthesis (GO:0015979)	11	1.24E-10
tetrapyrrole biosynthetic process (GO:0033014)	3	2.42E-02
response to high light intensity (GO:0009644)	3	3.93E-02
pigment metabolic process (GO:0042440)	4	2.26E-02
cofactor biosynthetic process (GO:0051188)	7	1.56E-04
response to light intensity (GO:0009642)	4	2.54E-02
generation of precursor metabolites and energy (GO:0006091)	9	1.59E-05
plastid organization (GO:0009657)	7	6.39E-04
chloroplast organization (GO:0009658)	5	1.98E-02
cofactor metabolic process (GO:0051186)	9	6.82E-05
cellular protein-containing complex assembly (GO:0034622)	6	2.53E-02
protein-containing complex assembly (GO:0065003)	6	3.68E-02
response to light stimulus (GO:0009416)	8	1.25E-02
response to radiation (GO:0009314)	8	1.48E-02
cellular biosynthetic process (GO:0044249)	13	2.52E-02
biosynthetic process (GO:0009058)	14	2.06E-02
organic substance biosynthetic process (GO:1901576)	13	2.51E-02
cellular metabolic process (GO:0044237)	27	2.66E-03
organic substance metabolic process (GO:0071704)	24	3.14E-02
metabolic process (GO:0008152)	27	2.19E-02
cellular process (GO:0009987)	32	1.42E-02

Table B.3 Genotyping results from Basta-selected, green primary transformants of *aae14-1/AAE14* plants transformed with full length, recoded AAE14.

<b>Genotype</b>	<b>Observed</b>	<b>Expected</b>	<b>Chi square test</b>
<i>AAE14/AAE14</i>	12	8.5	$\chi^2 = 1.941$
<i>aae14-1/AAE14</i>	15	17	p-value = 0.3789
<i>aae14-1/aae14-1</i>	7	8.5	

Table B.4 Genotyping results from hygromycin-selected, green primary transformants of *aae14-1/AAE14* plants transformed with EcMenE-PTS1

<b>Genotype</b>	<b>Observed</b>	<b>Expected</b>	<b>Chi square test</b>
<i>AAE14/AAE14</i>	4	2	$\chi^2 = 4.000$
<i>aae14-1/AAE14</i>	4	4	p-value = 0.1353
<i>aae14-1/aae14-1</i>	0	2	

Table B.5 The top 50 co-expressed genes with AAE14 retrieved from Atted-II database<sup>18</sup> (version 9.0)

#	Locus	Alias	Function
1	At5g35790	G6PD1	glucose-6-phosphate dehydrogenase 1
2	At2g34620	transcription	Mitochondrial transcription termination factor family protein
<b>3</b>	<b>At1g78180</b>	<b>Mitochondrial substrate carrier</b>	<b>Mitochondrial substrate carrier family protein</b> Cyclophilin-like peptidyl-prolyl cis-trans isomerase family protein
4	At1g74070	isomerase	protein
5	At5g52100	CRR1	Dihydrodipicolinate reductase, bacterial/plant
6	At4g34220	kinase	Leucine-rich repeat protein kinase family protein
7	At3g09580	oxidoreductase	FAD/NAD(P)-binding oxidoreductase family protein
<b>8</b>	<b>At2g37450</b>	<b>UMAMIT13</b>	<b>nodulin MtN21 /EamA-like transporter family protein</b> pentatricopeptide (PPR) repeat-containing protein / CBS domain-containing protein
9	At5g10690	PPR	domain-containing protein
10	At1g60550	ECHID	enoyl-CoA hydratase/isomerase D
11	At5g56850		
12	At1g12860	SCRM2	basic helix-loop-helix (bHLH) DNA-binding superfamily protein
13	At1g60600	ABC4	UbiA prenyltransferase family protein
14	At3g14930	HEME1	Uroporphyrinogen decarboxylase
15	At4g09010	TL29	ascorbate peroxidase 4
16	At3g13000	DUF547	Protein of unknown function, DUF547
17	At3g01480	CYP 38.00	cyclophilin 38
18	At5g01015		
19	At1g54820	kinase	Protein kinase superfamily protein
20	At2g47940	EMB3117	DEGP protease 2
21	At4g01460	DNA-binding	basic helix-loop-helix (bHLH) DNA-binding superfamily protein
22	At1g55370	NDF5	NDH-dependent cyclic electron flow 5
<b>23</b>	<b>At2g38330</b>	<b>MATE efflux</b>	<b>MATE efflux family protein</b> Bifunctional inhibitor/lipid-transfer protein/seed storage 2S albumin superfamily protein
24	At5g48490	inhibitor	albumin superfamily protein
		Tetratricopeptide repeat (TPR)-like	Tetratricopeptide repeat (TPR)-like superfamily protein
25	At4g28080	Tetratricopeptide repeat (TPR)-like	Tetratricopeptide repeat (TPR)-like superfamily protein
26	At5g66520	repeat (TPR)-like	Tetratricopeptide repeat (TPR)-like superfamily protein
27	At1g14030	LSMT-L	Rubisco methyltransferase family protein
28	At1g08520	V157	ALBINA 1

Table B.5 continued

#	Locus	Alias	Function
29	At4g25080	CHLM	magnesium-protoporphyrin IX methyltransferase
30	At1g71720	RLSB	Nucleic acid-binding proteins superfamily
31	At5g49390		
32	At1g19150	Lhca6	photosystem I light harvesting complex gene 6
33	At2g29290	Rossmann-fold	NAD(P)-binding Rossmann-fold superfamily protein
34	At3g29185	DUF3598	Domain of unknown function (DUF3598)
		Tetratricopeptide	
35	At1g31920	repeat (TPR)-like	Tetratricopeptide repeat (TPR)-like superfamily protein
36	At4g19985	NAT	Acyl-CoA N-acyltransferases (NAT) superfamily protein
		HMG box with	
		ARID/BRIGHT DNA-	HMG (high mobility group) box protein with ARID/BRIGHT
37	At1g76110	binding domain	DNA-binding domain
38	At3g10160	FPGS2	DHFS-FPGS homolog C
39	At3g08920	phosphatase	Rhodanese/Cell cycle control phosphatase superfamily protein
40	At1g21500		
41	At3g16000	MFP1	MAR binding filament-like protein 1
42	At2g39470	PPL2	PsbP-like protein 2
			Cyclophilin-like peptidyl-prolyl cis-trans isomerase family
43	At3g15520	isomerase	protein
44	At5g47900	DUF1624	Protein of unknown function (DUF1624)
45	At1g08390		
46	At3g25660	Amidase	Amidase family protein
47	At2g05160	zinc finger	CCCH-type zinc fingerfamily protein with RNA-binding domain
48	At1g03630	PORC	protochlorophyllide oxidoreductase C
49	At4g26520	FBA7	Aldolase superfamily protein
50	At4g33000	SCABP8	calcineurin B-like protein 10

Table B.6 Primers used in this study.

<b>Primer</b>	<b>Description</b>	<b>Sequence (5'-&gt;3')</b>
P1	<i>aae14-1</i> F	CCGGAATGGCTAATCACTCTC
P2	<i>aae14-1</i> R	TCCCGTTGTACCTATCCCAAG
P3	LBa1	TGGTTCACGTAGTGGGCCATCG
P4	CACC-CO-EcMenE-F	CACCATGATCTTTTCTGATTGGCCTTGGAGACATT
P5	CO-EcMenE-PTS1-R	TCAGAGCCTTGATTGCTGCCTTTGAACCCATTCTTTGA
P6	CACC-AAE14	CACCATGGCCAACCATTTCGCGA
P7	AAE14-no PTS1-stop-R	CAGGTCTTATCGCACTTTCAGATTATGACATAG
P8	native-EcMenE-F-KpnI	CACCGGTACCATGATCTTCTCTGACTGGCCGT
P9	native-EcMenE-R-Sall	GTGGGTGCAACGTCAGCAATAAGTCGACGTCG
P10	CO-EcMenE-F-KpnI	CACCGGTACCATGATCTTTTCTGATTGGCCTTGGAGA
P11	CO-EcMenE-PTS1-R-Sall	GGCAGCAATCAAGGCTCTGAGTCGACGTCG
P12	AAE14-no PTS1-R	CAGGTCTTATCGCACTTTCAGATTATGACA
P13	CACC-At1g60550	CACCATGGCGGATTCCAATGAGCTTGG
P14	At1g60550-no stop-R	AGGTCGCCGGTGAAATTTAGAGAAGTC

## APPENDIX C. SUPPLEMENTAL INFORMATION FROM CHAPTER 4

### C.1 Inclusion of the parameter $a$

The parameter  $a$  signifies the competitive advantage conveyed to allelopathic plants when competing for resources. When  $a < \frac{1}{2}$ , allelopathic plants are worse competitors for resources and pay an additional cost.

Without the inclusion of the parameter  $a$ , we assume that competing plants share the benefit in a given area equally (*i.e.*  $\frac{B}{2}$ ). This yields the following pay-off matrix:

		<b>Opponent</b>	
		$+A$	$-A$
<b>Player</b>	$+A$	$\frac{B}{2} - C$	$\frac{B}{2} - C$
	$-A$	$\frac{B}{2} - T$	$\frac{B}{2}$

Figure C.1 Symmetric pay-off matrix for competition between plants that either produce allelochemicals ( $+A$ ) or not ( $-A$ ) without the inclusion of the competitive parameter  $a$

In this case, for  $+A$  to be a pure ESS, (i)  $+A$  needs to be able to invade a population of  $-A$  and (ii) needs to resist invasion from  $-A$ . According to the ESS definition, this occurs when:

$$\frac{B}{2} - C > \frac{B}{2} \quad \text{and} \quad \frac{B}{2} - C > \frac{B}{2} - T \quad (\text{equations } 9a)$$

Both of which can be rearranged to:

$$-C > 0 \quad \text{and} \quad T > C \quad (\text{equations } 9b)$$

Therefore,  $+A$  can never be the ESS because  $C$  is by definition greater than zero, so the first condition in equations 9b cannot be met.

Conversely, for  $-A$  to be a pure ESS, (i)  $-A$  needs to be able to invade a population of  $+A$  and (ii) needs to resist invasion from  $+A$ . According to the ESS definition, this occurs when:

$$\frac{B}{2} - C < \frac{B}{2} \quad \text{and} \quad \frac{B}{2} - C < \frac{B}{2} - T \quad (\text{equations } 10a)$$

Both of which can be rearranged to:

$$-C < 0 \quad \text{and} \quad T < C \quad (\text{equations } 10b)$$

In this case,  $B$  has no bearing on the ESS. The only factors that matter are the relative values of  $C$  and  $T$ . Also, allelopathy can never be the ESS, which seems counterintuitive as we find allelopathic plants in nature.

## C.2 Inclusion of the parameter $T$

Without the inclusion of the parameter  $T$ , the pay-off matrix is as follows:

		Opponent	
		$+A$	$-A$
Player	$+A$	$\frac{B}{2} - C$	$aB - C$
	$-A$	$(1 - a)B$	$\frac{B}{2}$

Figure C.2 Symmetric pay-off matrix for competition between plants that either produce allelochemicals ( $+A$ ) or not ( $-A$ ) without the inclusion of  $T$ .

In this case, for  $+A$  to be a pure ESS, (i)  $+A$  needs to be able to invade a population of  $-A$  and (ii) needs to resist invasion from  $-A$ . According to the ESS definition, this occurs when:

$$aB - C > \frac{B}{2} \text{ and } \frac{B}{2} - C > B(1 - a) \quad (\text{equations 11a})$$

Both of which can be rearranged to:

$$B > \frac{2C}{2a-1} \quad (\text{equation 11b})$$

Conversely, for  $-A$  to be a pure ESS, (i)  $-A$  needs to be able to invade a population of  $+A$  and (ii) needs to resist invasion from  $+A$ . According to the ESS definition, this occurs when:

$$aB - C < \frac{B}{2} \text{ and } \frac{B}{2} - C < B(1 - a) \quad (\text{equations 12a})$$

Both of which can be rearranged to:

$$B < \frac{2C}{2a-1} \quad (\text{equation 12b})$$

Because there is only a single isocline (equations 11b and 12b), mixed ESS are not possible. In this situation, only pure ESS solutions can exist. Above the isocline  $B = \frac{2C}{2a-1}$ ,  $+A$  is ESS and below  $-A$  is ESS (Figure C.3).

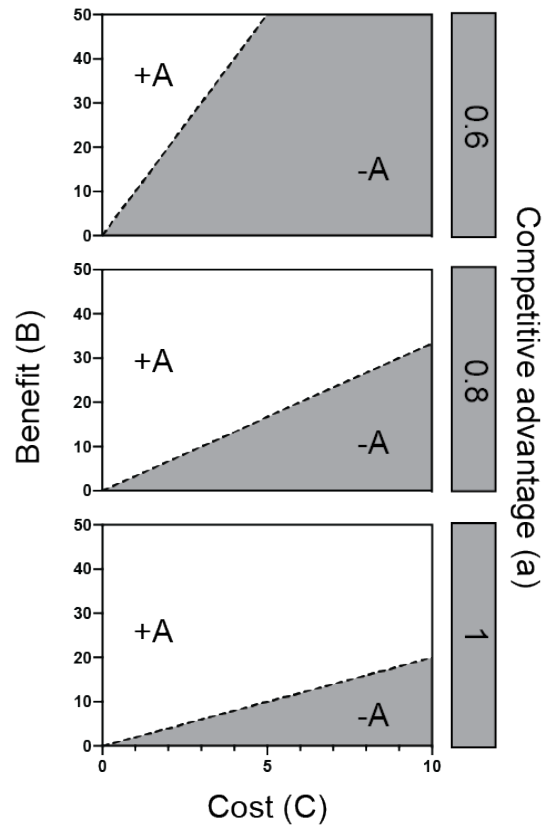


Figure C.3 Isoclines that depict ESS states in  $B$  and  $C$  phase space depending on the value  $a$  (rows). The dashed line represents the isocline  $B = \frac{2C}{2a-1}$ . White space is the area of parameter space where production of allelochemicals ( $+A$ ) is the ESS. Dark grey is where not producing allelochemicals is the ESS ( $-A$ ).

## PUBLICATIONS

1. Auber RP, Suttiyut T, **McCoy RM**, Ghaste M, Crook JW, Pendleton AL, Widhalm JR, and Wisecaver JH. (*accepted*). Hybrid *de novo* genome assembly of red gromwell (*Lithospermum erythrorhizon* Siebold & Zucc.) reveals evolutionary insight into shikonin biosynthesis. *Horticulture Research*.
2. **McCoy RM**, Meyer GW, Rhodes D, Sors TG, Murray GC, and Widhalm JR. (2020). Exploratory study on the foliar incorporation and stability of isotopically labeled amino acids applied to turfgrass. *Agronomy* 10:358. doi: 10.3390/agronomy10030358
3. Li Y, Brooks M, Yeoh-Wang J, **McCoy RM**, Rock T, Pasquino A, Moon CI, Patrick RM, Tanurdzic M, Ruffel S, Widhalm JR, McCombie WR, and Coruzzi GM. (2020). SDG8-mediated histone methylation and RNA processing function in the response to nitrate signaling. *Plant Physiology* 182: 215-227 doi: 10.1104/pp.19.00682.
4. **McCoy RM**, Utturkar S, Crook JW, Thimmapuram J, and Widhalm JR. (2018). The origin and biosynthesis of the naphthalenoid moiety of juglone in black walnut. *Horticulture Research* 5: 67 doi: 10.1038/s41438-018-0067-5.
5. Adebesin F, Widhalm JR, Lynch JH, **McCoy RM**, and Dudareva N. (2018) Auxillary peroxisomal thioesterases regulate flux distribution within the benzenoid/phenylpropanoid metabolism. *Plant Journal* 93: 905-916 doi: 10.1111/tpj.13818.
6. Wang P, Guo L, Jaini R, Klempein A, **McCoy RM**, Morgan JA, Dudareva N, and Chapple C. (2018) A <sup>13</sup>C isotope labeling method for the measurement of lignin metabolic flux in Arabidopsis stems. *Plant Methods* 14: 51 doi: 10.1186/s13007-018-0318-3.
7. Widhalm JR, Gutensohn M, Yoo H, Adebesin F, Qian Y, Guo L, Jaini R, Lynch JH, **McCoy RM**, Shreve JT, Thimmapuram J, Rhodes D, Morgan JA, and Dudareva N. (2015) Identification of a plastidial phenylalanine exporter that influences flux distribution through the phenylalanine biosynthetic network. *Nature Communications* 6: 8142 doi: 10.1038/ncomms9142.